CHARACTERIZATION OF BINDING AND ACTIVATION MECHANISMS OF BAK

CHARACTERIZATION OF BINDING AND ACTIVATION MECHANISMS OF BAK

By SABINA TREBINJAC, HBSC

A Thesis Submitted to the School of Graduate Studies in Partial Fulfilment of the Requirements for the Degree Master of Science

MASTER OF SCIENCE (2024) McMaster University

(Neuroscience) Hamilton, Ontario

TITLE: Characterization of the activation mechanism of Bak

AUTHOR: Sabina Trebinjac, H.B.Sc. (University of Toronto)

SUPERVISOR: Dr. Kathryn Mary Murphy

NUMBER OF PAGES: xxix, 99

Abstract

Background

Cell death is required for the development and function of all multicellular organisms by eliminating damaged cells, thereby maintaining physiological homeostasis. Dysregulation of cell death contributes to the development of diseases such as cancer, autoimmune and neurodegenerative diseases. The onset of cell death involves the activation of BCL-2 family executioner proteins Bax and Bak by the BH3-only activators Bid, Bim or Puma. Executioner proteins Bak and Bax are both involved in the pore formation process on the mitochondrial membrane, however, recent evidence suggests that Bax and Bak are differentially activated. Understanding such mechanistic differences opens the possibilities for pharmaceutical interventions via Bax/Bak-mediated apoptosis due to their differential expression profiles across various diseased/healthy tissues.

Methods

FLIM (Fluorescence Lifetime Imaging)-FRET (Förster resonance energy transfer) microscopy in live cells was done in BMK DKO and HCT116 DKO cell lines expressing the donor mCerulean3 or mTurquoise2 N-terminally fused to the protein-of-interest in cell lines stably expressing donor mCerulean3 (mC3)-fused to Bax or Bak without its carboxyl terminal, enabling survival of Bax/Bak expressing cells upon transient expression of the acceptor Venus-fused BH3-only activators. Transfected cells were imaged on the INO-FHS confocal microscope to obtain the fluorescence lifetime of mCerulean3.Fluorescent protein standards were used to convert intensity into concentration, and a Hill-slope fit of the binding curves was used to determine dissociation constants (K_D) in live cells. The apparent K_D values were obtained from the fitted Hill-equation (h=1) of the binding data after subtracting the fitted binding data of the negative collisional controls from each fitted construct's original binding data for each construct. If the final binding curves' BMAX y values (ΔGꞋ) were below the threshold of 0.04, the binding data were deemed insufficient (NSF). Unpaired student t-test with Welch's correction assuming Gaussian distribution with unequal standard deviation was used to determine statistical significance. Orthogonal *in*

vitro binding assays using recombinant proteins were carried out to validate our FLIM-FRET findings. Activation of Bak by BH3-only proteins was tested using terbium-release liposome permeabilization assay *in vitro* and dox-inducible mC3-Bak cell death assay in live cells.

Conclusion

Here, we report that Bid is more efficient than Bim at activating Bak, with the BH3 region of Bid enabling high affinity binding to Bak. Further, effective Bak activation by Bim or Bid requires both binding of the BH3-motifs to the BH3-binding pocket of Bak and additional interactions between the activator proteins and the Bak-CTS. For Bim, the additional interaction with the Bak-CTS necessary for robust Bak activation is with the CTS of Bim.

Acknowledgements

To Dr. Kathy Murphy and Dr. David Andrews, thank you for your tremendous support and mentorship, it has been an incredible privilege. Dr. Murphy, I hold deep gratitude for your kindness, guidance and writing mentorship. Dr. Andrews, thank you for your support and the opportunity to work on incredibly cool science.

I want to give a special thanks to my colleague Dang Nguyen. While we grappled with the complexities of Bak apoptosis, you made this challenging journey interesting and humorous. My dreams of bringing back the tradition of Viennese Kaffeehaus, where writers and scientists gather for intellectual exchange, were expressed in the many walks in nature around the hospital where there was ample opportunity for brainstorming and discussions.

To the Bcl-2 members of the Andrews lab, Dr. Justin Kale, Dr. Elizabeth Osterlund, Dr. James Pemberton, Dr. Wiebke Schormann, and Uyen Le, you were an incredible resource. I am fortunate to have received your insights.

I dedicate this thesis to my mom Radmila Trebinjac, who we lost too early and during the progress of this research but who built the foundation for the person I am today. I will forever miss sitting at the kitchen table with you working on our respective projects, but your presence lives on in your children and grandchildren.

Table of Contents

List of Figures

(D) Schematic describing the proteins used to measure in HCT116 $Bax^{-/-}$ $Bak^{-/-}$ (DKO) cells the binding of mCerulean3-fused CTS-truncated Bak (^{C}BakΔCTS) to Venus-fused tBid (^{V}tBid).

(E) Representative of FLIM-FRET images for ^{C}BakΔCTS (Time correlated single photon counting image, left panel) and ^{V}tBid (hyperspectral image, right panel). The middle panel shows the selection of Regions of Interest (ROIs) that resulted from the watershed algorithm on the mCerulean3 image. The scale bar indicates 100 μm. (F-H) The binding of acceptor ^{V}BH3-only proteins to (F, H) donor ^{C}BakΔCTS or (G) ^{C}BaxΔCTS in HCT116 DKO cells measured by FLIM-FRET.

(F) The protein ^{V}tBid bound to ^{C}BakΔCTS with an average K_D of 6 μM as indicated by the binding data in red that fits the Hill-equation (h=1) and has a s-ratio≥2. In contrast, binding to ^{C}BakΔCTS was not measurable for the other ^{V}BH3-only proteins tested.

(G) ^{V}tBid, ^{V}BimL, and ^{V}Puma bound to BaxΔCTS with K_D values ranging between 8 to 15 μM. Only collisions were detected for ^{V}Bik, ^{V}Noxa, ^{V}Bad, and the negative control protein Venus with either Bax or Bak, as the binding data best fit linear equations (s-ratio <2).

(H) Replacing the Bid BH3 motif with that of Bim in the ^{V}tBid(Bim BH3 h0-h4) chimera or mutating the key four hydrophobic residues (h1, h2, h3, and h4) to glutamic acid (^{V}tBid-4E) abolished binding of ^{V}tBid to ^{C}BakΔCTS. S-ratios for both ^{V}tBid(Bim BH3 h0-h4) and ^{V}tBid-4E and are below 2. (fit: R^2>0.9 and =0.7 for ^{V}tBid(Bim BH3 h0-h4) and ^{V}tBid-4E, respectively). (F-H) The dotted lines are the 95% confidence interval of fit of the data for the three technical replicates (solid symbols).

Figure 2.2. h0 residues within Bid BH3 confer binding to Bak but are insufficient to activate Bak.

(A) Schematic shows the alignment of residues in Bid and Bim BH3 motif. Mutations at the key hydrophobic residues in the Bid BH3 and Bim BH3 are highlighted in yellow. Chimeric mutants of BimL are highlighted in yellow where whole or parts of Bid BH3 are inserted in Bim BH3. A mutant of BimL with a scrambled BH3 sequence is shown at the bottom as a negative control for the *in vitro* cell-free liposome permeabilization assay.

(B) FLIM-FRET microscopy measured the binding of ^{V}tBid I82A I83A (purple) to ^{C}BakΔCTS in HCT116 DKO cells. The binding curve was linear (s-ratio <2), similar to the negative control ^{V}tBid-4E, indicating collisional interactions. In contrast, ^{V}tBid (red) exhibited binding fitted to the Hill equation (h=1), with an apparent K_D of 11 μM (s-ratio ≥2). Data from three technical replicates are shown, with summarized results in Table 1 and Appendix Table S1.

(C) FLIM-FRET microscopy measured the binding of ^{V}BimL(Bid BH3 h0+1) to ^{C}BakΔCTS with an apparent K_D of 10 µM (dark purple), fitted to the Hill equation (h=1). Enhanced binding was observed for ^{V}BimL(Bid BH3 h0-h4+3) (blue, K_D = 10 µM, s-ratio = 4.2), but not for ^{V}BimL(Bid BH3 h1-h4+3) (green), which displayed collisional interactions (s-ratio <2). ^{V}BimL, ^{V}BimL-4E, and ^{V}BimL(Bid BH3 h1-h4+3) all resulted in linear binding data that indicate collisions. Data from three technical replicates are summarized in Table 1 and Appendix Table S2.

(D) Terbium-release liposome assay with 100 nM Bak and cBid showed a partial reduction in Bak activation by cBid I82A I83A with the maximal terbium release was reduced from 70–80% for cBid to 50–60% for cBid I82A I83A while the EC50 values for both cBid and cBid I82A I83A were approximately 0.3±0.1 nM. Data points represent averages from four (cBid) and three (cBid I82A I83A) independent replicates.

(E) Terbium-release assay with 100 nM Bak showed minimal enhancement of BimL-mediated Bak activation when Bid BH3 residues were introduced into BimL. The EC50 decreased from 13 nM for BimL to 9 nM for BimL(Bid BH3 h0+1) and 5 nM for BimL(Bid BH3 h0-h4+3) chimera, while maximal terbium release remained at 70–80%. Scrambling the BH3 sequence abolished BimL-mediated activation. Data points are averages from six independent replicates fitted to a four-parameter dose-response curve.

Figure 2.3. Activation of Bak requires Bak CTS which binds selectively to Bim and Bid.

(A) Schematic representation of Bak and Bak-CTS mutants. The CTS, located at residues 186–211 in human Bak, was deleted in BakΔCTS or replaced with a scrambled sequence in Bak-CTSscr. The last three rows show schematic depictions of the Bak-CTS, Bax-CTS, and scrambled Bak-CTS sequences.

(B) Smac-mCherry release assay with mitochondria from BMK DKO cells. Deleting (red) or scrambling (gray) Bak-CTS abolished cBid-induced Bak activation. Recombinant cBid activates 100 nM Bak with an EC50 of 40 pM. BakΔCTS and Bak-CTSscr did not induce significant mitochondrial permeabilization. Data are from three independent experiments.

(C) The binding of 5 nM recombinant Donor A568-cBid to Acceptor A647-Bak or Bak-CTS mutants, measured via intensity-based FRET spectroscopy, showed reduced binding for BakΔCTS (dark red) and Bak-CTSscr (gray). The FRET data were fitted to a quadratic equation. Data are from three independent experiments.

(D) Quantifying A647-Bak binding to mitochondria isolated from BMK DKO cells showed that ~15% of full-length Bak, ~12% of Bak-CTSscr, and ~5% of BakΔCTS were in the mitochondrial fractions. Data represent five independent experiments.

(E) FLIM-FRET data showing $^{mT2}CTS_{BAK}$ bound to ^{V}BimL and ^{V}tBid in BMK DKO cells, with K_D values of 6.2 and 7.9 µM, respectively, as fitted to the Hill-equation (h=1). No binding was observed for ^{V}Bad, ^{V}Bik, or Venus, as indicated by their binding data fitted to the linear equation. Data are from three technical replicates. An independent biological replicate is in Figure 3—Figure Supplement 2D.

(F) FLIM-FRET data showed $^{mT2}CTS_{BAX}$ bound ^{V}tBid (K_D = 6.6 µM) but not ^{V}BimL, ^{V}Bad, ^{V}Bik, or ^{V}Noxa. S-ratio analysis indicates collisional interactions (s-ratio <2) for non-binding proteins. Data are from three technical replicates. An independent biological replicate is shown in Figure 3—Figure Supplement 2E.

Figure 2.4. The binding of Bak-CTS to Bid is independent of Bid BH3.

(A) FLIM-FRET analysis of ^{V}tBid and ^{V}tBid-4E binding to $^{mT2}CTS_{BAK}$ in BMK DKO cells. Mutating h1, h2, h3, and h4 residues in the BH3 motif of Bid (^{V}tBid-4E) did not abolish binding to $^{mT2}CTS_{BAK}$, but instead yielded a binding curve that was fitted to the Hill-equation (h=1) with an apparent K_D of 4.7 µM. Data represent three technical replicates. Figure 2.4 – Figure supplement 3 A and B show an independent replicate of the experiment in Panel A and B, respectively.

(B) Binding of ^{V}tBid I82A and ^{V}tBid I83A mutant to $^{mT2}CTS_{BAK}$ showed similar K_D values (~8–12 µM) compared to ^{V}tBid binding, indicating that mutations in the h0 residues of Bid did not affect the binding to the Bak-CTS. Data represent three technical replicates.

(C) FLIM-FRET analysis of ^{V}tBid, ^{V}tBid-4E, and ^{V}Bad examined their binding to mCerulean3-N-terminally fused full-length Bak with a G126S mutation in the BH3-binding pocket (^{C}Bak G126S). ^{V}tBid and ^{V}tBid-4E bound ^{C}Bak G126S with apparent K_D values of 24 and 37 µM, respectively, while ^{V}Bad exhibited collisional interactions (s-ratio <2). Results from two additional independent replicates were combined and shown in Figure 2.4—Figure Supplement 3C.

Figure 2.5. The Bim-CTS directly binds to the Bak-CTS.

(A) Schematic of murine BimL showing the alignment of Bim-BH3 and Bim-CTS murine sequences, which share homology at h0, h1, h2, and h3 residues but not h4. Negative controls include BimΔCTS (lacking residues 120–140), Bim-CTSscr (scrambled CTS residues 121–136), and the cancer-associated R134L mutant. Human Bad and a chimeric Bad protein (BadΔCTS-BimCTS) are included for comparison.

(B) FLIM-FRET microscopy revealed that Bim-CTS ($^{V}CTS_{BIM}$) bound to $^{mT2}CTS_{BAK}$ with an apparent K_D of 13 µM (Hill equation fit, h = 1). Full-length ^{V}BimL (K_D = 9 µM) and ^{V}BimL-4E (K_D = 16 µM) also bound $^{mT2}CTS_{BAK}$, confirming that the Bim BH3 is not required for binding $^{mT2}CTS_{BAK}$. Scrambling CTS in full-length Bim (^{V}BimL-CTSscr) or isolated CTS ($^{V}CTSscr_{BIM}$) abolished binding, with insufficient Δω (BMAX = 0.04, R^2 = −0.7 for ^{V}BimL-CTSscr; s-ratio < 2 for $^{V}CTSscr_{BIM}$). Binding data for ^{V}BimL-CTSscr and

^{V}CTSscr$_{BIM}$ were thus fitted to a linear equation which indicate collisions. Data represent three technical replicates; an independent replicate is shown in Figure 2.5—Figure Supplement 3A.

(C) ^{V}Bad did not bind ^{mT2}CTS$_{BAK}$ (linear fit, s-ratio = 1.1, $R^2 = 0.8$). Replacing the Bad-CTS with Bim-CTS (^{V}BadΔCTS-BimCTS) restored binding (K_D = 14 μM, s-ratio = 2.2). Truncating the Bim-CTS (^{V}BimΔCTS) eliminated binding to ^{mT2}CTS$_{BAK}$ (linear fit, s-ratio = 1.3). Data represent three technical replicates; an independent replicate is shown in Figure 2.5—Figure Supplement 3B.

(D) The R134L mutation in Bim-CTS (^{V}BimL R134L) abolished binding to ^{mT2}CTS$_{BAK}$, with insufficient FRET and low Δω (BMAX < 0.05, $R^2 = 0.2$, Hill equation fit, h = 1). Data represent three technical replicates; an independent replicate is shown in Figure 2.5—Figure Supplement 3C.

Figure 2.6. Bim CTS is necessary for BimL to activate Bak.

(A) Representative images of BMK DKO cells expressing Dox-inducible ^{C}Bak and transfected with ^{V}BimL or ^{V}BimL-R134L, showing caspase-3 activation (NucView530 intensity) as a marker of cell death.

(B) Cell death assay in ^{C}Bak-expressing BMK DKO cells demonstrates reduced cell death with ^{V}BimL mutants lacking an intact BH3 domain (4E), scrambled CTS (-CTSscr), or deleted CTS (ΔCTS). The cancer-associated R134L mutation (^{V}BimL-R134L) also significantly impaired cell death. Other constructs used in this experiment, including the negative control Venus, similarly did not induce significant cell death in cells expressing ^{C}Bak. Data from 3 independent replicates are shown with the solid line representing the mean %Dead of cells co-expressing ^{C}Bak and the indicated ^{V}BH3-only protein construct.

(C) Scrambling the Bim-CTS (BimL-CTSscr in light orange) reduced Bak activation by recombinant BimL in a terbium-release liposome permeabilization assay with 100 nM recombinant full-length Bak. Similarly, a BimL chimera mutant with Bad BH3 (BimL(Bad BH3 h1-h4+3) in dark red) failed to activate Bak with an increase in EC_{50} value and a decrease in maximal release. The data point represents an average of 6 independent replicates for BimL/BimL-CTSscr and 4 independent replicates for BimL (Bad BH3 h1-h4+3).

(D) Scrambled the Bim-CTS mildly reduced the binding of A568-BimL to MOM-like liposomes, as shown by size-exclusion chromatography, while ΔCTS eliminated liposome binding. Data from 3 independent experiments are shown with the solid line indicating the mean.

Figure 2.1. Figure Supplementary 1. ^{V}tBid BH3 chimera bind ^{C}BaxΔCTS and ^{C}Bcl-XL in live cells and kill primed BMK cells in a Bax/Bak-dependent manner.

(A) Schematic represents the BH3 sequences of murine Bid, Bim, and the ^{V}tBid chimera with its BH3 substituted for the BH3 of Bim from residue h0 to residue h4. Yellow-shaded sequences indicate the inserted Bim, Bad, or Puma BH3 replacing Bid BH3.

For both panels (B) and (C), the raw binding data for ^{V}tBid was from the same experiment as the main figure 2.1G and 1F, respectively, but was then plotted with higher bins of free Venus, resulting in an elongated x-axis.

(B) The chimera ^{V}tBid (Bim BH3 h0-h4) (orange) bound to ^{C}BaxΔCTS in HCT116 DKO cells, as fitted to the Hill-equation (h=1), with a lower affinity compared to ^{V}tBid (Table 1 and Appendix Table S3). The negative control ^{V}tBid-4E did not bind to ^{C}BaxΔCTS as indicated by the binding data fitting best to a linear equation, with the s-ration below 2. Data represent 3 technical replicates.

(C) ^{V}tBid and ^{V}tBid (Bim BH3 h0-h4) bound to ^{C}Bcl-XL in BMK DKO cells with similar apparent K_D ranging between 7 to 12 μM. In this experiment, we found that the binding data for the negative control ^{V}tBid-4E passed the threshold for s-ratio (>2) and BMAX of ΔGD (>0.05) to achieve an apparent K_D of 19 μM to ^{C}Bcl-XL demonstrating a lower binding affinity compared to ^{V}tBid.

(D) Cell death assay using BMK cells transfected with the indicated ^{V}BH3-only constructs showed that ^{V}tBid and ^{V}tBid (Bim BH3 h0-h4) induced approximately 60% to 70% cell death in the Venus-positive cell population, as measured by A647-Annexin V positivity. The negative control ^{V}tBid-4E only induced less than 10% cell death. BMK DKO cells were resistant to the expression of ^{V}tBid or ^{V}tBid (Bim BH3 h0-h4) chimera, confirming that cell death induced by ^{V}tBid or the chimera depends on the presence of Bax and Bak in these cells. Data represent 3 independent replicates.

Figure 2.2. Figure Supplementary 1. h0 residues of Bid BH3 are not required for ^{V}tBid binding to ^{C}Bax and ^{C}Bcl-XL.

(A) I83A mutation in Bid BH3 (^{V}tBid I83A in black) abolished the binding to ^{C}BakΔCTS in HCT116 DKO. Similarly, ^{V}tBid-4E (Blue) did not bind to ^{C}BakΔCTS as their binding data indicated collisions. ^{V}tBid I82A (Green) bound to ^{C}BakΔCTS with a reduced affinity with an apparent K_D of 21.3 μM, compared to ^{V}tBid binding to ^{C}BakΔCTS (K_d =7.6 μM). Apparent K_D values were obtained from the Hill-fitted binding curve after subtracting the original binding data from the collisional control ^{V}tBid-4E (Table 1, see Methods). Data from 3 technical replicates are shown.

(B) h0 mutants of ^{V}tBid bound ^{C}BaxΔCTS with similar (K_D = 8.8 μM for v-tBid I83A) or slightly reduced (K_D = 15.2 and 16.8 μM for ^{V}tBid I82 and ^{V}tBid I82A I83A, respectively) apparent K_D compared to ^{V}tBid (K_D = 12.7 μM) (Table 1). ^{V}tBid-4E did not bind to ^{C}BaxΔCTS, as the straight line (blue) fitted to the binding data shows. Data from 3 technical replicates are shown.

(C) h0 mutants of tBid did not affect the binding of ^{V}tBid to ^{C}Bcl-XL. ^{V}tBid I82A and ^{V}tBid I83A bind to ^{C}Bcl-XL with apparent K_D of 10.6 and 12.3 μM, respectively. ^{V}tBid bound ^{C}Bcl-XL with a K_D value of 9.4 μM, whereas ^{V}tBid-4E bound ^{C}Bcl-XL weakly with a K_D of 18.9 μM. These K_D values were obtained from the Hill-fitted binned binding data without subtracting the collisional binding control (Supplementary Table 3). The generated data for ^{V}tBid and ^{V}tBid-4E was from the same experiment that was done for Figure 2.1 – Figure Supplementary 1C. Data from 3 technical replicates are shown.

(D) Like ^{V}tBid, all h0 mutants of ^{V}tBid induced cell death as measured by Annexin V positivity in primed BMK WT cells. The mean %cell death of transfected cells induced by ^{V}tBid I82A, ^{V}tBid I83A, and ^{V}tBid I82A I83A were above 60%, as indicated by the solid lines in between the data points. All transfected cells selected for cell death analysis were positive for expression of Venus, as compared to the background Venus intensity in the non-transfected control group (see Methods). Data from 3 independent replicates are shown.

(E) Mutation in h0 residue I82A or I83A of stapled TMR-labeled Bid BH3 peptide (TMR-Bid SAHB) reduced the binding affinity to BakΔCTS recombinant proteins as measured by fluorescence polarization assay. 20 nM of TMR-Bid SAHB was added to an increasing concentration of BakΔCTS, as indicated on the x-axis. The negative control Bid SAHB with alanine replacing the h2 and h3+2 residues in Bid BH3 (TMR-Bid L90A D95A) had a ~12-fold reduction in binding affinity to BakΔCTS as compared to TMR-Bid SAHB. Binding data with the y-values (Polarization Unit) plotted against the concentration of the receptor BakΔCTS was fitted using the One Site-Total binding Equation in GraphPad Prism. Relative K_D values are shown on the graph. Data represent 3 independent replicates.

(F) I83A but not I82A mutation severely diminished the binding of TMR-Bid SAHB to BaxΔCTS recombinant proteins. The negative control TMR-Bid L90A D95A similarly lost the binding to BaxΔCTS. 20 nM of TMR-Bid SAHB was added to an increasing concentration of BaxΔCTS, as indicated by the values on the x-axis. The generated graph was done by the same analysis as for Panel E. Relative K_D values are displayed on the graph. Data represent 3 independent replicates.

Figure 2.2. Figure Supplementary 2. h0 residues of Bid BH3 are unnecessary for effective Bax and Bak activation by cBid.

(A) Measured by FLIM-FRET microscopy in BMK DKO cells, ^{V}BimL (grey) and ^{V}BimL with Bid BH3 chimera bind ^{C}BaxΔCTS in HCT116 DKO with a similar relative binding affinity as their apparent K_D values were between 8 and 13 μM (Table 1). Replacing the h0+1 residues of Bim (PEI) with that of Bid (IIH) in ^{V}BimL (Bid BH3 h0+1) (dark brown) or the entire Bim BH3 (h0-h4+3 in blue or h1-h4+3 in green) with the equivalent BH3 sequence from Bid had no significant effect on ^{V}BimL binding to mC3-BaxΔCTS. The negative control ^{V}BimL-4E (red) did not bind ^{C}BaxΔCTS, as indicated by a straight line fitted to the binding data at the bottom of the graph. Data from 3 technical replicates are shown.

(B) h0 mutations I82A and I83A did not significantly affect cBid-mediated Bak activation as measured by terbium release liposome permeabilization assay. cBid I82A and I83A activated 100 nM full-length recombinant Bak with a similar EC_{50} as WT cBid and only had a slightly reduced maximum % of terbium releases. Data from 4 independent replicates are shown. Errors bars indicate standard deviations.

(C) h0 mutations I82A, I83A, and I82A I83A had no effect on cBid-mediated Bax activation as measured by terbium release liposome permeabilization assay. For Bax activation, cBid and cBid h0 point mutants had similar EC_{50} around 1 nM and caused up to 80% terbium release at their highest concentrations when incubating with 100 nM full-length recombinant Bax. For cBid, cBid I82A, and cBid I83A, data from 4 independent replicates are shown. For cBid I82A I83A, data from 3 independent replicates are shown. Error bars indicate standard deviations.

(D) Table displays EC_{50} values in nanomolar for activation of 100 nM Bax or Bak by cBid or different cBid h0 mutants.

Figure 2.3. Figure Supplementary 1. Bak-CTS with the triple mutations V194K, L195S, and V198D can bind BimL and tBid despite poor mitochondrial localization.

(A) Western blot analysis of recombinant full-length Bak or Bak-CTS mutants (100 nM) incubated with isolated heavy membranes, including the mitochondrial fraction, in the presence or absence of cBid (10 nM). After a 1-hour incubation at 37°C, samples were centrifuged to separate the mitochondrial pellet (P) and soluble supernatant (S) fractions. Both fractions were analyzed by SDS-PAGE and immunoblotting with anti-Bak antibodies. The graph on the right quantified Bak binding to the mitochondrial fraction, showing that cBid enhanced mitochondrial localization of all Bak variants. Full-length Bak exhibited higher mitochondrial binding compared to Bak-CTSscr and BakΔCTS. cBid increased Bak recruitment for Bak and Bak-CTS mutants.

(B) ^{V}BimL and ^{V}tBid but not ^{V}Bad, ^{V}Bik, or Venus bind to Bak-CTS with the triple mutation V194K, L195S, and V198D (^{mT2}CTS-KSD$_{BAK}$). FLIM-FRET experiments were done on BMK DKO cell line stably expressing ^{mT2}CTS-KSD$_{BAK}$ and transfected with the indicated ^{V}BH3-only proteins. From the s-ratio analysis for the binding data, only ^{V}tBid and ^{V}BimL achieved an s-ratio value above 2, and thus their binding data were fitted to the Hill-equation (h=1), yielding the apparent K_D values of 32 and 23 µM, respectively. ^{V}Bad, ^{V}Bik, and Venus have an s-ratio lower than 2 and thus were fitted with a linear regression model indicating non-binding or collision (Appendix Table S3). Data represent 3 technical replicates.

(C) Scrambling the Bak-CTS (^{mT2}CTSscr$_{BAK}$) abolished binding to ^{V}tBid and ^{V}BimL in BMK DKO. From the s-ratio analysis, all ^{V}BH3-only proteins and Venus yield an s-ratio lower than 2, and thus, their binding data were fitted to linear models (Appendix Table S3). Data represent 3 technical replicates.

(D) Colocalization data of ^{mT2}CTS-KSD$_{BAK}$ and ^{mT2}CTSscr$_{BAK}$ (Blue channel) to MitoTracker Red (Red channel) revealed that both constructs, when expressed in BMK DKO, did not colocalize well to the mitochondrial membrane. ^{mT2}CTS-KSD$_{BAK}$ and ^{mT2}CTSscr$_{BAK}$ have mean Pearson's r values of 0.24 and 0.15, respectively, which are significantly lower than 0.8 – the mean Pearson's r value of ^{mT2}CTS$_{BAK}$ to MitoTracker Red (Beigl *et al*, 2024). The median and interquartile range are shown for n>2000 cells.

(E) Homodimerization of Bak-CTS in BMK DKO was detected by FLIM-FRET. Cells stably expressing ^{mT2}CTS$_{BAK}$ were transfected with either ^{mCitrine}CTS$_{BAK}$ or the mitochondria-binding control ^{mCitrine}CTS$_{TOM5}$. Bak-CTS bound to itself with an apparent K_D value of 11.1 µM (Appendix Table S3), whereas ^{mCitrine}CTS$_{TOM5}$ did not bind mT2-CTS$_{BAK}$ as its binding data has a s-ratio of 1.4 and thus was fit to a linear equation that represents collision. Data represent 3 technical replicates

(F) Colocalization data of ^{V}BH3-only proteins (Green channel) to ^{mT2}CTS-KSD$_{BAK}$ (Blue channel) shows that ^{V}tBid, ^{V}BimL, ^{V}Bad, and ^{V}Bik shared similar colocalization to ^{mT2}CTS-KSD$_{BAK}$ in BMK DKO cells. Confocal fluorescence images of the green and blue channels were used for colocalization analysis to obtain Pearson's r value for each cell. The mean Pearson's r values for ^{V}tBid, ^{V}BimL, ^{V}Bad, and ^{V}Bik were 0.21, 0.13, 0.12, and 0.18, respectively. The mean Pearson's r values for ^{V}BimL-ΔCTS and Venus were approximately zero, confirming their lack of binding to the mitochondrial membranes. The positive control MitoTracker Green, which stains the mitochondrial network, had a mean

Pearson's r of 0.45 for colocalization to ^{mT2}CTS-KSD$_{BAK}$. The median and interquartile range are shown for a minimum of 2000 cells per transfectant.

(G) Colocalization data of ^{V}BH3-only proteins (Green channel) to ^{mT2}CTSscr$_{BAK}$ (Blue channel) show that the ^{V}BH3-only proteins did not colocalize well to ^{mT2}CTSscr$_{BAK}$ in BMK DKO. Similarly, the negative control ^{V}BimL-ΔCTS and Venus had poor colocalization with ^{mT2}CTSscr$_{BAK}$. The mean Pearson's r values for ^{V}tBid, ^{V}BimL, ^{V}Bad, ^{V}Bik, ^{V}BimΔCTS, and Venus are 0.28, 0.15, 0.17, 0.27, 0.13, and 0.15, respectively. The median and interquartile range are shown for a minimum of 2000 cells per transfectant.

Figure 2.3. Figure Supplementary 2. The binding of Bak-CTS to ^{V}BimL and ^{V}tBid in cells is not due to collision on the MOM.

(A) Colocalization data of ^{V}BH3-only proteins (Green channel) to MitoTracker Red (Red channel) show that ^{V}tBid, ^{V}BimL, ^{V}Bad, and ^{V}Bik shared similar subcellular localization to the mitochondrial membranes with mean Pearson's r values around 0.1 in BMK DKO cells stably expressing ^{mT2}CTS$_{BAK}$. Using both parametric unpaired t-test for the mean and non-parametric Mann-Whitney test for the median, we confirm that there was no statistical significance in the differences between the mean or median Pearson's r values of ^{V}tBid, ^{V}BimL, ^{V}Bad, and ^{V}Bik colocalizing to MitoTracker Red. The comparison was made to ^{V}tBid, with $p>0.05$. On the other hand, ^{V}BimL-ΔCTS and Venus did not colocalize to MitoTracker Red with the mean Pearson's r values of 0.02 and 0, respectively, and were significantly different from the colocalization data for ^{V}tBid ($p<0.0001$). The median and interquartile range are shown for 1500 cells.

(B) Equally poor colocalization of ^{V}BH3-only proteins (Green channel) to ^{mT2}CTS$_{BAK}$ (Blue channel) as shown by their median Pearson's r values of ~0.1 in BMK DKO cells stably expressing ^{mT2}CTS$_{BAK}$. The mean Pearson's r values of ^{V}tBid, ^{V}BimL, ^{V}Bad, and ^{V}Bik were 0.14, 0.17, 0.1, and 0.14, respectively. ^{V}BimL-ΔCTS and Venus have the lowest mean Pearson's r values of ~0.03. The median and interquartile range are shown for 1500 cells.

(C) Selected confocal images display the subcellular localization of ^{V}BimL, ^{V}tBid, and ^{V}Bad in comparison to ^{mT2}CTS$_{BAK}$ in BMK DKO cells used for colocalization microscopy in Panel (A) and (B). BMK DKO stably expressing ^{mT2}CTS$_{BAK}$ were transfected to transiently express the indicated VBH3-only protein constructs for this experiment. The scale bar equates to 50 μm.

(D) An independent replicate showed that ^{V}BimL and ^{V}tBid bind to ^{mT2}CTS$_{BAK}$ in BMK DKO, as measured by FLIM-FRET, with apparent K_D values of 9 μM and 12 μM, respectively, and s-ratio >2 for both. The binding data were fitted to a Hill equation with h=1. ^{V}Bad, ^{V}Bik, ^{V}Noxa, and Venus did not interact with $^{mT2}CTS_{BAK}$, as demonstrated by their binding data fitting a linear equation (s-ratio <2). Data represent 3 technical replicates.

(E) An independent replicate of the FLIM-FRET experiment in BMK DKO cells expressing $^{mT2}CTS_{BAX}$, which demonstrates that ^{V}BimL, ^{V}Bad, ^{V}Noxa, and ^{V}Bik did not bind $^{mT2}CTS_{BAX}$ as their binding data were best fitted to the linear regression model (s-ratio<2). In contrast, ^{V}tBid bound $^{mT2}CTS_{BAX}$ with an apparent K_D value of 28 μM. Data represent 3 technical replicates.

Figure 2.4. Figure Supplementary 1. Mutations in the Bid h0 residues do not affect tBid binding to the MOM.

(A) Colocalization of ^{V}tBid (Green channel) to MitoTracker Red (Red channel) was not significantly affected by mutation in the Bid h0 residues. ^{V}tBid, ^{V}tBid I82A, and ^{V}tBid I83A shared similar subcellular localization to the mitochondrial membranes with the mean Pearson's r values of 0.11, 0.12, and 0.15, respectively, in BMK DKO cells stably expressing $^{mT2}CTS_{BAK}$. ^{V}tBid-4E had a higher mean Pearson's r value of 0.25, showing a better localization than ^{V}tBid to the MitoTracker Red, which stains mitochondrial membranes. In contrast, Venus- the negative control, had a mean Pearson's r value of 0.03, correlating to a cytoplasmic subcellular localization (images not shown). Horizontal lines indicating the median and interquartile range are shown for a minimum of 1500 cells.

(B) Colocalization of ^{V}tBid (Green channel) to $^{mT2}CTS_{BAK}$ (Blue channel) was not reduced by mutations in the Bid h0 residues as shown by their median Pearson's r values of >0.1 in BMK DKO cells, stably expressing $^{mT2}CTS_{BAK}$. The mean Pearson's r values of v-tBid, ^{V}tBid-4E, ^{V}tBid I82A, and ^{V}tBid I83A were 0.13, 0.28, 0.17, and 0.21, respectively. Venus had the lowest mean Pearson's r values of ~0.03. The median and interquartile range are shown for a minimum of 1500 cells.

(C) Scrambling Bak-CTS ($^{mT2}CTSscr_{BAK}$) abolished binding to ^{V}tBid as measured by FLIM-FRET microscopy. S-ratio analysis of the binding data in BMK DKO cells stably expressing $^{mT2}CTSscr_{BAK}$ showed that ^{V}tBid, ^{V}tBid-4E, ^{V}tBid-I82A, and ^{V}tBid-I83A have s-ratio values < 2. Therefore, their binding data were fit to the linear regression model, which represents collision. Data represent 3 technical replicates.

(D) G126S mutation in ^{C}BakΔCTS was insufficient to abolish the binding of ^{V}tBid (red) to ^{C}BakΔCTS in HCT116 DKO cells, as measured by FLIM-FRET. The binding of ^{C}BakΔCTS G126S to ^{V}tBid yielded an apparent K_D value of 10.4 μM when fitted to the Hill-equation (h=1). Mutation in the Bid BH3 (^{V}tBid-4E in blue) was sufficient to abrogate the binding of ^{V}tBid to ^{C}BakΔCTS G126S, as indicated by the straight line (in blue) fitted to the binding data for ^{V}tBid-4E. Likewise, ^{V}Bad (green), a negative control, did not bind ^{C}BakΔCTS G126S. Data represent 3 technical replicates.

Figure 2.4. Figure Supplementary 2. G126S Bak does not become activated and kills cells upon binding to tBid.

(A) TMRE intensity of HCT116 DKO cells stably expressing ^{C}Bak G126S was not significantly altered when cells were transfected with ^{V}tBid or ^{V}tBid-4E as compared to non-transfected cells (n≥1000 cells). Only cells positive for both Venus and mCerulean3 24 hours after transfection were selected for analysis in the transfected groups. TMRE fluorescence dye stains metabolically active mitochondria and was used to evaluate the viability of cells co-expressing ^{V}tBid or ^{V}tBid-4E and ^{C}Bak G126S mutant. The mean raw TMRE intensity for ^{V}tBid-4E and non-transfected groups was within 25% of the standard deviation of the ^{V}tBid transfected group. Horizontal bars indicating the median and interquartile ranges are shown.

(B) A647-Annexin V intensity of cells expressing ^{C}Bak G126S does not significantly increase upon transfected with ^{V}tBid or ^{V}tBid-4E as compared to non-transfected control (n≥1000 cells). The mean raw A647 intensity for ^{V}tBid-4E and non-transfected groups are within 25% of the standard deviation of ^{V}tBid transfected group. The median and interquartile ranges are shown.

(C) Selected confocal images display HCT116 DKO cells stably expressing ^{C}Bak G126S, transfected with ^{V}tBid and ^{V}tBid-4E, and stained with TMRE 24 hours post-transfection. The scale bar equates to 100 µm.

Figure 2.4. Figure Supplementary 3. FLIM-FRET replicate shows binding of ^{V}tBid to Bak-CTS

(A) An independent FLIM-FRET replicate confirms the binding of ^{V}tBid and ^{V}tBid-4E to $^{mT2}CTS_{BAK}$ in BMK DKO cells. ^{V}tBid and ^{V}tBid-4E bind to $^{mT2}CTS_{BAK}$with an apparent K_D of 8.7 and 6.7 µM, respectively, as fitted to Hill-equation (h=1). Data represent 3 technical replicates.

(B) An independent FLIM-FRET replicate shows mutations at Bid h0 residue did not affect ^{V}tBid binding to $^{mT2}CTS_{BAK}$ in BMK DKO cells. ^{V}tBid I82A and ^{V}tBid I83A bound to $^{mT2}CTS_{BAK}$ with an apparent K_D of 9.1 and 7.2 μM, respectively, as fitted to Hill-equation (h=1). Data represent 3 technical replicates.

(C) Combined data from 2 independent FLIM-FRET replicates in HCT116 DKO cells (2 technical replicates from each) show that ^{C}Bak G126S bound both ^{V}tBid and ^{V}tBid-4E with K_D of 34 and 33 μM, respectively, as fitted to the Hill-equation (h=1). In contrast, ^{V}Bad did not bind ^{C}Bak G126S as its binding data were best fitted to a linear equation that represents collision. S-ratio values for all binding curves are shown in Appendix Table S3.

Figure 2.5. Figure Supplementary 1. The binding of Bim-CTS to Bak-CTS is not due to the colocalization of BimL and Bak to the MOM.

(A) Scrambling the Bak-CTS ($^{mT2}CTSscr_{BAK}$) eliminated binding to ^{V}BimL (grey) and $^{V}CTS_{BIM}$ (purple). FLIM-FRET experiments were done in BMK DKO cell line, stably expressing $^{mT2}CTSscr_{BAK}$ and transfected with the indicated ^{V}BimL or $^{V}CTS_{BIM}$ construct. From the s-ratio analysis for the binding data, none of the transfectants yielded an s-ratio value above 2 and passed the BMAX threshold of 0.05. Thus, their binding data were all fitted to the linear regression model, indicating collision with the donor $^{mT2}CTSscr_{BAK}$ fusion proteins. Data represent 3 technical replicates.

(B) The triple V194K, L195S, and V198D mutation in Bak-CTS ($^{mT2}CTS\text{-}KSD_{BAK}$) did not affect binding to ^{V}BimL in BMK DKO. ^{V}BimL binds $^{mT2}CTS\text{-}KSD_{BAK}$ with an apparent K_D value of 23 μM. Scrambling the Bim-CTS in full-length BimL abolished this interaction (^{V}BimL-CTSscr in light orange), as indicated by the straight line fitted to its binding data (s-ratio = 1.2). Data represent 3 technical replicates.

(C) The triple V194K, L195S, and V198D mutation in Bak-CTS ($^{mT2}CTS\text{-}KSD_{BAK}$) did not affect binding to $^{V}CTS_{BIM}$ in BMK DKO. $^{V}CTS_{BIM}$ binds $^{mT2}CTS\text{-}KSD_{BAK}$ with an apparent K_D value of 17 μM. Scrambling the Bim-CTS was sufficient to abolish this interaction ($^{V}CTSscr_{BIM}$ in green), as indicated by the straight line fitted to its binding data (s-ratio =1). Data represent 3 technical replicates.

(D) Colocalization data of ^{V}BH3-only proteins (Green channel) to MitoTracker Red (Red channel) show that both ^{V}BimL-CTSscr and $^{V}CTSscr_{BIM}$ (columns 4 and 5) colocalized to the mitochondria equally well as compared to ^{V}BimL and $^{V}CTS_{BIM}$ in BMK DKO cells. Confocal fluorescence images of the green and red channels were used for colocalization analysis to obtain Pearson's r value for each cell. The mean Pearson's r values for ^{V}BimL, ^{V}BimL-CTSscr, ^{V}BimL-4E, $^{V}CTS_{BIM}$, and

$^{V}CTSscr_{BIM}$ were 0.1, 0.09, 0.15, 0.1, and 0.18. On the other hand, the mean Pearson's r for v-BimL-ΔCTS and the negative control Venus were both zero, confirming their lack of colocalization to the mitochondrial membranes. ^{V}Bad and ^{V}BadΔCTS-Bim-CTS colocalize to MitoTracker Red with the mean Pearson's r values of 0.1 and 0.14, respectively, suggesting that the Bim-CTS can replace the Bad-CTS to localize Bad to the mitochondrial membranes. Horizontal bars indicating the median and interquartile range are shown for a minimum of 1500 cells. The colocalization data for ^{V}BimL, Venus, ^{V}Bad, and ^{V}BimL-ΔCTS are the same as in Figure 2.3 – Figure Supplement 2A, as both graphs were generated from data collected in the same experiment.

(E) $^{V}CTS_{BIM}$ bound specifically to $^{mT2}CTS_{BAK}$ and not to the mitochondrial binding region of ActA ($^{C}CTS_{ActA}$) in BMK DKO cells, as measured by FLIM-FRET microscopy. $^{V}CTS_{BIM}$ binds $^{mT2}CTS_{BAK}$ with an apparent K_D value of 9.3 μM and a s-ratio of 5. On the other hand, $^{V}CTS_{BIM}$ and $^{C}CTS_{ActA}$ had a collisional interaction as the s-ratio value for their binding data was 1.5, and thus, was fitted to the linear regression model. Data represent 3 technical replicates.

(F) Cell death assay in BMK cells demonstrates that mutation in the BH3 of BimL (^{V}BimL-4E) but not in the Bim-CTS (^{V}BimL-CTSscr) eliminated the pro-apoptotic sensitizer function of BimL. As BMK cells are primed, this killing assay does not differentiate BimL-induced cell death due to direct activation of Bax/Bak from cell death due to inhibition of anti-apoptotic proteins. ^{V}BimL-CTSscr induced similar A647-Annexin V positivity in the transfected cells as ^{V}BimL (60-70%). ^{V}Bad only caused about 25% cell death in the transfected population. Mutating the Bad BH3 with two alanine at position h2 (L114) and h4 (F121) (^{V}Bad-L114A F121A) slightly reduced the %cell death to 16%. Surprisingly, replacing the Bad-CTS with that of Bim (^{V}BadΔCTS-Bim-CTS) increased Bad-mediated cell death to 40%. BMK DKO cells transfected with the same ^{V}BH3-only constructs yielded insignificant %cell death, confirming the observed ^{V}BH3-only protein-induced cell death was Bax/Bak dependent. Data from 3 technical replicates are shown.

Figure 2.5. Figure Supplementary 2. Cancer-associated mutations in the Bim-CTS reduce the binding of Bim to Bak-CTS, thereby impairing Bim-mediated Bak activation.

(A) Schematic shows cancer-associated missense mutation in the CTS of BimL. The mutations were found through cbioportal.com for BCL2L11 (gene encoding Bim) across all human cancers. The equivalent residues in murine BimL were mutated accordingly for ^{V}BimL mammalian expression constructs.

(B) Binding of ^{V}BimL to ^{mT2}CTS$_{BAK}$ in BMK DKO was detected by FLIM-FRET, with an apparent K_D value of 7 µM, as fitted to the Hill-equation (h=1). I125V (Blue) and M123I (dark red) mutations in BimL did not affect the binding of ^{V}BimL to ^{mT2}CTS$_{BAK}$, whereas R130L (green) and I132N (black) abolished this binding. The negative control, ^{V}BimL-CTSscr (light orange), did not bind to ^{mT2}CTS$_{BAK,}$ as indicated by the binding data fitting a linear equation. Data represent 2 technical replicates.

(C) Colocalization data of ^{V}BimL or ^{V}BimL cancer-associated mutants (Green channel) to MitoTracker Red (Red channel) in BMK DKO cells show that the mitochondrial localization of ^{V}BimL was not affected by M123I and R134L mutations. ^{V}BimL, ^{V}BimL-M123I, and ^{V}BimL-R134L all shared a mean Pearson's r value of approximately 0.1 and were not significantly different from one another as determined by unpaired t-test ($p>0.05$). On the other hand, ^{V}BimΔCTS, ^{V}BimL-I125V, ^{V}BimL-R130L, and ^{V}BimL-I132N colocalized poorly to MitroTracker Red, compared to ^{V}BimL, with the mean Pearson's r values of 0.02, 0.07, 0.04, and 0.04, respectively. These mean Pearson's r values were significantly different from that of ^{V}BimL, as determined by unpair t-test ($p<0.0001$). The colocalization data for ^{V}BimL and ^{V}BimL-ΔCTS are the same as in Figure 2.3 – Figure Supplement 2A, as both graphs were generated from the same experiment. Horizontal bars indicating the median and interquartile range are shown for a minimum of 1500 cells.

(D) Colocalization data of ^{V}BimL or ^{V}BimL cancer-associated mutants (Green channel) to ^{mT2}CTS$_{BAK}$ (Blue channel) in BMK DKO cells show colocalization of ^{V}BimL and to ^{mT2}CTS$_{BAK}$ was minimally affected by M123, I125V, and R134L mutation. ^{V}BimL, ^{V}BimL-M123I, ^{V}BimL-I125V, and ^{V}BimL-R134L had the mean Pearson's r values of 0.17, 0.15, 0.13, and 0.13, respectively. On the other hand, ^{V}BimL-ΔCTS, ^{V}BimL-R130L, and ^{V}BimL-I132N colocalized significantly less to ^{mT2}CTS$_{BAK}$, compared to ^{V}BimL, with the mean Pearson's r values of 0.03, 0.04, and 0.07, respectively. The colocalization data for ^{V}BimL and ^{V}BimL-ΔCTS are the same as in Figure 2.3 – Figure Supplement 2B, as both graphs were generated from data collected in the same experiment. Horizontal bars indicating the median and interquartile range are shown for a minimum of 1500 cells.

Figure 2.5. Figure Supplementary 3. FLIM-FRET replicate shows the binding of ^{V}BimL and ^{V}CTS$_{BIM}$ to the Bak-CTS in cells.

(A) An independent FLIM-FRET replicate shows ^{V}BimL and ^{V}CTS$_{BIM}$ directly bound ^{mT2}CTS$_{BAK}$ in BMK DKO cells. Mutating the BH3 of BimL (^{V}BimL-4E in red) did not affect the binding of ^{V}BimL to ^{mT2}CTS$_{BAK}$, whereas scrambling the Bim-CTS

(^{V}BimL-CTSscr in light orange) significantly reduced the BMAX values for $\Delta\boldsymbol{\omega}$ to below the threshold of 0.05 for Hill-equation fitting. The apparent K_D values for the binding curves are displayed on the graph. The s-ratio values for all curves are in Appendix Table S3. Data represent 3 technical replicates.

(B) An independent FLIM-FRET replicate demonstrates that the Bim-CTS when replaced the Bad-CTS in full-length Bad (^{V}BadΔCTS-BimCTS in light purple), converted ^{V}Bad into a $^{mT2}CTS_{BAK}$ binder with an apparent K_D value of 16.5 μM, as fitted to the Hill-equation (h=1). ^{V}Bad did not bind to $^{mT2}CTS_{BAK}$, as indicated by the linear binding data (s-ratio = 1.3). Truncating the Bim-CTS (^{V}BimL-ΔCTS in brown) abolished the binding of ^{V}BimL to $^{mT2}CTS_{BAK}$ (s-ratio = 1.2). Data represent 3 technical replicates.

(C) An independent FLIM-FRET replicate shows that the cancer-associated mutation R134L in the Bim-CTS (^{V}BimL R134L in dark yellow) abolished the binding of ^{V}BimL to $^{mT2}CTS_{BAK}$, as demonstrated by a linear fit to the binding data as the calculated BMAX value for $\Delta\boldsymbol{\omega}$ were below the threshold of 0.05 for Hill-equation fitting. Data represent 3 technical replicates.

Figure 2.6. Figure Supplementary 1. Restoring membrane-binding to CTS-truncated BimL is insufficient to activate Bak.

(A) Binding of full-length Bak with the G126S mutation in the BH3-binding pocket (^{C}Bak G126S) to the $^{V}CTS_{BIM}$ was detected by FLIM-FRET in BMK DKO cells. $^{V}CTS_{BIM}$ bound ^{C}Bak G126S with an apparent K_D value of 28 μM (Dark purple), as fitted with the Hill-equation (h=1). Scrambling the CTS of Bim ($^{V}CTSscr_{BIM}$) abolished the binding to ^{C}Bak G126S (light green) as its binding data was best fitted to a linear equation (s-ratio=0.7). Data represent 3 technical replicates.

(B) Truncating the CTS of full-length Bak G126S (^{C}BakΔCTS G126S) eliminated binding to $^{V}CTS_{BIM}$ in BMK DKO cells. FLIM-FRET binding data shows that both $^{V}CTS_{BIM}$ and $^{V}CTSscr_{BIM}$ had collisional interactions with ^{C}BakΔCTS G126S (s-ratios < 1) and thus were fitted to the linear regression model. Data represent 3 technical replicates.

(C) Mutating BH3 of Bim (^{V}BimL-4E in red) did not affect the binding of ^{V}BimL to ^{C}Bak G126S in BMK DKO cells, as measured by FLIM-FRET microscopy. ^{V}BimL and ^{V}BimL-4E bound ^{C}Bak G126S with the apparent K_D values of 34 and 36 μM, respectively. Scrambling (^{V}BimL-CTSscr in light orange) or mutating Bim-CTS with R134L missense mutation (^{V}BimL R134L in dark yellow) eliminated the binding of ^{V}BimL to ^{C}Bak G126S, as the binding data were best fitted to a linear equation (s-ratio < 1.5). Data represent 3 technical replicates.

(D) Restoring liposome-binding to BimL-ΔCTS by replacing Bim-CTS with the CTS of Monoamine Oxidase (MAO) in recombinant BimL-ΔCTS-MAO did not restore Bak activation. Terbium release liposome permeabilization assay with 100 nM recombinant full-length Bak demonstrates that BimL-induced Bak activation caused an increase in %Terbium release as the concentration of BimL went from 0.1 to 10 nM. Above 10 nM of BimL, % terbium release reached a plateau as BimL-mediated Bak activation reached its maximum constraints set by the amount of Bak present in the experiment. Unlike BimL, BimL-ΔCTS-MAO (in black) did not activate Bak despite being targeted to liposomes better than BimL (Chi *et al*, 2020). This is apparent as an increasing amount of BimL-ΔCTS-MAO, incubated with the same amount of Bak, failed to produce any increase in % terbium release. Data from 4 independent replicates are shown.

List of Tables

Appendix Table 2.S3. Calculated S-ratio, BMAX, and apparent K_D values for all FLIM-FRET experiments in this study are displayed. K_D values are obtained from the Hill-fitted original binding data for each binding curve in both main and supplementary figures. For each binding curve, the most complete independent replicate is chosen for s-ratio analysis. If the s-ratio is smaller than 2, the binding data is fitted to the linear regression model, and the energy transfer or FRET is interpreted as collisions between the acceptor and donor fluorophores. Suppose the binding data has an s-ratio larger than 2; in that case, the binding data for 3 technical replicates are fitted to the Hill equation to obtain a K_D value in μM of Free Acceptor (x-axis) and a BMAX value of the ΔGↃ (y-axis). If the BMAX value is below 0.05, the binding data is deemed insufficient, and the binding data is re-fitted to a linear regression model. Interpretation of the binding data is on the right. N/A = not applicable; binding data fails to qualify for the next step in the analysis.

Appendix Table 2.S4: All cell lines were tested for Mycoplasma using MycoAlert® Mycoplasma Detection Kit from Lonza. Ratio A/B is an indicator of ATP level which is measured by the luminescence intensity before (read A) and after (read B) adding the substrate. Samples with ratio A/B <1 are negative for Mycoplasma. N/A: not applicable.

Appendix Figure 2.S5. Western blot of cell lysates from cell lines used for FLIM-FRET. Expression of the donor-fusion proteins was verified by immunoblotting on the left panel. GAPDH loading control is shown on the right panel.

List of all Abbreviations

Bad	Bcl2-associated agonist of cell death
Bak	Bcl-2 antagonist/killer
Bax	Bcl-2 associated X protein
Bcl-2	B-cell CLL/lymphoma 2
Bcl-XL	B-cell lymphoma extra long
BH	Bcl-2 homology
Bid	BH3 interacting domain death agonist
Bim	Bcl-2-like protein 11
Bok	Bcl-2-related ovarian killer protein
^{C}	mCerulean 3
cBid	cleaved Bid
CTS	carboxyl-terminal sequence
DKO	double knockout
DPA	dipicolinic acid
EDTA	ethylenediaminetetraacetic acid
FLIM	Fluorescence Lifetime Imaging
FRET	Förster resonance energy transfer
K_D	dissociation constant
kDa	kiloDalton
Mcl-1	induced myeloid leukemia cell differentiation protein Mcl-1
MOM	mitochondrial outer membrane
MOMP	mitochondrial outer membrane permeabilization
Ni2+-NTA	nickel-nitrilotriacetic acid
OMM	outer mitochondria membrane
Puma	p53 upregulated modulator of apoptosis
Tb	terbium III
tBid	truncated Bid
TNF	tumour necrosis factor

VDAC2	voltage-dependent anion channel isoform 2
v	venus
WT	wild-type

1 Introduction

1.1 Initiating Programmed Cell Death

Cell death is required to develop and function all multicellular organisms by eliminating damaged cells, thereby maintaining physiological homeostasis. In adult humans, approximately 50 to 70 billion cells are eliminated daily through apoptosis, a process balanced in the body by concurrent cell division. Dysregulation of cell death contributes to the pathogenesis of many diseases, including cancer, neurodegeneration, and autoimmune diseases. The initiation of programmed cell death involves the activation of BCL-2 family executioner proteins, namely Bak and Bax, by the activators Bid, Bim or Puma. Recent evidence suggests that Bak and Bax are differentially activated; however, we do not understand how (Cartron *et al*, 2003; Sarosiek *et al*, 2013). Understanding such mechanistic differences opens avenues for potential pharmaceutical interventions targeting Bak/Bax-mediated apoptosis due to their differential expression profiles across various diseased and healthy tissues.

Cells activate an intracellular cell death program called apoptosis, either physiological stimuli (e.g. receptors such as the p55 tumour necrosis factor receptor (TNRF1)) (Tartaglia *et al*, 1993) or pathophysiological stimuli (e.g. cellular stress, radiation or growth factor deprivation) (Alberts, 2022; Kerr *et al*, 1972). Distinctive alterations in apoptotic cell morphology include mitochondrial swelling, chromatin condensation, DNA fragmentation, and cell shrinkage without causing lysis or damage to neighboring cells (Kerr *et al.*, 1972; Wyllie *et al*, 1980; Wyllie *et al*, 1984). Apoptotic cells retain their cell membrane integrity, enclosing cellular contents and fragments, facilitating swift and precise removal and digestion by local phagocytes (Kurosaka *et al*, 2003; Morris *et al*, 1984; Sandow *et al*, 1979; Savill & Fadok, 2000). Phagocytic cells such as macrophages in humans, recognize various apoptotic signals on the surface of the cell. This process prevents the initiation of an inflammatory response in adjacent tissues by preventing their exposure to the harmful content of the dying cell.

1.2 The role of Bcl-2 family of proteins in intrinsic apoptosis

Intrinsic programmed cell death is largely regulated by the B cell lymphoma-2 (BCL-2) family of proteins, whose namesake protein was first characterized in a patient with acute B-cell lymphocytic leukemia (Tsujimoto *et al*, 1985). Since then furher discovery of other family members has been expanded and characterized by their ability to activate or inhibit apoptosis, thereby the complex balance of intrinsic cell death or survival is orchestrated by this single protein family (Figure 1.1).

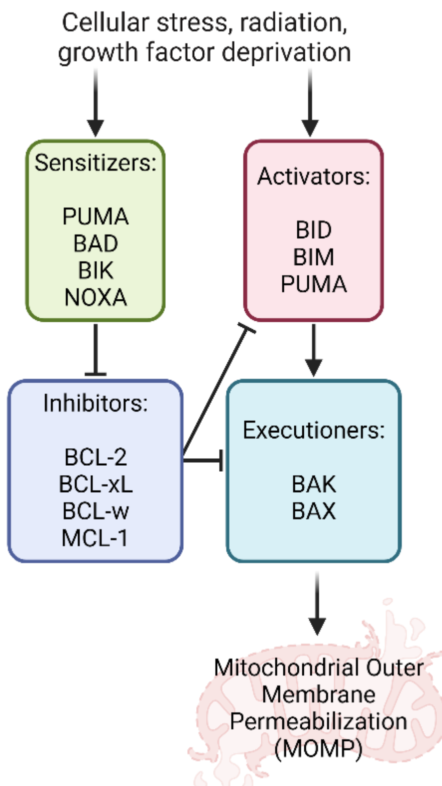

Figure 1.1. Schematic characterization of the Bcl-2 family of proteins. Activators Bid, Bim, Puma activate the executioner proteins Bak/Bax. Bak/Bax can be inhibited by binding to the anti-apoptotic proteins Bcl-2, Bcl-XL, Bcl-W, and Mcl-1. Sensitizer proteins Bad, Bik, and Noxa, bind anti-apoptotic proteins to disrupt the inhibited heterodimeric complexes, further promoting MOMP.

All members of the family share the highly conserved hydrophobic BCL-2 homology (BH) domain 3 (BH3) motif, and most share the conserved carboxyl terminal sequence (CTS) membrane domain whose main function is characterized by localization of Bcl-2 family proteins to intracellular membranes (Figure 1.2) (Nechushtan *et al,* 1999). Beyond localization, recent evidence suggests that dimerization and oligomerization requires the interaction of transmembrane domains, leading to mitochondrial pore formation and permeabilization of the mitochondrial outer membrane (MOMP) (Chi X *et al*, 2020; Lucendo *et al*, 2020; Pemberton *et al*, 2023).

Figure 1.2. Schematic representation of the highly conserved hydrophobic BCL-2 homology (BH) domains motifs and the conserved carboxyl terminal sequence (CTS). BH3 regions and binding sites on Bcl-2 family proteins govern MOMP by regulating the activation and subsequent oligomerization of pore-forming executioner proteins Bak and Bax.

BH3-only activator proteins Bid, Bim, Puma activate the executioner proteins Bak/Bax. To inhibit Bax/Bak activation, the multi-domain anti-apoptotic proteins, including Bcl-2, Bcl-XL, Bcl-W and Mcl-1, bind direct activators such as Bid and Bim and to activated Bax/Bak, forming mutually sequestered inactive heterodimeric complexes (Hockings *et al*, 2018; Ku *et al*, 2011; Lee *et al*, 2016). Sensitizers, including Bad and Bik, bind anti-apoptotic proteins and compete with formation of or disrupt the the inhibited heterodimeric complexes. As the Bax/Bak bound by anti-apoptotic proteins is in the active state, releasing these proteins rapidly results in MOMP. Additionally, released direct activator BH3-only proteins can subsequently activate Bax/Bak to induce MOMP (Day *et al*, 2008; Huang *et al*, 2019; Osterlund *et al*, 2022).

Bak inactive state in healthy cells involves its binding to the voltage-dependent anion channel isoform 2 (VDAC2) (Cheng et al., 2003), which localizes Bak constitutively to the mitochondrial outer membrane (MOM) (Naghdi *et al*, 2015). While the precise mechanism of the VDAC2-Bak interaction remains unclear, the Bak-CTS is essential for VDAC2 to sequester Bak into an inhibitory complex (Lazarou et al., 2010). Further, mutating the BAK BH3 domain has been shown to disrupt the VDAC2 interaction with Bak (Cheng *et al*, 2003). Alternatively, Bak is inhibited by binding to the anti-apoptotic proteins Bcl-XL and Mcl-1 (Hockings et al., 2018). This interaction is mediated by the Bak BH3 motif binding to the BH3-binding pocket of Bcl-XL and Mcl-1, establishing a dependence on these anti-apoptotic proteins for cell survival.

Oligomerization of the executioner protein Bax is initiated by direct binding of activators Bid and/or Bim (Kim *et al*, 2009; Korsmeyer *et al*, 2000; Leshchiner *et al*, 2013). The mechanisms leading to efficient Bak activation remain less clear. Activation of Bak triggers dissociation of the core domain from the latch domain (helix α6- α8) (Brouwer *et al*, 2014), exposing the Bak BH3, which subsequently binds the BH3-binding pocket of another Bak, to form Bak BH3-in-groove dimers. As the Bak dimers become oligomers, the Bak-CTS was shown to provide an additional dimer interface in the pore-forming high-order Bak complexes (Iyer *et al*, 2015). However, the Bak-CTS has been considered to be primarily a hydrophobic transmembrane sequence that binds Bak to the MOM (Martínez-Senac Mdel *et al*, 2002) therefore, the precise role of Bak-CTS has not been well-characterized in mediating protein-protein interactions or functioning in Bak activation.

In humans, caspases are broadly classified in three groups: inflammatory (caspase 1, 4 and 5, 12L), initiator (caspase 2, 8, 9 and 10) and executioner (caspase 3, 6 and 7) (McIlwain *et al*, 2013). Inactive monomers of initiator caspases, specifically caspase-8 and caspase-9, dimerize to form larger activation complexes. Activation of initiator caspases that cleave and activate the executioner caspases triggers apoptosis (McIlwain *et al.*, 2013). The main role of the initiator caspases is to activate the effector caspases: caspase-3, caspase-6, and caspase-7. Each dimer of an initiator caspase can cleave one or more inactive dimers of effector caspases, triggering an amplified caspase cascade. This cascade results in widespread protein cleavage, leading to apoptosis (McIlwain *et al.*, 2013). The apoptotic cells are then quickly engulfed and digested by nearby phagocytes (Figure 1.3).

Caspase-8 cleaves full-length cytosolic inactive Bid (Li *et al*, 1998) to generate cleaved cBid. cBid consists of two fragments p15 and p7 that remain attached together due to hydrophobic interactions. tBid includes only the p15 fragment that subsequently interacts with the mitochondria outer membrane and is separated from the p7 fragment (Shivakumar *et al*, 2014). Bid contains the BH3 (alpha helix) and BH4 (alpha helix) domains, while the cleaved tBid shares only the BH3 homology with other members of the Bcl-2 family (Wang *et al*, 1996). Upon cleavage, Bid is converted into tBid, which activates Bak and Bax.

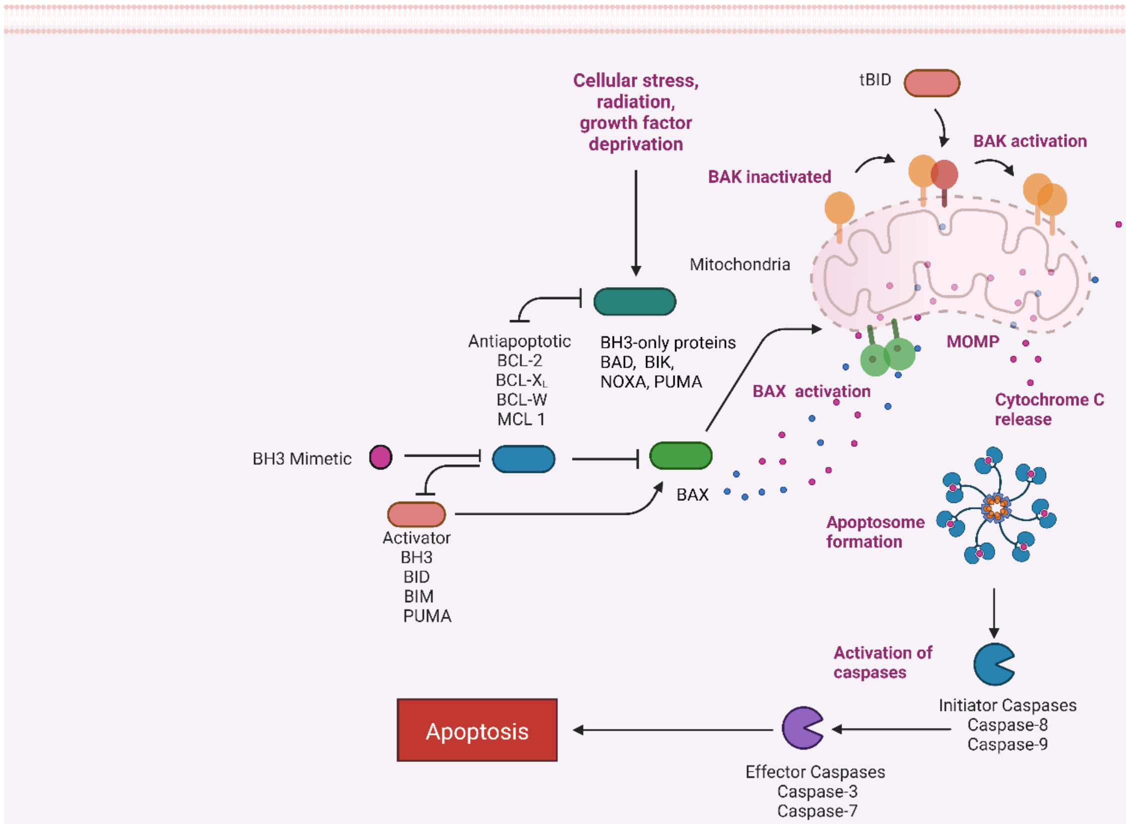

Figure 1.3. Schematic of the intrinsic apoptosis pathway. An intracellular cell death program is activated after cellular stress, radiation, or growth factor deprivation. BH3-only activator proteins Bid, Bim, and Puma govern mitochondrial outer membrane permeabilization by regulating the activation and subsequent homoligomerization of pore-forming executioner proteins Bax, Bak. The activation of Bak leads to the exposure of its BH3 domain, allowing it to bind to nearby Bak proteins. Inactive monomers of initiator caspases, specifically caspase-8 and caspase-9, dimerize to form larger activation complexes. The main role of these initiator caspases is to activate the effector caspases: caspase-3, caspase-6, and caspase-7. Each dimer of an initiator caspase can cleave one or more inactive dimers of effector caspases, triggering a caspase cascade.

Mouse models deficient in Bcl-2 exhibit abnormalities after birth, including smaller size, immunodeficiency, polycystic kidney disease, hair hypopigmentation and shortened lifespan (Kamada *et al*, 1995; Nakayama *et al*, 1993; Veis *et al*, 1993). Mice deficient in Bcl-XL die at embryonic day 13, exhibiting significant apoptosis in immature neurons in the brain, spinal cord, and dorsal root ganglia (Motoyama *et al*, 1995). Proapoptotic Bax knockout mice are viable, however, males display infertility due to developmental dysfunction of the seminiferous tubules (Knudson *et al*, 1995). Further, Bax-deficient mice display a decrease in neuronal death occurring naturally during development or due to trophic factor deprivation (Deckwerth *et al*, 1996). Bak is widely expressed across most tissue types (Kiefer *et al*, 1995; Krajewski *et al*, 1996). Bak knockout mice display limited developmental abnormalities and retain fertility (Lindsten *et al*, 2000), pointing to the overlapping function of Bax and Bak in maintaining apoptosis and homeostasis in cells. However, double knockout bax−/−bak−/− mice exhibit profound developmental dysfunction, including excess cells within the central nervous system, lymphocyte accumulation, female fertility dysfunction, deafness and circling behaviour (Lindsten *et al.*, 2000). Only 10% of the animals survive to adulthood (Lindsten *et al.*, 2000).

1.3 Current pharmacological interventions using BH3 memetics

Small molecules called BH3 mimetics have been developed to mimic BH3-proteins by binding to anti- apoptotic proteins to displace Bid/Bim activators, allowing Bid/Bim to bind to Bak/Bax and trigger MOMP. To date, more than 20 compounds have been identified while 6 BH3 mimetics are currently in clinical development. Venitoclax (formerly known as ABT-199 or GDC0199) is a BH3 memetic targeting Bcl-2 that successfully induces apoptosis while preserving platelets, received approval from the FDA in 2016 for the treatment of patients with previously treated chronic lymphocytic leukemia (CLL) (Souers *et al*, 2013). BH3 mimetics do not induce cell death in healthy cells as both priming and the presence of BH3 mimetics is required for apoptosis to occur in targeted cells (Jakubowska *et al*, 2019). Unlike healthy cells, cancer cells select for mechanisms that resist apoptosis by upregulating one or more antiapoptotic proteins and become dependent on them (Deng *et al*, 2007). The dependence on antiapoptotic proteins “primes cells for cell death” leaving them vulnerable to toxic insults (Certo *et al*, 2006; Del Gaizo Moore & Letai, 2013). Introducing BH3 mimetics targets the antiapoptotic proteins, which primarily affect cancer cells. For instance, in the case of BCL-2, when bound to an activator, adding a BH3 mimetic displaces the activator from BCL-2, freeing the activator to bind to Bax and Bak, leading to their activation triggering MOMP and subsequent cell death.

1.4 Thesis Synopsis

This thesis aims to fill a gap in understanding the mechanisms of executioner protein Bak activation by BH3-only activators. Chapter 2 demonstrates that the activator protein Bid is more efficient than the activator protein Bim at binding and activating Bak. The h0 region of the Bid BH3 sequence confers high-affinity binding of activator Bim. The thesis demonstrates further the surprising result of recovery of binding of BimL to truncated Bak (without CTS) by adding Bid h0 sequence in the Bim BH3. However, when purified, recombinant BimL with the Bid h0 does not significantly enhance Bak activation. The thesis further demonstrates that the specific sequence of the Bak CTS is required for efficient activation of Bak by cBid and that the Bak CTS binds directly to activator proteins tBid and Bim. The further surprising and complex aspects of the activation of Bak demonstrate that specifically, for Bim, strong Bak activation also requires interaction with Bim's own CTS.

Overall this thesis demonstrates that the carboxyl terminal sequence of Bak is required for activation by BH3-only proteins.

1.5 References

Alberts B (2022) Molecular biology of the cell. W. W. Norton & Company, New York

Beigl TB, Paul A, Fellmeth TP, Nguyen D, Barber L, Weller S, Schäfer B, Gillissen BF, Aulitzky WE, Kopp HG et al (2024) BCL-2 and BOK regulate apoptosis by interaction of their C-terminal transmembrane domains. EMBO Rep 25: 3896-3924

Brouwer JM, Westphal D, Dewson G, Robin AY, Uren RT, Bartolo R, Thompson GV, Colman PM, Kluck RM, Czabotar PE (2014) Bak core and latch domains separate during activation, and freed core domains form symmetric homodimers. Mol Cell 55: 938-946

Cartron PF, Juin P, Oliver L, Martin S, Meflah K, Vallette FM (2003) Nonredundant role of Bax and Bak in Bid-mediated apoptosis. Mol Cell Biol 23: 4701-4712

Certo M, Del Gaizo Moore V, Nishino M, Wei G, Korsmeyer S, Armstrong SA, Letai A (2006) Mitochondria primed by death signals determine cellular addiction to antiapoptotic BCL-2 family members. Cancer Cell 9: 351-365

Cheng EH, Sheiko TV, Fisher JK, Craigen WJ, Korsmeyer SJ (2003) VDAC2 inhibits BAK activation and mitochondrial apoptosis. Science 301: 513-517

Chi X, Nguyen D, Pemberton JM, Osterlund EJ, Liu Q, Brahmbhatt H, Zhang Z, Lin J, Leber B, Andrews DW (2020) The carboxyl-terminal sequence of bim enables bax activation and killing of unprimed cells. Elife 9

Day CL, Smits C, Fan FC, Lee EF, Fairlie WD, Hinds MG (2008) Structure of the BH3 domains from the p53-inducible BH3-only proteins Noxa and Puma in complex with Mcl-1. J Mol Biol 380: 958-971

Deckwerth TL, Elliott JL, Knudson CM, Johnson EM, Jr., Snider WD, Korsmeyer SJ (1996) BAX is required for neuronal death after trophic factor deprivation and during development. Neuron 17: 401-411

Del Gaizo Moore V, Letai A (2013) BH3 profiling--measuring integrated function of the mitochondrial apoptotic pathway to predict cell fate decisions. Cancer Lett 332: 202-205

Deng J, Carlson N, Takeyama K, Dal Cin P, Shipp M, Letai A (2007) BH3 profiling identifies three distinct classes of apoptotic blocks to predict response to ABT-737 and conventional chemotherapeutic agents. Cancer Cell 12: 171-185

Hockings C, Alsop AE, Fennell SC, Lee EF, Fairlie WD, Dewson G, Kluck RM (2018) Mcl-1 and Bcl-x(L) sequestration of Bak confers differential resistance to BH3-only proteins. Cell Death Differ 25: 721-734

Huang K, O'Neill KL, Li J, Zhou W, Han N, Pang X, Wu W, Struble L, Borgstahl G, Liu Z et al (2019) BH3-only proteins target BCL-xL/MCL-1, not BAX/BAK, to initiate apoptosis. Cell Res 29: 942-952

Iyer S, Bell F, Westphal D, Anwari K, Gulbis J, Smith BJ, Dewson G, Kluck RM (2015) Bak apoptotic pores involve a flexible C-terminal region and juxtaposition of the C-terminal transmembrane domains. Cell Death Differ 22: 1665-1675

Jakubowska MA, Kerkhofs M, Martines C, Efremov DG, Gerasimenko JV, Gerasimenko OV, Petersen OH, Bultynck G, Vervliet T, Ferdek PE (2019) ABT-199 (Venetoclax), a BH3-mimetic Bcl-2 inhibitor, does not cause Ca(2+) -signalling dysregulation or toxicity in pancreatic acinar cells. Br J Pharmacol 176: 4402-4415

Kamada S, Shimono A, Shinto Y, Tsujimura T, Takahashi T, Noda T, Kitamura Y, Kondoh H, Tsujimoto Y (1995) bcl-2 deficiency in mice leads to pleiotropic abnormalities:

accelerated lymphoid cell death in thymus and spleen, polycystic kidney, hair hypopigmentation, and distorted small intestine. Cancer Res 55: 354-359

Kerr JF, Wyllie AH, Currie AR (1972) Apoptosis: a basic biological phenomenon with wide-ranging implications in tissue kinetics. Br J Cancer 26: 239-257

Kiefer MC, Brauer MJ, Powers VC, Wu JJ, Umansky SR, Tomei LD, Barr PJ (1995) Modulation of apoptosis by the widely distributed Bcl-2 homologue Bak. Nature 374: 736-739

Kim H, Tu HC, Ren D, Takeuchi O, Jeffers JR, Zambetti GP, Hsieh JJ, Cheng EH (2009) Stepwise activation of BAX and BAK by tBID, BIM, and PUMA initiates mitochondrial apoptosis. Mol Cell 36: 487-499

Knudson CM, Tung KS, Tourtellotte WG, Brown GA, Korsmeyer SJ (1995) Bax-deficient mice with lymphoid hyperplasia and male germ cell death. Science 270: 96-99

Korsmeyer SJ, Wei MC, Saito M, Weiler S, Oh KJ, Schlesinger PH (2000) Pro-apoptotic cascade activates BID, which oligomerizes BAK or BAX into pores that result in the release of cytochrome c. Cell Death Differ 7: 1166-1173

Krajewski S, Krajewska M, Reed JC (1996) Immunohistochemical analysis of in vivo patterns of Bak expression, a proapoptotic member of the Bcl-2 protein family. Cancer Res 56: 2849-2855

Ku B, Liang C, Jung JU, Oh BH (2011) Evidence that inhibition of BAX activation by BCL-2 involves its tight and preferential interaction with the BH3 domain of BAX. Cell Res 21: 627-641

Kurosaka K, Takahashi M, Watanabe N, Kobayashi Y (2003) Silent cleanup of very early apoptotic cells by macrophages. J Immunol 171: 4672-4679

Lee EF, Grabow S, Chappaz S, Dewson G, Hockings C, Kluck RM, Debrincat MA, Gray DH, Witkowski MT, Evangelista M et al (2016) Physiological restraint of Bak by Bcl-xL is essential for cell survival. Genes Dev 30: 1240-1250

Leshchiner ES, Braun CR, Bird GH, Walensky LD (2013) Direct activation of full-length proapoptotic BAK. Proc Natl Acad Sci U S A 110: E986-995

Li H, Zhu H, Xu CJ, Yuan J (1998) Cleavage of BID by caspase 8 mediates the mitochondrial damage in the Fas pathway of apoptosis. Cell 94: 491-501

Lindsten T, Ross AJ, King A, Zong WX, Rathmell JC, Shiels HA, Ulrich E, Waymire KG, Mahar P, Frauwirth K et al (2000) The combined functions of proapoptotic Bcl-2 family members bak and bax are essential for normal development of multiple tissues. Mol Cell 6: 1389-1399

Lucendo, E., Sancho, M., Lolicato, F., Javanainen, M., Kulig, W., Leiva, D. et al. (2020) Mcl-1 and Bok transmembrane domains: unexpected players in the modulation of apoptosis. Proc. Natl Acad. Sci. U.S.A. 117, 27980–27988.

Martínez-Senac Mdel M, Corbalán-García S, Gómez-Fernández JC (2002) The structure of the C-terminal domain of the pro-apoptotic protein Bak and its interaction with model membranes. Biophys J 82: 233-243

McIlwain DR, Berger T, Mak TW (2013) Caspase functions in cell death and disease. Cold Spring Harb Perspect Biol 5: a008656

Morris RG, Hargreaves AD, Duvall E, Wyllie AH (1984) Hormone-induced cell death. 2. Surface changes in thymocytes undergoing apoptosis. Am J Pathol 115: 426-436

Motoyama N, Wang F, Roth KA, Sawa H, Nakayama K, Nakayama K, Negishi I, Senju S, Zhang Q, Fujii S et al (1995) Massive cell death of immature hematopoietic cells and neurons in Bcl-x-deficient mice. Science 267: 1506-1510

Naghdi S, Várnai P, Hajnóczky G (2015) Motifs of VDAC2 required for mitochondrial Bak import and tBid-induced apoptosis. Proc Natl Acad Sci U S A 112: E5590-5599

Nakayama K, Nakayama K, Negishi I, Kuida K, Shinkai Y, Louie MC, Fields LE, Lucas PJ, Stewart V, Alt FW et al (1993) Disappearance of the lymphoid system in Bcl-2 homozygous mutant chimeric mice. Science 261: 1584-1588

Nechushtan, A., Smith, C.L., Hsu, Y. and Youle, R.J. (1999) Conformation of the Bax C-terminus regulates subcellular location and cell death. EMBO J. 18, 2330–2341

Osterlund EJ, Hirmiz N, Pemberton JM, Nougarède A, Liu Q, Leber B, Fang Q, Andrews DW (2022) Efficacy and specificity of inhibitors of BCL-2 family protein interactions assessed by affinity measurements in live cells. Sci Adv 8: eabm7375

Pemberton, J.M., Nguyen, D., Osterlund, E.J., Schormann, W., Pogmore, J.P., Hirmiz, N. et al. (2023) The carboxyl-terminal sequence of PUMA binds to both anti-apoptotic proteins and membranes. eLife 12, e88329

Pogmore JP, Pemberton JM, Chi X, Andrews DW (2016) Using Förster-Resonance Energy Transfer to Measure Protein Interactions Between Bcl-2 Family Proteins on Mitochondrial Membranes. Methods Mol Biol 1419: 197-212

Sandow BA, West NB, Norman RL, Brenner RM (1979) Hormonal control of apoptosis in hamster uterine luminal epithelium. Am J Anat 156: 15-35

Sarosiek KA, Chi X, Bachman JA, Sims JJ, Montero J, Patel L, Flanagan A, Andrews DW, Sorger P, Letai A (2013) BID preferentially activates BAK while BIM preferentially activates BAX, affecting chemotherapy response. Mol Cell 51: 751-765

Savill J, Fadok V (2000) Corpse clearance defines the meaning of cell death. Nature 407: 784-788

Shivakumar S, Kurylowicz M, Hirmiz N, Manan Y, Friaa O, Shamas-Din A, Masoudian P, Leber B, Andrews DW, Fradin C (2014) The proapoptotic protein tBid forms both superficially bound and membrane-inserted oligomers. Biophys J 106: 2085-2095

Souers AJ, Leverson JD, Boghaert ER, Ackler SL, Catron ND, Chen J, Dayton BD, Ding H, Enschede SH, Fairbrother WJ et al (2013) ABT-199, a potent and selective BCL-2 inhibitor, achieves antitumor activity while sparing platelets. Nat Med 19: 202-208

Tartaglia LA, Ayres TM, Wong GH, Goeddel DV (1993) A novel domain within the 55 kd TNF receptor signals cell death. Cell 74: 845-853

Tsujimoto Y, Cossman J, Jaffe E, Croce CM (1985) Involvement of the bcl-2 gene in human follicular lymphoma. Science 228: 1440-1443

Veis DJ, Sorenson CM, Shutter JR, Korsmeyer SJ (1993) Bcl-2-deficient mice demonstrate fulminant lymphoid apoptosis, polycystic kidneys, and hypopigmented hair. Cell 75: 229-240

Wang K, Yin XM, Chao DT, Milliman CL, Korsmeyer SJ (1996) BID: a novel BH3 domain-only death agonist. Genes Dev 10: 2859-2869

Wyllie AH, Kerr JF, Currie AR (1980) Cell death: the significance of apoptosis. Int Rev Cytol 68: 251-306

Wyllie AH, Morris RG, Smith AL, Dunlop D (1984) Chromatin cleavage in apoptosis: association with condensed chromatin morphology and dependence on macromolecular synthesis. J Pathol 142: 67-77

2 The carboxyl terminal sequence of Bak is required for activation by BH3-only proteins

2.1 Preface

This chapter is prepared for submission for publication:

Sabina Trebinjac*, Dang Nguyen*, Tobias B Beigl[4], Uyen Le, Kathryn Mary Murphy, Frank Essmann[4], David W. Andrews. (2025). The carboxyl terminal sequence of Bak is required for activation by BH3-only proteins. In draft.

*These authors contributed equally.

Author Contributions: Trebinjac S carried out the FLIM-FRET and cell death assay experiments and data analysis, co-drafted the manuscript. Nguyen D conducted FLIM-FRET and cell death and analysis, and performed protein purification, labeling, and conducted in vitro cell-free assays using liposomes and mitochondria and analysis and co-drafted the manuscript. Andrews DW was involved in the conception of the manuscript, directed the layout of the figures and edited the manuscript. Uyen conducted experiments for Figure 3 - figure supplementary 1E. T Beigl cloned the constructs for mT2-CTSBak/Bax for FLIM-FRET. All authors reviewed the manuscript.

Objective: Characterization of binding and activation mechanisms of Bak by interactions with BH3-only activator proteins.

Highlights:

- Bid is more efficient than Bim at activating Bak
- The BH3 region of Bid enables high affinity binding to Bak
- The h0 region of the Bid BH3 sequence confers high-affinity binding of BimL to Bak
- High-affinity binding of BimL to Bak is insufficient to enable Bak activation by Bim
- The specific sequence of the Bak CTS is required for efficient activation of Bak by cBid
- The Bid BH3 region is not required for tBid to bind to the CTS of Bak
- The Bim-CTS binds to the BAK-CTS and is required for the efficient activation of Bak
- The Bim-CTS is required for binding and activating full-length Bak.

2.2 Abstract

The Bcl-2 family of proteins plays a pivotal role in regulating the mitochondrial pathway of apoptosis through direct binding interactions among its members. Bak, a key executioner protein in this family, localizes to the mitochondrial outer membrane via its carboxyl terminal sequence (CTS) and becomes activated through interactions with the BH3-only proteins Bid and Bim. The BH3-motifs of these proteins are essential for binding to the BH3-binding pocket of Bak, triggering conformational changes that lead to Bak oligomerization. However, here, we demonstrate that efficient activation of Bak by Bim or Bid requires additional binding interactions between the activator proteins and the Bak-CTS. The additional interaction of Bim with the Bak-CTS necessary for robust Bak activation is with the CTS of Bim.

2.3 Introduction

The Bcl-2 family of proteins controls the commitment step to the onset of programmed cell death by initiating mitochondrial outer membrane permeabilization (MOMP) (Kale *et al*, 2018). Dysregulation of homeostasis with either excessive or deficient apoptosis contributes to the pathogenesis of many diseases, and as such, it is essential to understand how the Bcl-2 family regulates this form of cell death (Singh *et al*, 2019). The current model of apoptosis posits that the interactions between Bcl-2 homology 3 (BH3) regions and binding sites on Bcl-2 family proteins govern MOMP by regulating the activation and subsequent oligomerization of pore-forming executioner proteins Bax, Bak, and Bok. In one mechanism, the oligomerization of the executioner protein Bax is initiated by direct binding of activators Bid and/or Bim (Kim *et al.*, 2009; Korsmeyer *et al.*, 2000; Leshchiner *et al.*, 2013). The mechanisms leading to efficient Bak activation remain less clear. Understanding mechanistic differences in the activation process opens avenues for potential pharmaceutical interventions selectively targeting Bak- or Bax-mediated apoptosis.

To inhibit Bax/Bak activation, the multi-domain anti-apoptotic proteins, including Bcl-2, Bcl-XL, Bcl-W and Mcl-1, bind direct activators such as Bid and Bim and to activated Bax/Bak, forming mutually sequestered inactive heterodimeric complexes (Hockings *et al.*, 2018; Ku *et al.*, 2011; Lee *et al.*, 2016). A second group of BH3-only proteins, known as sensitizers, that includes Bad and Bik, bind anti-apoptotic proteins and compete with formation of or disrupt the the inhibited heterodimeric complexes. As the Bax/Bak bound by anti-apoptotic proteins is in the active state, releasing these proteins rapidly results in MOMP. Additionally, released direct activator BH3-only proteins can subsequently activate Bax/Bak to induce MOMP (Day *et al.*, 2008; Huang *et al.*, 2019; Osterlund *et al.*, 2022).

Biochemical evidence from multiple studies suggests that the BH3 motifs of BH3-only proteins are key factors distinguishing sensitizers from direct activators as they determine which anti-apoptotic or executioner proteins the BH3-only proteins bind to (Letai *et al*, 2002). For example, the BH3 motifs of Bim and Bid, but not Bad, bind to and thereby activate Bax and Bak. However, measurements of the selectivity of the BH3 regions of Bid and Bim for Bax and Bak are ambiguous. The BH3 peptide of Bid, alone or in the context of the active form of Bid (cBid), preferentially activates Bak compared to Bax. In contrast, the Bim BH3 peptide and recombinant BimL are more efficient at activating Bax than Bak (Sarosiek *et al.*, 2013). However, when these BH3 motifs were compared using a recombinant chimera of cBid with either the Bim or Bid BH3 no difference in the activation of Bax or Bak was observed(Hockings *et al*, 2015). Thus, the context in which the BH3 motif is presented likely contributes to specificity. The mechanisms by which BimL and cBid activate Bak remain unclear as despite both requiring BH3 motifs for pro-apoptotic function, the two BH3-only proteins differ in tertiary structure. Additionally, the chimeric cBid with a Bim BH3 used in this study contained only 16 residues from the Bim BH3 sequence and did not include the h0 region (Hockings *et al.*, 2015). Thus, whether the importance of the Bid BH3 motif or the h0 region in selective binding and preferential activation of Bak over Bax is unclear.

There is also evidence that similar to Bax, Bak can be activated by interactions with other small molecules (Brahmbhatt *et al*, 2016) and that active Bak binds and activates dormant Bak (Singh *et al*, 2022). Binding to VDAC2 has been proposed as a mechanism for recruiting Bak to the mitochondrial outer membrane (MOM) (Naghdi *et al.*, 2015) and to maintaining Bak in a dormant state in healthy cells (Cheng *et al.*, 2003). Although the exact mechanism for VDAC2 binding to Bak is still unknown, the Bak-CTS is required for VDAC2 to sequester Bak in an inactive complex (Lazarou *et al*, 2010). Alternatively, Bak can be inhibited by binding to the anti-apoptotic proteins Bcl-XL and Mcl-1 (Hockings *et al.*, 2018). This interaction is mediated by the Bak BH3 binding to the BH3-binding pocket of Bcl-XL and Mcl-1 and instills a survival dependence on the anti-apoptotic proteins. It remains unclear whether in live cells Bid and Bim induced by apoptotic stimuli displace active Bak from these inhibitory complexes to elicit Bak-driven MOMP. Adding to the complexity, inactive Bak has a structural constraint where the N-terminal BH4 region of Bak binds to its core domain (helix α2- α5), thereby blocking access to the BH3-binding pocket (Sandow *et al*, 2021). It is unclear how Bid and Bim overcome this auto-regulatory mechanism to enable BH3-mediated Bak activation.

Irrespective of the initiating step, BH3-mediated activation of Bak triggers dissociation of the core domain from the latch domain (helix α6- α8) (Brouwer *et al.*, 2014), exposing the Bak BH3, which then binds the BH3-binding pocket of another Bak, to form Bak BH3-in-groove dimers. As the Bak dimers become oligomers, the Bak-CTS was shown to provide an additional dimer interface in the pore-forming high-order Bak complexes (Iyer *et al.*, 2015). However, the Bak-CTS has been considered to be primarily a hydrophobic transmembrane sequence that binds Bak to the MOM (Martínez-Senac Mdel *et al.*, 2002) therefore, the precise role of Bak-CTS has not been well-characterized in mediating protein-protein interactions or functioning in Bak activation. A previous study using recombinant CTS-truncated Bak in which the Bak-CTS was replaced with a poly-histidine tag (BakΔCTS-His) to enable binding to liposomes containing Ni^{2+}-NTA lipids showed that in this context the Bak-CTS is not essential for Bak activation (Oh *et al*, 2010). However, this chimeric mutant of Bak also lacked the N-terminal segment (16 residues) hypothesized to be involved in the inherent structural restraint that keeps Bak inactive (Dewson *et al*, 2009). Moreover, BakΔCTS-His is prone to auto-activation at concentrations above 100 nM. Another study that examined the binding site of the Bid BH3 on Bak used recombinant full-length murine Bak with three mutations in the Bak-CTS (I192K, F193S, and V196D, similar to residues in the Bax-CTS) to reduce overall hydrophobicity and enable a better purification yield (Leshchiner *et al.*, 2013).The results of this study suggested that binding a BH3 sequence to the canonical binding pocket is necessary and sufficient to activate Bak. Altogether, these studies highlight the lack of consensus on the mechanism(s) governing Bak activation, particularly in cells.

Here we demonstrate using FLIM (Fluorescence Lifetime Imaging)-FRET (Förster resonance energy transfer) microscopy in live cells, that the efficient activation of Bak by Bim or Bid results from both binding of the BH3 motifs to the BH3-binding pocket of Bak and a separate binding interaction of the activator proteins to the Bak-CTS. Importantly, we show that the second Bak-binding site on BimL is the Bim-CTS, that binds directly to the Bak-CTS on the MOM. This mechanism of Bak activation differs significantly from previous data for Bax activation in which the Bim-CTS binds to Bax in solution and, therefore, activates Bax independently from its role in localizing Bim/Bax complexes to the MOM (Chi *et al.*, 2020).

2.4 Results

2.4.1 Bid is more efficient than Bim at activating Bak.

To examine how Bid and Bim differ in their Bak-activating function, recombinant full-length His-tagged proteins were expressed in bacteria and purified. Even though the N-terminal His tags were not removed, for simplicity, the proteins are referred to here as BimL and Bid. When the latter was activated via cleavage by recombinant Caspase 8, it is referred to as cBid. To enable the expression of human Bak in *E. Coli*, we used a Bak mutant with three alterations in the carboxyl terminal sequence (CTS) of Bak (V194K, L195S, V198D) analogous to the I192K, F193S, V196D murine Bak mutant that was previously purified to study Bak (Leshchiner *et al.*, 2013). These mutations enhance the hydrophilicity of the Bak-CTS, thereby improving the purification yield of the full-length protein. All full-length recombinant Bak proteins used in this study contained the three aforementioned mutations in the Bak-CTS and were purified with a carboxyl terminal chitin-binding domain (CBD) tag, linked via an intein sequence that enabled cleavage to release the full-length Bak proteins.

The function of the recombinant proteins was assayed utilizing liposomes with a lipid composition similar to that of mitochondria and encapsulating DPA:Terbium. In this assay, cBid was much more efficient than BimL at activating BAK-mediated liposome permeabilization (Figure 2.1A). In contrast, cBid and BimL both activated recombinant BAX equally with EC_{50}'s of 2.5 and 2.3 nM, respectively (Figure 2.1B) demonstrating that even though cBid was much more efficient at activating Bak, both BH3-only proteins were functional. As expected, the negative control BimL-4E in which the BH3 region was disrupted by the introduction of 4 glutamic acid residues, did not activate BAK or BAX.

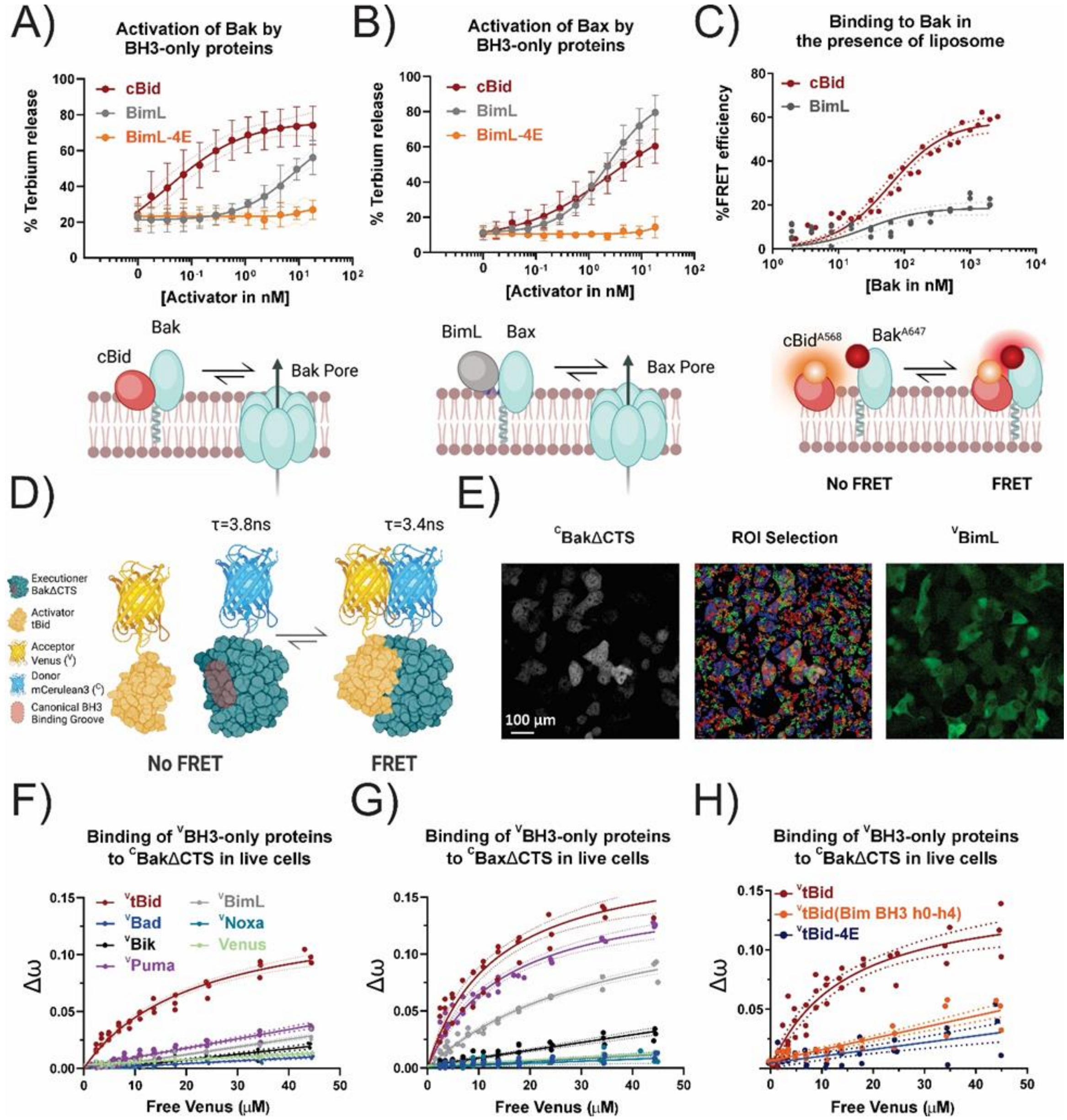

Figure 2.1. Bid binds to Bak and Bax, while Bim preferentially binds to Bax. Activation of **(A)** 100 nM Bak or **(B)** 100 nM Bax by the indicated proteins results in permeabilization of MOM-like liposomes.cBid is more efficient than BimL at inducing Bak activation. Measured by % terbium release, cBid resulted in an EC_{50} for terbium release of ~40 pM. In contrast, 4-5 nM BimL were required to result in detectable terbium release, which had not plateaued by 2 μM. Both cBid and BimL activate Bax equivalently with EC_{50}s of 2.5 and 2.3 nM, respectively. As expected, the negative control, BimL-4E, did not activate Bax or Bak (horizontal orange line). Data points (solid color) show the

mean of 5 independent replicates for cBid and BimL and 3 independent replicates for BimL-4E. The dotted lines indicate 95% confidence intervals of the fit to a four-parameter logistic equation, and error bars represent the standard deviation of the replicates. **(C)** The binding of 5 nM Donor Alexa 568-labelled (A568-) single-cysteine recombinant cBid (C126) or BimL (Q41C) to the Acceptor Alexa 647-labelled (A647-) single-cysteine recombinant Bak in the presence of liposomes was measured by stimulated emission intensity-based FRET. In this assay, cBid bound to full-length Bak with a K_D of ~58 nM and BMAX of 58% (R^2>0.9), data fit as previously (Pogmore *et al.*, 2016). BimL bound to Bak similarly with a K_D of ~24 nM. However, the BMAX of only 19% (R^2 = 0.41) suggests high uncertainty in this measurement. **(D)** Schematic describing the proteins used to measure in HCT116 $Bax^{-/-}$ $Bak^{-/-}$ (DKO) cells the binding of mCerulean3-fused CTS-truncated Bak (^{C}BakΔCTS) to Venus-fused tBid (^{V}tBid). **(E)** Representative of FLIM-FRET images for ^{C}BakΔCTS (Time correlated single photon counting image, left panel) and ^{V}tBid (hyperspectral image, right panel). The middle panel shows the selection of Regions of Interest (ROIs) that resulted from the watershed algorithm on the mCerulean3 image. The scale bar indicates 100 µm. (F-H) The binding of acceptor ^{V}BH3-only proteins to (F, H) donor ^{C}BakΔCTS or (G) ^{C}BaxΔCTS in HCT116 DKO cells measured by FLIM-FRET. **(F)** The protein ^{V}tBid bound to ^{C}BakΔCTS with an average K_D of 6 µM as indicated by the binding data in red that fits the Hill-equation (h=1) and has a s-ratio≥2. In contrast, binding to ^{C}BakΔCTS was not measurable for the other ^{V}BH3-only proteins tested. **(G)** ^{V}tBid, ^{V}BimL, and ^{V}Puma bound to BaxΔCTS with K_D values ranging between 8 to 15 µM. Only collisions were detected for ^{V}Bik, ^{V}Noxa, ^{V}Bad, and the negative control protein Venus with either Bax or Bak, as the binding data best fit linear equations (s-ratio <2). **(H)** Replacing the Bid BH3 motif with that of Bim in the ^{V}tBid(Bim BH3 h0-h4) chimera or mutating the key four hydrophobic residues (h1, h2, h3, and h4) to glutamic acid (^{V}tBid-4E) abolished binding of ^{V}tBid to ^{C}BakΔCTS. S-ratios for both ^{V}tBid(Bim BH3 h0-h4) and ^{V}tBid-4E and are below 2. (fit: R^2>0.9 and =0.7 for ^{V}tBid(Bim BH3 h0-h4) and ^{V}tBid-4E, respectively). (F-H) The dotted lines are the 95% confidence interval of fit of the data for the three technical replicates (solid symbols).

2.4.2 The BH3 region of Bid enables high affinity binding to Bak

To investigate whether the difference in Bak activation—where Bid is more effective than BimL—results from the Bid BH3 motif providing higher binding affinity of cBid to Bak compared to the binding of the Bim BH3 motif in BimL to Bak, we measured the apparent binding affinities of purified recombinant proteins labeled with fluorescent dyes using Förster resonance energy transfer (FRET) (Figure 1C). The binding of BimL and cBid to full-length Bak, expressed as %FRET efficiency, resulted in dissociation constants (K_D) of 58 nM for cBid and 24 nM for BimL. However, compared to the maximum FRET efficiency of ~60% observed for cBid binding to Bak C166, the maximum FRET efficiency ~20% resulting from binding of BimL to Bak C166, was so low that a saturable curve was difficult to distinguish from a linear increase that might be just due to collisions. Moreover, the maximum FRET efficiency cannot be interpreted directly because it is determined by binding, distance, and dye orientation. Since FRET decreases by 10^6 with distance, differences in the distance between donor dyes (in this case at Bid C126 and Bim C41) and the acceptor dye on Bak C166 (in the BH3-binding pocket) likely contribute substantially to the maximum FRET efficiencies observed for Bid/Bak and Bim/Bak heterodimers. Therefore, measurements in vitro were inconclusive regarding the affinity of BimL binding to Bak C166.

To further examine the binding affinity between BimL/Bid and Bak, we measured live cells by FLIM-FRET microscopy (Figure 2.1F-H). For these measurements, the proteins were exogenously expressed as fluorescence protein fusions (Liu *et al*, 2012; Osterlund *et al*, 2019; Osterlund *et al*, 2015; Pemberton *et al*, 2023). Expression of full-length Bak and a direct activator protein in cells resulted in rapid apoptosis. To enable measurement of binding interactions, CTS-truncated Bak (BakΔCTS) with an N-terminally fused mCerulean3 (^{C}BakΔCTS), as the donor fluorophore of the FRET pair, was stably expressed in Bax -/-Bak-/- HCT116 cells (Figure 2.1D). ^{C}BakΔCTS is cytoplasmic and does not bind to MOM but has an intact canonical BH3-binding pocket and thus can bind to direct activator BH3-only proteins (Dai *et al*, 2011; Ye *et al*, 2020) without inducing significant MOMP (Stehle *et al*, 2018). As FRET acceptor proteins, Venus (V) was N-terminally fused to the BH3-only proteins. The acceptor was expressed transiently to obtain cells with a wide range of expression levels to measure binding curves. The binding of ^{V}BH3-protein to ^{C}BakΔCTS results in a decrease in the fluorescence lifetime of mCerulean3 that is quantified by time-correlated single photon counting. FLIM FRET is expressed as an increase in change in angular frequency (ΔϢ) derived from phasor plots of the lifetime data (Osterlund *et al.,* 2022; Ranjit *et al*. 2018). In these experiments, significant binding was observed for Venus-fused to the p15 fragment of cleaved Bid (^{V}tBid) but not for other

BH3-only proteins or the negative control Venus (Figure 2.1F). As tBid, BimL, and Puma are known direct activators of Bax (Chi *et al.*, 2020; Gallenne *et al*, 2009; Korsmeyer *et al.*, 2000), binding of these BH3-only proteins to ^{C}BaxΔCTS was used to demonstrate that the ^{V}BH3-only proteins were functional (Figure 2.1G). The measured K_D values for ^{V}tBid, ^{V}BimL, and ^{V}Puma binding to ^{C}BaxΔCTS in live cells were relatively similar (8-15 μM). As expected, the sensitizer BH3 proteins, ^{V}Bad, ^{V}Bik, and ^{V}Noxa, that bind to anti-apoptotic Bcl-2 family proteins did not bind to ^{C}BakΔCTS or ^{C}BaxΔCTS. Instead of a binding curve, the data fit into a straight line, indicating that only collisions were detected, similar to the Venus negative control. Taken together, this data suggests that in live cells, tBid has a higher affinity than BimL for binding to BakΔCTS.

Our FLIM-FRET binding data with ^{C}BakΔCTS contrasts with previously published results for Bim BH3 peptides, which were shown to interact with Bak (Brouwer *et al*, 2017; Ye *et al.*, 2020). To ensure that the lack of binding between ^{V}BimL and ^{C}BakΔCTS is not due to the orientation of the Venus acceptor fluorescence protein (FP) relative to the mCerulean3 donor FP on ^{C}BakΔCTS, we transiently expressed a ^{V}tBid chimera, ^{V}tBid (Bim BH3), wherein the Bim BH3 replaced the Bid BH3 from residue h0 to h4 (Figure 2.1 – Figure Supplement 1A). The binding of the chimera to mC3-BakΔCTS was not observed (Figure 2.1H, orange line). As a negative control, we used the mutant tBid-4E in which the four conserved hydrophobic residues (h1, h2, h3, and h4) were mutated to glutamic acid (E). As expected, disrupting the Bid BH3 with 4E mutations (^{V}tBid-4E) abolished binding to ^{C}BakΔCTS (Blue line). These data indicate that the Bid BH3 is required for binding to BakΔCTS in live cells that can be detected by FLIM FRET.

To ensure that substituting the Bim BH3 for the Bid BH3 did not eliminate the pro-apoptotic function of tBid, we tested the binding to ^{C}BaxΔCTS instead of ^{C}BakΔCTS. Our data shows that the ^{V}tBid (Bim BH3) chimera bound ^{C}BaxΔCTS (Figure 2.1 – Figure Supplement 1B) and ^{C}Bcl-XL (Figure 2.1 – Figure Supplement 1C). Finally, the ^{V}tBid (Bim BH3) chimera induced cell death effectively compared to WT tBid when expressed in primed BMK cell lines (Chi *et al.*, 2020) (Figure 2.1 – Figure Supplement 1D). This confirms that the ^{V}tBid chimera retained its sensitizer function and indirectly activated Bax or Bak by inhibiting anti-apoptotic proteins such as Bcl-XL. Taken together, our data demonstrates that the Bid BH3 sequence enables high-affinity binding to ^{C}BakΔCTS while Bid BH3 and Bim BH3 can bind to both ^{C}BaxΔCTS and ^{C}Bcl-XL.

	h0 h1 h2 h3 h4	^{C}BakΔCTS	^{C}BaxΔCTS
Bid BH3	EE I I H N I A R H L A Q I G D E M D H N IQPT		
Bim BH3	LR P E I R I A Q E L R R I G D E F N E T YTRR		
tBid	EE I I H N I A R H L A Q I G D E M D H N IQPT	7.6	12.7
tBid (Bim h0-h4)	EE P E I R I A Q E L R R I G D E F D H N IQPT	Non-binding	18.7
tBid (Bim h0-h3)	EE P E I R I A Q E L R R I G D E M D H N IQPT	Non-binding	15.1t
tBid (Bim h1-h4)	EE I I H N I A Q E L R R I G D E F D H N IQPT	8.1	7.4
tBid H84I N85R	EE I I I R I A R H L A Q I G D E M D H N IQPT	7.8	10.1
tBid I82P I83E	EE P E H N I A R H L A Q I G D E M D H N IQPT	Non-binding	Non-binding
tBid I82A I83A	EE A A H N I A R H L A Q I G D E M D H N IQPT	Non-binding	16.8
tBid I82A	EE A I H N I A R H L A Q I G D E M D H N IQPT	21.3	15.2t
tBid I82P	EE P I H N I A R H L A Q I G D E M D H N IQPT	Non-binding	20.2
tBid I83A	EE I A H N I A R H L A Q I G D E M D H N IQPT	Non-binding	8.8
tBid I83E	EE I E H N I A R H L A Q I G D E M D H N IQPT	Non-binding	8.4
tBid (Bim h0±2)	LR P E I R I A R H L A Q I G D E M D H N IQPT	Non-binding	27.9
tBid (Bim h0+2)	EE P E I R I A R H L A Q I G D E M D H N IQPT	Non-binding	19.4
tBid (Bim h0±1)	ER P E I N I A R H L A Q I G D E M D H N IQPT	Non-binding	Non-binding
tBid (Bim h0-1,+2)	ER P E I R I A R H L A Q I G D E M D H N IQPT	Non-binding	27.7
BimL	LR P E I R I A Q E L R R I G D E F N E T YTRR	Non-binding	8.2
BimL (Bid h0-h4+3)	LR I I H N I A R H L A Q I G D E M D H N YTRR	10.1	10
BimL (Bid h1-h4+3)	LR P E I R I A R H L A Q I G D E M D H N YTRR	Non-binding	13.2
BimL I88H R89N	LR P E H N I A Q E L R R I G D E F N E T YTRR	Non-binding	9
BimL P86I E87I	LR I I I R I A Q E L R R I G D E F N E T YTRR	17.2	21.9
BimL (Bid h0±2)	EE I I H N I A Q E L R R I G D E F N E T YTRR	6.4	6
BimL (Bid h0+2)	LR I I H N I A Q E L R R I G D E F N E T YTRR	11.2	9

BimL (Bid h0+1)	LR I I H R I A Q E L R R I G D E F N E T YTRR	10	8.9
BimEL	LR P E I R I A Q E L R R I G D E F N E T YTRR	Non-Binding	11.9
BimEL (Bid h0-h4+3)	LR I I H N I A R H L A Q I G D E M D H N YTRR	16.3	9.9
BimEL (Bid h1-h4+3)	LR P E I R I A R H L A Q I G D E M D H N YTRR	22.4	14.3
BimEL I144H R145N	LR P E H N I A Q E L R R I G D E F N E T YTRR	Non-binding	19.2
BimEL P142I E143I	LR I I I R I A Q E L R R I G D E F N E T YTRR	12.7	10.3
BimEL (Bid h0±2)	EE I I H N I A Q E L R R I G D E F N E T YTRR	Non-binding	17.9
BimEL (Bid h0+2)	LR I I H N I A Q E L R R I G D E F N E T YTRR	8.4	8.8
BimEL (Bid h0+1)	LR I I H R I A Q E L R R I G D E F N E T YTRR	6.4	6.8

Table 2.1. BH3 sequences of Bim, tBid, and the mutants used in FLIM-FRET experiments with BaxΔCTS and BakΔCTS. The yellow-shaded residues are mutated or swapped-in sequences from the other activator proteins. Key hydrophobic residues of the BH3 motif are in red. The average apparent dissociation constant (K_D) values in µM of all independent replicates for each construct are shown in the color-shaded squares in the columns on the right. Red-shaded squares highlight constructs that do not bind the indicated executioner protein. Dark-blue-shaded squares indicate strong binding, while light-blue-shaded squares indicate weak binding.

2.4.3 The h0 region of the Bid BH3 sequence confers high-affinity binding of BimL to Bak

To identify which residues in the Bid BH3 are required for preferential binding of tBid to the BH3-binding pocket on Bak, we created different chimeric mutants of ^{V}tBid where parts of Bim BH3 were swapped for the equivalent residues in the Bid BH3 (Table 1). The binding of these ^{V}tBid mutants to both ^{C}BakΔCTS and ^{C}BaxΔCTS was quantified using FLIM-FRET to determine the apparent K_D values for each ^{V}tBid construct. From these experiments, we identified residues I82 and I83 of Bid at the h0 residues that could not be exchanged with the corresponding PE residues of Bim without losing binding to ^{C}BakΔCTS. As PE is not a conservative substitution, we also examined a series of alanine substitutions at the Bid h0 residues, specifically I82A, I83A, I82A, and I83A (Figure 2.2A). All of these substitutions significantly impaired the binding of ^{V}tBid to ^{C}BakΔCTS (Figure

2.2B and Figure 2 - Figure Supplement 1A) as indicated by an increase in the apparent K_D values or the binding data fitting to a linear model that represents collisions rather than binding. In contrast, these mutants retained significant binding to ^{C}BaxΔCTS (Figure 2.2 - Figure Supplement 1B), although the I82A and I82A/I83A mutations moderately reduced the binding of tBid to BaxΔCTS (Table 1). Moreover, these h0 mutations in the BH3 of tBid did not affect the binding of tBid to Bcl-XL (Figure 2.2-figure supplement 1C) or the Bax/Bak dependent death-inducing function of tBid in BMK cells (Figure 2.2- figure supplement 1D). As an orthogonal assay, we used fluorescence polarization (FP) with recombinant BakΔCTS and TMR-labelled stapled human Bid BH3 peptide (Bid SAHB) (Walensky *et al*, 2004). In this assay, the I82A and I83A mutations decreased binding of Bid BH3 to BakΔCTS by 4- and 14-fold, respectively (Figure 2.2-Figure supplement 1E). As expected, the I82A mutation minimally affected the binding of Bid SAHB to BaxΔCTS. However, the I83A mutation decreased the binding of Bid SAHB to BaxΔCTS by 6-fold (Figure 2.2 – Figure supplement 1F). Collectively, our data strongly demonstrate the importance of the h0 residues for the preferential binding of tBid to the BH3-binding pocket of Bak.

To examine if the h0 residues or other parts of Bid BH3 are sufficient to confer Bak binding to Bim, we created BimL and BimEL chimera in which residues in the Bim BH3 were replaced with the corresponding residues from the Bid BH3 sequence. Mutating h0 residues of Bim (P86I E87I in murine BimL) to that of Bid (2 isoleucines) substantially increased binding to BakΔCTS (Table 1). The BimL chimera with the highest binding affinity for BakΔCTS in live cells (lowest K_D) was achieved for BimL (Bid h0±2) in which the Bid h0 residues EEIIHN replace the corresponding BimL residues LRPEIR (Table 1). However, substitution of BimL residues PEI with Bid residues IIH BimL (h0+1) (Figure 2.2C) resulted in a nearly equivalent K_D of 10 μM when fitting the binding data to a Hill-equation (h=1). Significantly, substituting the entire Bim BH3 from h0 (P86, in murine BimL) to h4+3 (T103) did not improve binding to ^{C}BakΔCTS further suggesting that it is the H0 region that confers binding specificity (Figure 2.2C). The ^{V}BimL chimera with the Bid

BH3 substitutions or Bid h0 residues have similar binding to ^{C}BaxΔCTS (Table 1 and Figure 2.2 – Figure supplement 2A), suggesting that the BH3-binding pocket/sites on ^{C}BaxΔCTS can accommodate the binding of either Bim or Bid BH3 despite their different h0 residues. Finally, most of the substitution mutations had similar effects on the binding of ^{V}BimL and ^{V}BimEL to ^{C}BakΔCTS and ^{C}BaxΔCTS, as expected.

2.4.4 High-affinity binding of BimL to Bak is insufficient to enable Bak activation by Bim

As Bid h0 residues are necessary and sufficient for binding to BakΔCTS, we tested whether these residues are required for Bak activation. Surprisingly, the h0 I82A I83A mutation reduced but did not abolish Bid-mediated Bak activation in the terbium-release liposome permeabilization assay using full-length Bak (Figure 2.2D). Mutating individual h0 residue on cBid slightly reduced the maximum Bak-induced % terbium release from ~75% to ~60% (Figure 2.2 – Figure Supplementary 2B). In this experiment, the EC50 of cBid and cBid h0 mutants (I82A, I83A, and I82A I83A) activating Bak are all between 0.2 and 0.4 nM, suggesting no significant differences in their Bak-activating efficacy. Likewise, there were no differences in Bax activation by cBid and cBid h0 mutants (Figure 2.2- Figure Supplement 2C and 2D). We also tested the functional effect of inserting Bid h0 residues into Bim BH3 in BimL chimera protein by testing recombinant chimera BimL mutant with full-length Bak in the same terbium release liposome assay. We found no significant improvement to BimL-mediated Bak activation upon inserting the h0+1 (IIH) residues from Bid BH3 into the equivalent residues in BimL (Figure 2.2E). Replacing the entire Bim BH3 with that of Bid (h0-h4+3) slightly enhances Bak activation as the EC_{50} decreases from 13 nM for WT BimL to 5 nM for BimL(Bid BH3 h0+1). Nevertheless, the Bak-activating efficacy of these BimL (Bid BH3) chimeras is an order of magnitude lower than that of cBid as cBid can activate Bak with EC_{50} in the picomolar range. Scrambling the BH3 of BimL results in a complete loss of Bak (Figure 2.2E). Taken together, the functional data with the liposome permeabilization assay indicates that the additional binding affinity to the BH3-binding pocket of Bak conferred by Bid h0 residues is insufficient to improve BimL-mediated Bak activation.

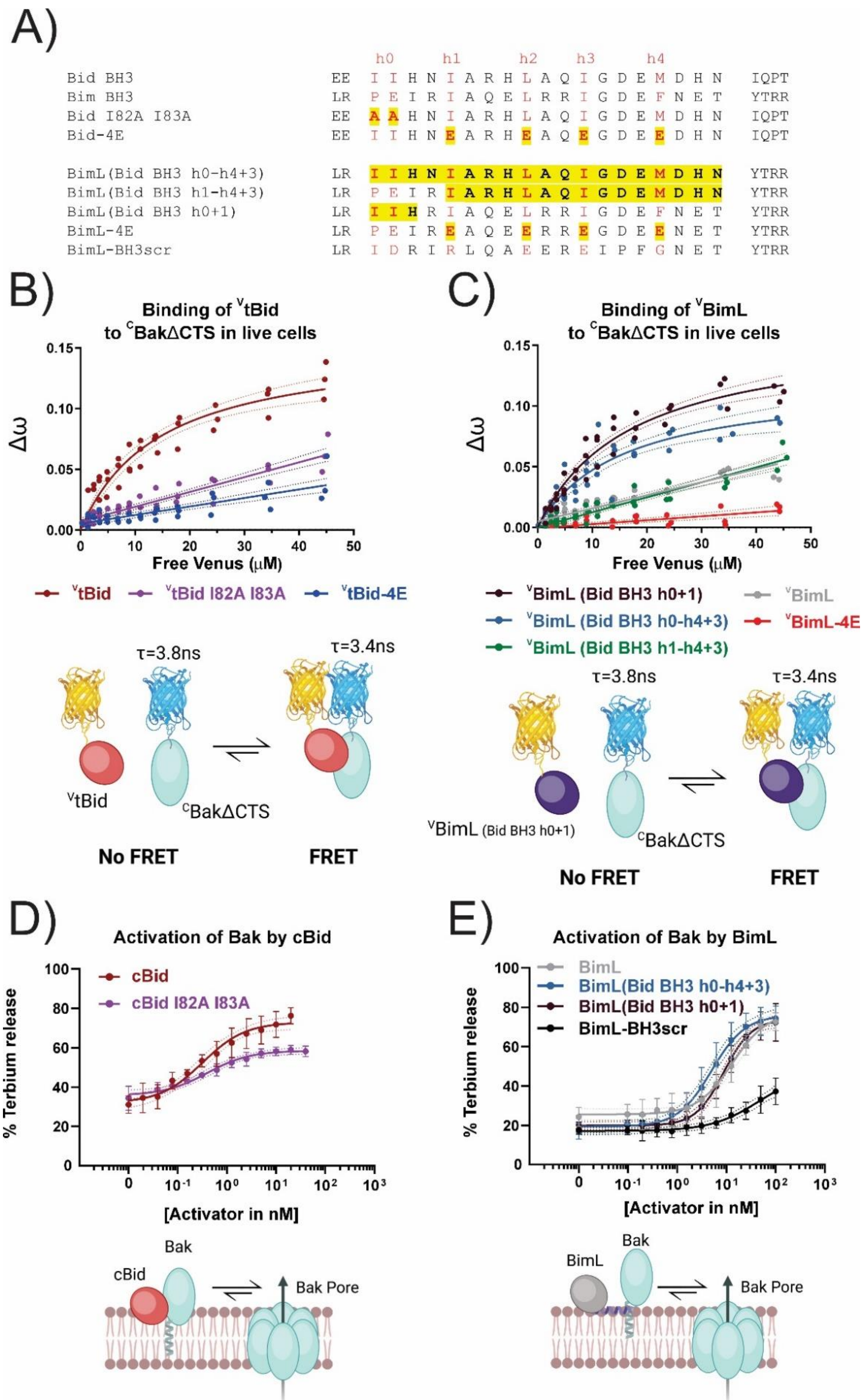
A)
h0 h1 h2 h3 h4
Bid BH3 EE I I H N I A R H L A Q I G D E M D H N IQPT
Bim BH3 LR P E I R I A Q E L R R I G D E F N E T YTRR
Bid I82A I83A EE A A H N I A R H L A Q I G D E M D H N IQPT
Bid-4E EE I I H N E A R H E A Q E G D E E D H N IQPT
BimL(Bid BH3 h0-h4+3) LR I I H N I A R H L A Q I G D E M D H N YTRR
BimL(Bid BH3 h1-h4+3) LR P E I R I A R H L A Q I G D E M D H N YTRR
BimL(Bid BH3 h0+1) LR I I H R I A Q E L R R I G D E F N E T YTRR
BimL-4E LR P E I R E A Q E E R R E G D E E N E T YTRR
BimL-BH3scr LR I D R I R L Q A E E R E I P F G N E T YTRR
B)
Binding of vtBid to cBakΔCTS in live cells
Δω
Free Venus (μM)
vtBid
vtBid I82A I83A
vtBid-4E
τ=3.8ns
τ=3.4ns
vtBid
cBakΔCTS
No FRET
FRET
C)
Binding of vBimL to cBakΔCTS in live cells
Δω
Free Venus (μM)
vBimL (Bid BH3 h0+1)
vBimL
vBimL (Bid BH3 h0-h4+3)
vBimL-4E
vBimL (Bid BH3 h1-h4+3)
τ=3.8ns
τ=3.4ns
vBimL (Bid BH3 h0+1)
cBakΔCTS
No FRET
FRET
D)
Activation of Bak by cBid
cBid
cBid I82A I83A
% Terbium release
[Activator in nM]
cBid
Bak
Bak Pore
E)
Activation of Bak by BimL
BimL
BimL(Bid BH3 h0-h4+3)
BimL(Bid BH3 h0+1)
BimL-BH3scr
% Terbium release
[Activator in nM]
BimL
Bak
Bak Pore

Figure 2.2. h0 residues within Bid BH3 confer binding to Bak but are insufficient to activate Bak. (A) Schematic shows the alignment of residues in Bid and Bim BH3 motif. Mutations at the key hydrophobic residues in the Bid BH3 and Bim BH3 are highlighted in yellow. Chimeric mutants of BimL are highlighted in yellow where whole or parts of Bid BH3 are inserted in Bim BH3. A mutant of BimL with a scrambled BH3 sequence is shown at the bottom as a negative control for the *in vitro* cell-free liposome permeabilization assay. **(B)** FLIM-FRET microscopy measured the binding of ^{V}tBid I82A I83A (purple) to ^{C}BakΔCTS in HCT116 DKO cells. The binding curve was linear (s-ratio <2), similar to the negative control ^{V}tBid-4E, indicating collisional interactions. In contrast, ^{V}tBid (red) exhibited binding fitted to the Hill equation (h=1), with an apparent K_D of 11 µM (s-ratio ≥2). Data from three technical replicates are shown, with summarized results in Table 1 and Appendix Table S1.**(C)** FLIM-FRET microscopy measured the binding of ^{V}BimL(Bid BH3 h0+1) to ^{C}BakΔCTS with an apparent K_D of 10 µM (dark purple), fitted to the Hill equation (h=1). Enhanced binding was observed for ^{V}BimL(Bid BH3 h0-h4+3) (blue, K_D = 10 µM, s-ratio = 4.2), but not for ^{V}BimL(Bid BH3 h1-h4+3) (green), which displayed collisional interactions (s-ratio <2). ^{V}BimL, ^{V}BimL-4E, and ^{V}BimL(Bid BH3 h1-h4+3) all resulted in linear binding data that indicate collisions. Data from three technical replicates are summarized in Table 1 and Appendix Table S2. **(D)** Terbium-release liposome assay with 100 nM Bak and cBid showed a partial reduction in Bak activation by cBid I82A I83A with the maximal terbium release was reduced from 70–80% for cBid to 50–60% for cBid I82A I83A while the EC50 values for both cBid and cBid I82A I83A were approximately 0.3±0.1 nM. Data points represent averages from four (cBid) and three (cBid I82A I83A) independent replicates. **(E)** Terbium-release assay with 100 nM Bak showed minimal enhancement of BimL-mediated Bak activation when Bid BH3 residues were introduced into BimL. The EC50 decreased from 13 nM for BimL to 9 nM for BimL(Bid BH3 h0+1) and 5 nM for BimL(Bid BH3 h0-h4+3) chimera, while maximal terbium release remained at 70–80%. Scrambling the BH3 sequence abolished BimL-mediated activation. Data points are averages from six independent replicates fitted to a four-parameter dose-response curve.

2.4.5 The specific sequence of the Bak CTS is required for efficient activation of Bak by cBid

The discrepancy between FLIM-FRET binding data with ^{C}BakΔCTS and functional liposome permeabilization data with full-length Bak regarding the role of Bid h0 residues revealed to us that there must be other regions outside of Bid BH3 and BH3-binding pocket of Bak, which contribute to the highly potent Bak activation by cBid. This led us to investigate the potential role of the carboxyl terminal sequence (CTS) of Bak in its activation. The canonical function of Bak CTS is to localize Bak to the MOM (Todt *et al*, 2015). Bak-CTS has also been reported to be required for binding Bak to VDAC2 (Lazarou *et al.*, 2010). This enables the formation of the VDAC2-Bak complex, which inhibits Bak activation.

To investigate the role of Bak-CTS in its activation, we generated recombinant human Bak proteins that have a complete CTS truncation (ΔCTS) or a scrambled CTS sequence (CTSscr) (Figure 2.3A). We then tested the activity of these recombinant Bak proteins with the Smac-mCherry release mitochondria-permeabilization assay (Shamas-Din *et al*, 2014; Tait *et al*, 2010). Incubation of mitochondria with Bak and increasing concentration of cBid causes Bak activation, which permeabilizes the MOM, releasing Smac-mCherry into the soluble fraction. Unsurprisingly, cBid activates Bak efficiently with an EC_{50} of 40 pM and a maximum release of around 70-80% at a concentration above 1 nM (Figure 2.3B). Scrambling or truncating Bak CTS abolished Bak activation by cBid as indicated by the horizontal linear fit through the release data for Bak-CTSscr (grey) and BakΔCTS (dark red). This data suggests that cBid, even at higher concentrations, does not effectively activate CTS-mutated Bak.

Next, we examined if the binding of Bak to cBid in the presence of mitochondrial membrane is affected by mutation in the Bak-CTS using FRET spectroscopy (Figure 2.3C). Using a fixed concentration of the donor 5 nM A568-labelled single cysteine cBid (C126) and increasing concentration of the acceptor A647-labelled single cysteine Bak (C14A C166) or Bak-CTSscr/ΔCTS incubated together isolated mitochondria, we found that scrambling Bak CTS decreased the binding of cBid to Bak as indicated by a drop in K_D from 400 nM for WT Bak to 5000 nM for Bak-CTSscr. Truncating the Bak CTS effectively eliminated the binding of cBid to Bak as indicated by a gradual linear increase in %FRET efficiency with increasing concentration of BakΔCTS acceptor protein. Scrambling or truncating Bak-CTS negatively affected its binding to cBid, thereby substantiating the role of Bak-CTS in Bid-mediated Bak activation.

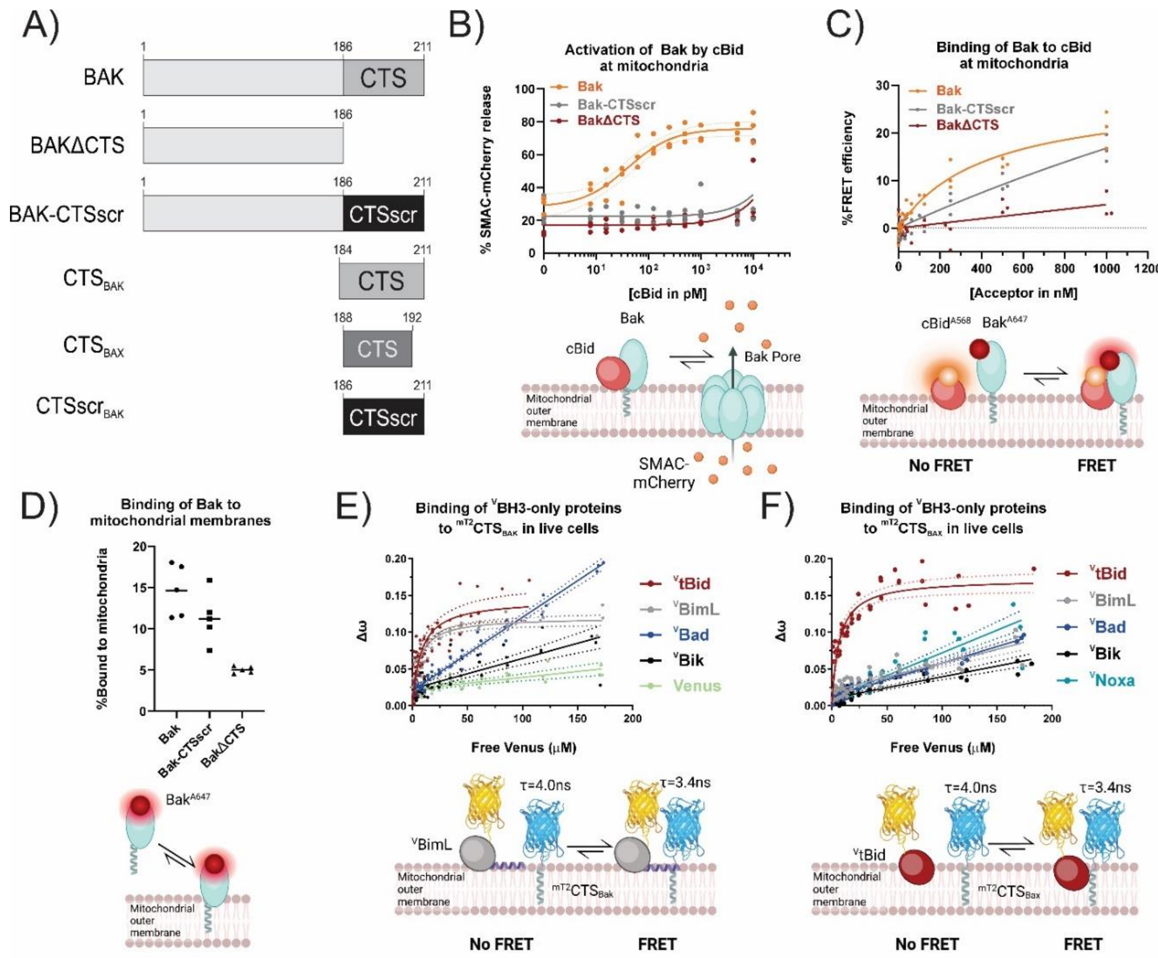

Figure 2.3. Activation of Bak requires Bak CTS which binds selectively to Bim and Bid. (A) Schematic representation of Bak and Bak-CTS mutants. The CTS, located at residues 186–211 in human Bak, was deleted in BakΔCTS or replaced with a scrambled sequence in Bak-CTSscr. The last three rows show schematic depictions of the Bak-CTS, Bax-CTS, and scrambled Bak-CTS sequences. **(B)** Smac-mCherry release assay with mitochondria from BMK DKO cells. Deleting (red) or scrambling (gray) Bak-CTS abolished cBid-induced Bak activation. Recombinant cBid activates 100 nM Bak with an EC50 of 40 pM. BakΔCTS and Bak-CTSscr did not induce significant mitochondrial permeabilization. Data are from three independent experiments. **(C)** The binding of 5 nM recombinant Donor A568-cBid to Acceptor A647-Bak or Bak-CTS mutants, measured via intensity-based FRET spectroscopy, showed reduced binding for BakΔCTS (dark red) and Bak-CTSscr (gray). The FRET data were fitted to a quadratic equation. Data are from three independent experiments. **(D)** Quantifying A647-Bak binding to mitochondria isolated from BMK DKO cells showed that ~15% of full-length Bak, ~12% of Bak-CTSscr, and ~5% of BakΔCTS were in the mitochondrial fractions. Data represent five independent experiments. **(E)** FLIM-FRET data showing $^{mT2}CTS_{BAK}$ bound to ^{V}BimL and ^{V}tBid in BMK DKO cells, with K_D values of 6.2 and 7.9 μM, respectively, as fitted to the Hill-

equation (h=1). No binding was observed for ^{V}Bad, ^{V}Bik, or Venus, as indicated by their binding data fitted to the linear equation. Data are from three technical replicates. An independent biological replicate is in Figure 2.3—Figure Supplement 2D. **(F)** FLIM-FRET data showed ^{mT2}CTS$_{BAX}$ bound ^{V}tBid (K_D = 6.6 μM) but not ^{V}BimL, ^{V}Bad, ^{V}Bik, or ^{V}Noxa. S-ratio analysis indicates collisional interactions (s-ratio <2) for non-binding proteins. Data are from three technical replicates. An independent biological replicate is shown in Figure 2.3—Figure Supplement 2E.

To ensure that the observed differences in activities between Bak and Bak-CTSscr are not simply due to differences in binding to mitochondria, we measured fluorescence intensity reflecting the amount of A647-labelled Bak in the mitochondrial fraction after incubating the recombinant Bak with isolated mitochondria from BMK DKO (Figure 2.3D). Scrambling Bak-CTS slightly reduced the binding of Bak to mitochondria from ~15% to 11%, whereas truncating Bak-CTS reduced it further to 5%. We also calculated the band intensity for the anti-Bak immunoblot for the mitochondrial and soluble fraction of unlabelled Bak protein incubating with isolated mitochondria (Figure Supplement 3 – Figure Supplement 1A). Here, we found that scrambling Bak-CTS reduced Bak binding to the mitochondrial membrane from 29% to 12%. Furthermore, only 3% of BakΔCTS was found in the mitochondrial fraction. Importantly, adding 10 nM cBid increased the %bound of Bak and Bak-CTS mutants. In detail, 42% Bak, 27% Bak-CTSscr, and 16% BakΔCTS bound to mitochondrial membranes upon incubation with cBid. These results show that Bak CTS mutants can still be recruited to the MOM by cBid as they possess functional BH3-binding pockets that bind the Bid BH3 motif.

2.4.6 The Bak CTS binds directly to activator proteins tBid and Bim but not to sensitizers Bad or Bik

Bak-CTSscr recombinant protein can bind and be recruited by cBid to the MOM, albeit at a reduced level, indicating that the BH3-binding pocket of Bak still plays a dominant role in this interaction. However, previous studies also suggested that Bak-CTS interacts with other Bak-CTS to form a secondary interface within Bak homodimer and oligomeric complex upon its activation by tBid (Iyer *et al.*, 2015). To investigate the potential functions of the Bak-CTS independent of its BH3-binding pocket, we conducted experiments to test if Bak-CTS can directly interact with BH3-only proteins using FLIM-FRET in BMK DKO cells. We indeed found that Bak-CTS (denoted as CTS_{BAK}), when fused with the donor mTurquoise2 ($^{mT2}CTS_{BAK}$) (Figure 2.3E), can undergo efficient FRET with both ^{V}BimL and ^{V}tBid as indicated by their binding data fitting to the Hill equation (h=1) and yielded a relative apparent K_D of 6.2 and 7.9 μM respectively. ^{V}Bad, ^{V}Bik, or the negative control Venus did not bind $^{mT2}CTS_{BAK}$, as indicated by the straight lines fitting their binding data. Importantly, introducing the triple mutations V194K, L195S, and V198D (KSD) used in the full-length recombinant Bak into Bak-CTS ($^{mT2}CTS\text{-}KSD_{BAK}$) reduced but did not abolish the binding of Bak-CTS to ^{V}tBid and ^{V}BimL (Figure 2.3-Figure supplement 1B), whereas scrambling the Bak-CTS ($^{mT2}CTSscr_{BAK}$) was sufficient to abolish these binding (Figure 2.3 – Figure Supplement 1C). However, this could be due to the poor localization of the donor $^{mT2}CTSscr_{BAK}$ fusion protein to the mitochondria (Figure 2.3 – Figure Supplement 1D). Nevertheless, our findings revealed that the Bak-CTS can selectively bind direct activators but not sensitizer BH3-only proteins. We also confirm that the Bak-CTS can bind to itself upon co-expressing the donor $^{mT2}CTS_{BAK}$ with the acceptor $^{mCitrine}CTS_{BAK}$ fusion proteins in BMK DKO, yielding an apparent K_D of 11-12 μM (Figure 2.3-Figure supplement 1E). To determine if CTS-binding by BH3-only proteins is unique for Bak, we conducted FLIM-FRET experiments to test the binding of ^{V}BH3-only proteins to the Bax-CTS ($^{mT2}CTS_{BAX}$), which localizes to the MOM similarly to $^{mT2}CTS_{BAK}$ in BMK DKO cells (Beigl *et al.*, 2024). Unlike $^{mT2}CTS_{BAK}$, $^{mT2}CTS_{BAX}$ did not bind to ^{V}BimL (Figure 2.3F) despite their subcellular localization at the MOM. Similarly, the sensitizer proteins ^{V}Bad, ^{V}Bik, and ^{V}Noxa exhibited collisional interactions with $^{mT2}CTS_{BAX}$. In contrast to ^{V}BimL and the sensitizer proteins, ^{V}tBid was found to bind $^{mT2}CTS_{BAX}$ with a K_D value of 6.6 μM (Figure 2.3F).

To ensure that the differences in Bak-/Bax-CTS-binding among the ^{V}BH3-only proteins, as discovered in our FLIM-FRET experiments, were not due to dissimilar subcellular localization of the exogenously expressed Venus-fusion proteins, we stained the transfected

BMK DKO cells stably expressing $^{mT2}CTS_{BAK}$ with MitoTracker Red and measured the Pearson correlation coefficients (Pearson's r) for the colocalization of the ^{V}BH3-only proteins (Green channel) to MitoTracker Red (Red Channel) (Figure 2.3 – Figure supplement 2A) or to $^{mT2}CTS_{BAK}$ (Figure 2.3 – Figure supplement 2B and 2C). We found no significant differences in colocalization to MitoTracker Red or $^{mT2}CTS_{BAK}$ between ^{V}tBid, ^{V}BimL, ^{V}Bad, and ^{V}Bik as their median Pearson's r were all approximately 0.1. On the other hand, Venus by itself or CTS-truncated BimL (^{V}BimL-ΔCTS) had a median Pearson's r of 0, suggesting that both Venus and BimΔCTS were localized to the cytoplasm in cells. The colocalization data confirms that the differences in Bak-/Bax-CTS-binding of different ^{V}BH3-only proteins to $^{mT2}CTS_{BAK}$ and $^{mT2}CTS_{BAX}$ were not due to any detectable differences in their subcellular colocalization. Altogether, our FLIM-FRET data demonstrates the binding of Bak-CTS to ^{V}BimL and ^{V}tBid. This is the first report of the direct binding between direct activator BH3-only proteins and the CTS of Bak.

2.4.7 The Bid BH3 region is not required for tBid to bind to the CTS of Bak

Scrambling of the Bak-CTS likely impacts Bak dimerization and oligomerization, thereby diminishing its mitochondrial permeabilizing function upon adding cBid. Such mutation in the Bak-CTS also impaired binding to cBid (or tBid). This suggests that during the initial step of Bak activation, Bak-CTS is involved in the binding to direct activators independently of the BH3-binding pocket binding to Bid or Bim-BH3 motifs. To test this hypothesis, we examined the binding of ^{V}tBid and ^{V}tBid BH3 mutants to $^{mT2-}CTS_{BAK}$ using FLIM-FRET (Figure 2.4). The results highlighted that ^{V}tBid BH3 mutants (4E, I82A, and I83A) still bound to $^{mT2}CTS_{BAK}$ like ^{V}tBid with the apparent relative K_D values ranging from 7 to 9 µM (Figure 2.4A and 4B), showing no effect of the BH3 mutations on binding to Bak-CTS in BMK DKO. We also found similar colocalization of ^{V}tBid and ^{V}tBid BH3-h0 mutants with MitoTracker Red (Figure 2.4 – Figure Supplement 1A) or to $^{mT2-}CTS_{BAK}$ (Figure 2.4 – Figure Supplement 1B). Scrambling the Bak-CTS in $^{mT2}CTSscr_{BAK}$ prevented the binding to ^{V}tBid or any ^{V}tBid BH3 mutants (Figure 2.4 – Figure Supplement 1C). These data strongly indicate that the Bid BH3 motif is dispensable for binding ^{V}tBid to $^{mT2-}$CTS$_{BAK}$.

Following this result, we hypothesized that a mutation in the BH3-binding pocket of full-length Bak (G126S) that prevents the binding of BH3 motifs thereby disabling Bak activation, should not affect the binding of ^{V}tBid to the Bak-CTS (Dai *et al.*, 2011; Ye *et al.*, 2020). Thus, the HCT116 DKO cell line expressing Bak G126S mutant fused N-terminally to mCerulean3 (^{C}Bak G126S) was created for the FLIM-FRET experiments with transient expression of ^{V}tBid, ^{V}tBid-4E, or ^{V}Bad. We found that ^{V}tBid and ^{V}tBid-4E but not ^{V}Bad bound ^{C}Bak G126S with the apparent relative K_D of 24 and 37 μM, respectively (Figure 2.4C). Intriguingly, we detected binding of ^{V}tBid but not ^{V}tBid-4E or ^{V}Bad to ^{C}BakΔCTS G126S by FLIM-FRET (Figure 2.4 – Figure supplement 1D). This data implied that the G126S mutation did not entirely abolish the binding of Bid BH3 to the BH3-binding pocket of ^{C}BakΔCTS. Importantly, we showed that transient expression of ^{V}tBid or ^{V}tBid-4E did not affect the viability or survival of HCT116 DKO cells stably expressing ^{C}Bak G126S (Figure 2.4-Figure supplement 2A-C) as compared to non-transfected ^{C}Bak G126S-expressing HCT116 DKO cells. This affirmed that the G126S mutation in the BH3-binding pocket of Bak impaired its pro-apoptotic function. Collectively, our data support a model in which the Bak-CTS functions independently of the BH3-binding pocket of Bak, acting as a secondary binding site that interacts with a non-BH3 region in ^{V}tBid.

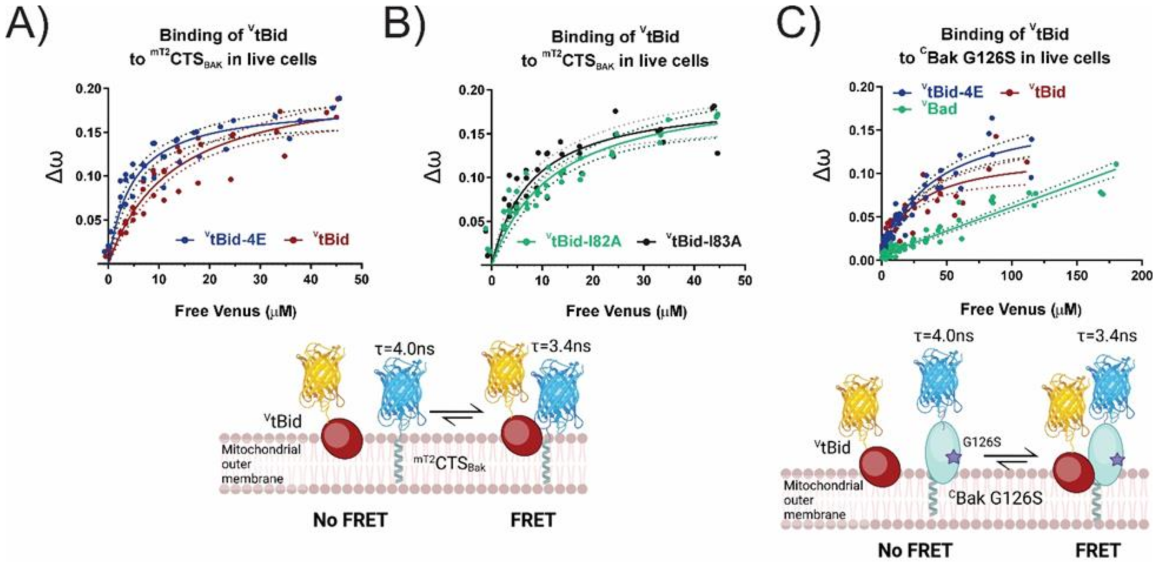

Figure 2.4. The binding of Bak-CTS to Bid is independent of Bid BH3. (A) FLIM-FRET analysis of ^{V}tBid and ^{V}tBid-4E binding to ^{mT2}CTS$_{BAK}$ in BMK DKO cells. Mutating h1, h2, h3, and h4 residues in the BH3 motif of Bid (^{V}tBid-4E) did not abolish binding to ^{mT2}CTS$_{BAK}$, but instead yielded a binding curve that was fitted to the Hill-equation (h=1) with an apparent K_D of 4.7 µM. Data represent three technical replicates. Figure 2.4 – Figure supplement 3 A and B show an independent replicate of the experiment in Panel A and B, respectively. **(B)** Binding of ^{V}tBid I82A and ^{V}tBid I83A mutant to ^{mT2}CTS$_{BAK}$ showed similar K_D values (~8–12 µM) compared to ^{V}tBid binding, indicating that mutations in the h0 residues of Bid did not affect the binding to the Bak-CTS. Data represent three technical replicates. **(C)** FLIM-FRET analysis of ^{V}tBid, ^{V}tBid-4E, and ^{V}Bad examined their binding to mCerulean3-N-terminally fused full-length Bak with a G126S mutation in the BH3-binding pocket (^{C}Bak G126S). ^{V}tBid and ^{V}tBid-4E bound ^{C}Bak G126S with apparent K_D values of 24 and 37 µM, respectively, while ^{V}Bad exhibited collisional interactions (s-ratio <2). Results from two additional independent replicates were combined and shown in Figure 2.4—Figure Supplement 3C.

2.4.8 The Bim-CTS binds to the BAK-CTS

As BimL can bind to the Bak-CTS and activate Bak, albeit requiring a higher concentration than cBid, we investigated where this binding interface is located on BimL. Previously we found that the membrane-binding carboxyl terminal sequence (CTS) of Bim can interact with Bcl-XL (Liu *et al*, 2019) and Bax (Chi *et al.*, 2020). Thus, we hypothesized that the Bim-CTS could interact with Bak-CTS and that it is required for BimL-mediated Bak activation. To test this hypothesis, we generated mutants of BimL where the Bim-CTS is truncated (ΔCTS), scrambled (-CTSscr), or mutated (Figure 2.5A). We then tested the binding of these ^{V}BimL mutants to $^{mT2}CTS_{BAK}$ using FLIM-FRET. We also created a Venus-Bim-CTS fusion construct ($^{V}CTS_{BIM}$) to test the direct binding of the Bim-CTS to the Bak-CTS as $^{V}CTS_{BIM}$ does not contain the Bim BH3 motif or any other regions of BimL. We found that both ^{V}BimL (grey) and $^{V}CTS_{BIM}$ (purple) bound to $^{mT2}CTS_{BAK}$ with apparent K_D of 9 and 13 μM, respectively (Figure 2.5B). Mutating Bim-BH3 with 4E does not affect ^{V}BimL binding to $^{mT2}CTS_{BAK}$ (In red). On the other hand, scrambling Bim-CTS abolishes the binding of full-length BimL (^{V}BimL-CTSscr in light orange) or the Bim-CTS by itself ($^{V}CTSscr_{BIM}$ in dark green) to $^{mT2}CTS_{BAK}$. Likewise, scrambling the Bak-CTS abolished binding to ^{V}BimL and $^{V}CTS_{BIM}$ (Figure 2.5 – Figure Supplement 1A). Notably, the triple mutations V194K, L195S, and V198D in Bak-CTS (^{mT2}CTS-KSD_{BAK}) did not affect the binding of ^{V}BimL or $^{V}CTS_{BIM}$ (Figure 2.5 – Figure Supplement 1 B and C). To ensure that the lack of binding to the Bim-CTSscr mutant is not due to improper subcellular localization caused by the scrambled mutation, we imaged $^{mT2}CTS_{BAK}$ BMK DKO cells stained with MitoTracker Red and transfected with ^{V}BimL, ^{V}BimL-CTSscr, or ^{V}BimΔCTS for fluorescence colocalization microscopy. We found that scrambling the Bim-CTS, unlike truncating the Bim-CTS (^{V}BimΔCTS), did not significantly change its mitochondrial colocalization as compared to ^{V}BimL as reflected by their similar Pearson's r of ~0.1 (Figure 2.5- Figure supplement 1D). Additionally, $^{V}CTS_{BIM}$ did not bind to the mitochondria-localized membrane-binding region of ActA ($^{C}CTS_{ActA}$) (Figure 2.5 – Figure Supplement 1E), confirming that the direct binding observed between $^{V}CTS_{BIM}$ and $^{mT2}CTS_{BAK}$ was not a result of their colocalization to the MOM. Crucially, ^{V}BimL-CTSscr can still induce Bax/Bak-dependent cell death in primed BMK cells (Figure 2.5 – Figure Supplement 1F), validating that it can act as a sensitizer due to its intact BH3 motif and that the Bim-CTS is not required for Bim to bind anti-apoptotic proteins.

Next, we employed a chimeric Bad mutant where Bad-CTS is replaced by Bim-CTS (^{V}BadΔCTS-BimCTS) to verify the binding of the Bim-CTS to the Bak-CTS in a different ^{V}BH3-only protein (Figure 2.5C). ^{V}Bad has a high collisional rate to $^{mT2}CTS_{BAK}$ as indicated by the straight line (dark blue) that increased steeply with higher amount of free

Venus. Significantly, ^{V}BadΔCTS-Bim-CTS (light blue) bound to $^{mT2}CTS_{BAK}$ with a K_D of 14 μM, similar to that of $^{V}CTS_{BIM}$. In contrast, ^{V}BimΔCTS did not bind to $^{mT2}CTS_{BAK}$ (brown) and localizes significantly less to the mitochondria compared to ^{V}BimL, as shown by a near 0 Pearson's r value for colocalization with MitoTracker Red (see above). The binding data illustrated that Bim-CTS is necessary and sufficient for binding to Bak-CTS.

We then screened multiple cancer-associated missense mutations, as found on cBioportal (Cerami *et al*, 2012; de Bruijn *et al*, 2023; Gao *et al*, 2013), in the Bim-CTS to identify a point mutation that blocks the binding of ^{V}BimL to $^{mT2}CTS_{BAK}$ but does not impair the localization of ^{V}BimL to mitochondria (Figure 2.5D and Figure 2.5 - Figure Supplement 2A-C). Of the five mutants tested, ^{V}BimL-R134L is the only one that localized to the mitochondrial membranes, similar to ^{V}BimL (Figure 2.5 - Figure supplement 2C), and did not bind to $^{mT2}CTS_{BAK}$ (Figure 2.5D). Other point mutants of Bim-CTS either had no effects on binding to $^{mT2}CTS_{BAK}$ (I125V and M123I) or did not localize to the mitochondria (R130L and I132N). This suggests that the cancer-associated mutation R134L potentially affects BimL-mediated Bak activation by disrupting the interaction between Bim-CTS and Bak-CTS. Overall, our colocalization and binding data indicate that there is no correlation between mitochondrial localization and binding to Bak-CTS, as the ^{V}BH3-only protein fusion proteins were localized to multiple subcellular compartments when overexpressed in the FLIM-FRET experiments. Importantly, we show that cancer-associated mutation in the Bim-CTS can impair its binding to the CTS of Bak.

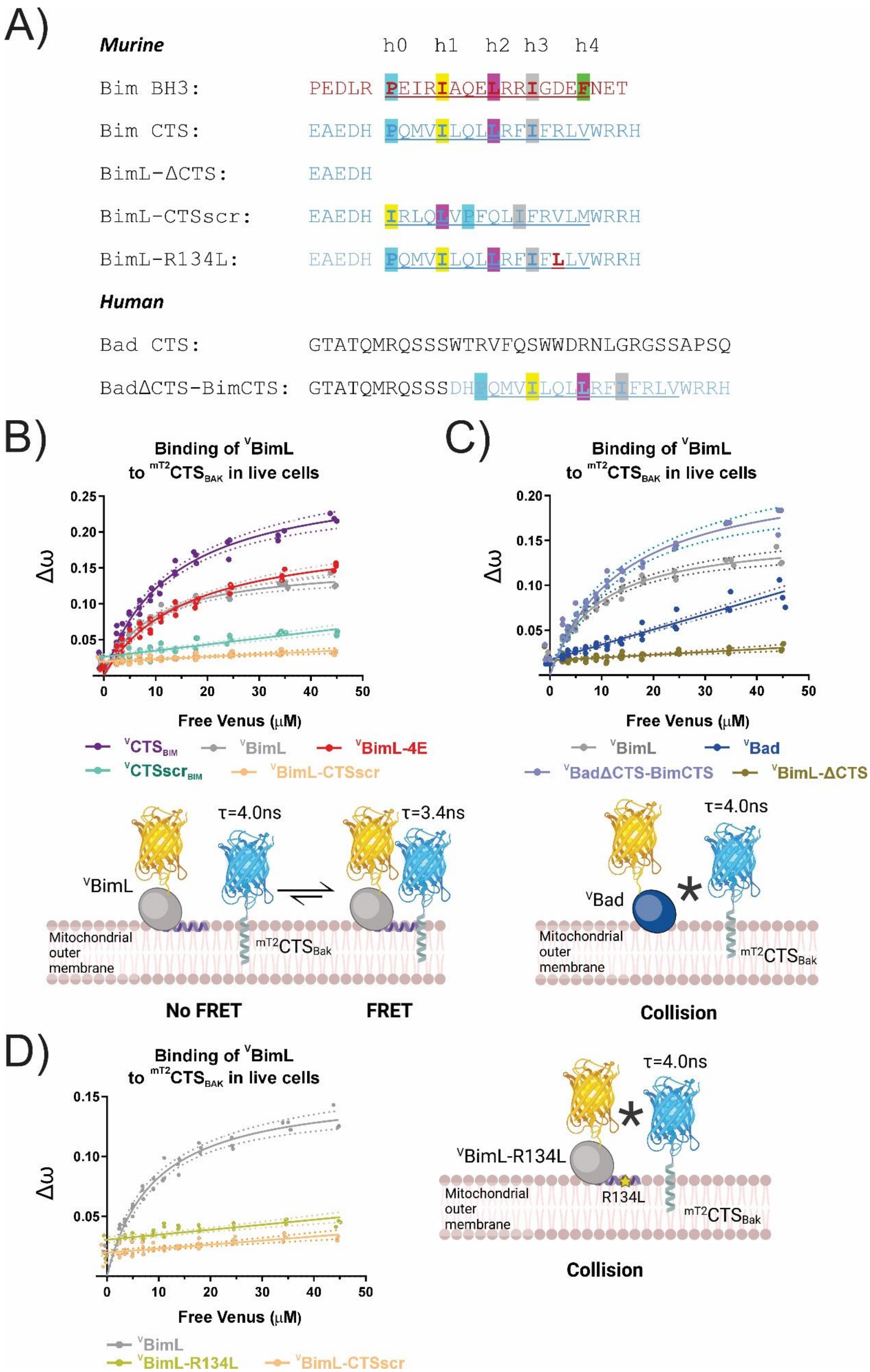
A)
Murine
h0 h1 h2 h3 h4
Bim BH3: PEDLR PEIRIAQELRRIGDEFNET
Bim CTS: EAEDH PQMVILQLLRFIFRLVWRRH
BimL-ΔCTS: EAEDH
BimL-CTSscr: EAEDH IRLQLVPFQLIFRVLMWRRH
BimL-R134L: EAEDH PQMVILQLLRFIFLLVWRRH
Human
Bad CTS: GTATQMRQSSSWTRVFQSWWDRNLGRGSSAPSQ
BadΔCTS-BimCTS: GTATQMRQSSSDHPQMVILQLLRFIFRLVWRRH
B)
Binding of VBimL to mT2CTSBAK in live cells
Δω
Free Venus (μM)
VCTSBIM
VBimL
VBimL-4E
VCTSscrBIM
VBimL-CTSscr
τ=4.0ns
τ=3.4ns
VBimL
Mitochondrial outer membrane
mT2CTSBak
No FRET
FRET
C)
Binding of VBimL to mT2CTSBAK in live cells
Δω
Free Venus (μM)
VBimL
VBad
VBadΔCTS-BimCTS
VBimL-ΔCTS
τ=4.0ns
VBad
Mitochondrial outer membrane
mT2CTSBak
Collision
D)
Binding of VBimL to mT2CTSBAK in live cells
Δω
Free Venus (μM)
VBimL
VBimL-R134L
VBimL-CTSscr
τ=4.0ns
VBimL-R134L
R134L
Mitochondrial outer membrane
mT2CTSBak
Collision

Figure 2.5. The Bim-CTS directly binds to the Bak-CTS. (A) Schematic of murine BimL showing the alignment of Bim-BH3 and Bim-CTS murine sequences, which share homology at h0, h1, h2, and h3 residues but not h4. Negative controls include BimΔCTS (lacking residues 120–140), Bim-CTSscr (scrambled CTS residues 121–136), and the cancer-associated R134L mutant. Human Bad and a chimeric Bad protein (BadΔCTS-BimCTS) are included for comparison. **(B)** FLIM-FRET microscopy revealed that Bim-CTS ($^{V}CTS_{BIM}$) bound to $^{mT2}CTS_{BAK}$ with an apparent K_D of 13 μM (Hill equation fit, h = 1). Full-length ^{V}BimL (K_D = 9 μM) and ^{V}BimL-4E (K_D = 16 μM) also bound $^{mT2}CTS_{BAK}$, confirming that the Bim BH3 is not required for binding $^{mT2}CTS_{BAK}$. Scrambling CTS in full-length Bim (^{V}BimL-CTSscr) or isolated CTS ($^{V}CTSscr_{BIM}$) abolished binding, with insufficient Δω (BMAX = 0.04, $R^2 = -0.7$ for ^{V}BimL-CTSscr; s-ratio < 2 for $^{V}CTSscr_{BIM}$). Binding data for ^{V}BimL-CTSscr and $^{V}CTSscr_{BIM}$ were thus fitted to a linear equation which indicate collisions. Data represent three technical replicates; an independent replicate is shown in Figure 2.5—Figure Supplement 3A. **(C)** ^{V}Bad did not bind $^{mT2}CTS_{BAK}$ (linear fit, s-ratio = 1.1, R^2 = 0.8). Replacing the Bad-CTS with Bim-CTS (^{V}BadΔCTS-BimCTS) restored binding (K_D = 14 μM, s-ratio = 2.2). Truncating the Bim-CTS (^{V}BimΔCTS) eliminated binding to $^{mT2}CTS_{BAK}$ (linear fit, s-ratio = 1.3). Data represent three technical replicates; an independent replicate is shown in Figure 2.5—Figure Supplement 3B. **(D)** The R134L mutation in Bim-CTS (^{V}BimL R134L) abolished binding to $^{mT2}CTS_{BAK}$, with insufficient FRET and low Δω (BMAX < 0.05, R^2 = 0.2, Hill equation fit, h = 1). Data represent three technical replicates; an independent replicate is shown in Figure 2.5—Figure Supplement 3C.

2.4.9 The Bim-CTS is required for the efficient activation of Bak

To evaluate the functional effect of ^{V}BimL-R134L, ^{V}BimL-CTSscr, ^{V}BimL-ΔCTSmutants in cells with Bak but not Bax, we transiently expressed ^{V}BimL or ^{V}BimL mutant in BMK DKO cell line stably expressing rtTA3 and the full-length ^{C}Bak fusion protein under a Doxycycline-inducible promoter (Tet-ON system) (Das *et al*, 2016; Gossen *et al*, 1995) (Figure 2.6A and B). In cells positive for Venus and mCerulean3, cell death induced by Bak activation was scored by Nucview 530 Caspase 3 substrates, which accumulate in the nucleus of dead cells. Upon addition of Doxycycline, we observed that 70-80% of cells with both ^{V}BimL and ^{C}Bak were positive for caspase 3 activation and were scored as dead cells. Mutating Bim BH3 (2.4E), scrambling, or truncating the Bim-CTS reduced %dead cells to ~30%. Introducing the R134L cancer-associated mutation to Bim-CTS abrogated the Bak-activating function of BimL, reducing the % cell death to approximately 10-15%, similar to the negative control Venus. Bad functions as a sensitizer protein and does not activate Bax or Bak (Letai *et al.*, 2002). However, we observed that the Bad chimera containing Bim-CTS could bind to Bak-CTS in cells. To investigate whether the Bim-CTS alone could activate Bak when substituted for Bad-CTS, we tested the ^{V}BadΔCTS-BimCTS construct in the cell death assay. Our results showed that ^{V}BadΔCTS-BimCTS did not enhance Bak-dependent cell death in Tet-inducible ^{C}Bak BMK DKO cells compared to ^{V}Bad, with both constructs inducing only 20 to 30% cell death. Importantly, in this system, the addition of Doxycycline induced ^{C}Bak expression at a low level, which did not cause significant cell death imparted by Bak autoactivation (data not shown). These findings confirm that the BH3 motif of BimL is necessary for Bak activation and suggest that the Bim-CTS alone is insufficient to trigger Bak activation.

We then conducted an *in-vitro* Bak activation assay with the terbium-encapsulated liposomes to verify the cell death data. Scrambling BimL-CTS abrogated BimL-mediated activation of Bak in the terbium release liposome assay with 100 nM full-length Bak (Figure 2.6C). Furthermore, using a recombinant chimera BimL with the Bad BH3 replacing Bim BH3 from residue h1 (I90 in murine BimL equivalent to Y110 in human Bad) to residue h4+3 (T104 in murine BimL equivalent to S124 in human Bad), we showed that BimL (Bad BH3 h1-h4+3) chimera did not activate Bak similarly to BimL-CTSscr, confirming that the Bim BH3 is required for BimL-mediated Bak activation. Crucially, the differences in Bak-activating activity between BimL and BimL-CTSscr were unlikely due to differences in binding to liposomes as purified recombinant A568-labeled BimL and BimL-CTSscr have similar liposome binding activity (Figure 2.6D). By using gel-filtration chromatography, 11% BimL and 9% BimL-CTSscr were shown to be eluted in the liposome fraction, whereas only 2-3% of BimLΔCTS were eluted in the same fraction as the liposomes. We concluded that scrambling the Bim-CTS did not impair the binding of BimL to the liposomes and that the Bim-CTS together with the Bim BH3 are both necessary to activate Bak.

We conclude that both the Bim-BH3 and the Bim-CTS are necessary to activate Bak. Bim-CTS by itself is sufficient for binding to Bak-CTS but is not for Bak activation. Altogether, our functional data in cells and with liposomes validate the FLIM-FRET binding data, supporting the role of Bim-CTS in Bak activation via direct binding to the Bak-CTS to form a secondary binding site in addition to the Bim BH3 binding interface with BH3-binding groove of Bak.

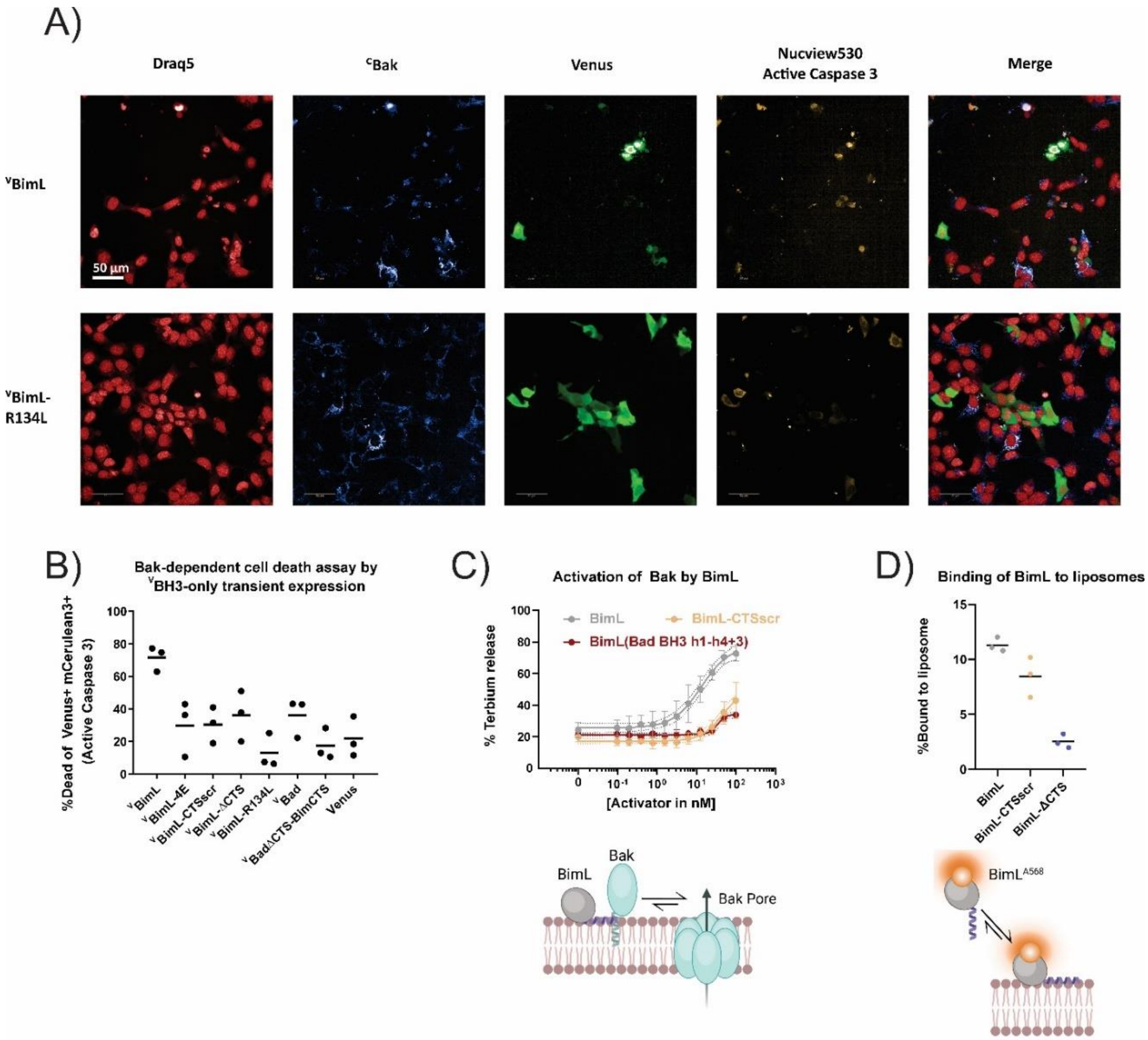

Figure 2.6. Bim CTS is necessary for BimL to activate Bak. (A) Representative images of BMK DKO cells expressing Dox-inducible ^{C}Bak and transfected with ^{V}BimL or ^{V}BimL-R134L, showing caspase-3 activation (NucView530 intensity) as a marker of cell death. **(B)** Cell death assay in ^{C}Bak-expressing BMK DKO cells demonstrates reduced cell death with ^{V}BimL mutants lacking an intact BH3 domain (4E), scrambled CTS (-CTSscr), or deleted CTS (ΔCTS). The cancer-associated R134L mutation (^{V}BimL-R134L) also significantly impaired cell death. Other constructs used in this experiment, including the negative control Venus, similarly did not induce significant cell death in cells expressing ^{C}Bak. Data from 3 independent replicates are shown with the solid line representing the mean %Dead of cells co-expressing ^{C}Bak and the indicated ^{V}BH3-only protein construct.

(C) Scrambling the Bim-CTS (BimL-CTSscr in light orange) reduced Bak activation by recombinant BimL in a terbium-release liposome permeabilization assay with 100 nM recombinant full-length Bak. Similarly, a BimL chimera mutant with Bad BH3 (BimL(Bad BH3 h1-h4+3) in dark red) failed to activate Bak with an increase in EC_{50} value and a decrease in maximal release. The data point represents an average of 6 independent replicates for BimL/BimL-CTSscr and 4 independent replicates for BimL (Bad BH3 h1-h4+3) **(D)** Scrambled the Bim-CTS mildly reduced the binding of A568-BimL to MOM-like liposomes, as shown by size-exclusion chromatography, while ΔCTS eliminated liposome binding. Data from 3 independent experiments are shown with the solid line indicating the mean.

2.4.10 The Bim-CTS and not membrane-binding is required for binding and activating full-length Bak

As we observed direct binding of the Bim-CTS to the Bak-CTS and that the Bim-CTS is required for effective Bim-mediated activation of Bak, we next examined if the Bim-CTS by itself can bind to full-length Bak in cells and if such binding is dependent on the Bim BH3 and the BH3-binding pocket of Bak. To this end, we expressed $^{V}CTS_{BIM}$ in HCT116 DKO cells stably expressing the inactive ^{C}Bak G126S or ^{C}BakΔCTS G126S mutant. We found that $^{V}CTS_{BIM}$ but not $^{V}CTSscr_{BIM}$ bound to ^{C}Bak G126S (Figure 2.6 – Figure Supplement 1A). Truncating the Bak-CTS eliminated the binding of Bak to both $^{V}CTS_{BIM}$ and $^{V}CTSscr_{BIM}$ (Figure 2.6 – Figure Supplement 1B). Furthermore, consistent with our binding data using $^{mT2}CTS_{BAK}$, ^{V}BimL-4E with the mutated BH3 still bound full-length ^{C}Bak G126S comparable to ^{V}BimL. In contrast, scrambling the Bim-CTS or introducing the R134L mutation was sufficient to abolish binding to ^{C}Bak G126S (Figure 2.6 – Figure Supplement 1C). Overall, our FLIM-FRET data indicate that the Bim BH3 and the BH3-binding pocket of Bak are not required for the Bim-CTS to bind full-length Bak.

Because the Bim-CTS has dual functions mediating both membrane binding and protein-protein interaction, it is vital to separate between these two functions when we study the role of Bim-CTS in Bak activation. For this purpose, we created a BimL chimera, where we replaced Bim-CTS with the carboxyl terminal membrane-binding sequence of the tail-anchor Monoamine oxidase (MAO) protein (BimΔCTS-MAO). The BimΔCTS-MAO chimera was shown to bind liposomes and isolated mitochondria but could not activate Bax

(Chi *et al.*, 2020). Here, we found that recombinant BimΔCTS-MAO did not activate Bak in the terbium release liposome permeabilization assay compared to BimL (Figure 2.6 – Figure Supplement 1D) as indicated by a low % terbium release (~20-30%) which was unchanged with increasing amount of BimΔCTS-MAO. This confirms that the Bim-CTS but not membrane-binding is required for Bim-mediated Bak activation.

2.5 Discussion

Activation of Bak by BH3-only proteins requires the binding of BH3 sequences of activators to the BH3-binding pocket of Bak. In this study, we demonstrate that BimL is less efficient than cBid in activating Bak (Figure 2.1A and B). These results are consistent with previous data (Sarosiek et al., 2013) where cBid preferentially activates Bak to release cytochrome C from isolated heavy membranes (enriched in mitochondria without detectable Bax) isolated from WT mouse livers (Letai et al., 2002). To examine if the inefficient Bak activation by BimL but not cBid is due to insufficient binding, we performed FRET assay using labeled single-cysteine recombinant Bak, cBid, and BimL proteins. However, we found that, unlike A568-cBid, A568-BimL had low FRET efficiency with A647-Bak while both had similar K_D. Because of this low FRET dynamic range for recombinant BimL and Bak that made it difficult to differentiate binding from collisions, we switched to using FLIM-FRET microscopy to acquire relative apparent K_D for these proteins in live cells.

To figure out whether the differences in the BH3 motifs of Bid and BimL can explain the differences in their Bak-activating activity, we performed FLIM-FRET using different BH3-swapped chimera mutants of Bid and BimL (Figure 22. and Figure 2.2 – Figure Supplement 2). We demonstrated the preference and selectivity of the BH3-binding pocket of Bak to Bid BH3 but not to Bim BH3 using exogenously expressed ^{C}BakΔCTS, which does not become activated to induce MOMP (Figure 2.1F and 2.1G). Specifically, we identified the region of h0 residues (I82 and I83) in Bid BH3 as necessary for ^{V}tBid to bind ^{C}BakΔCTS (Figure 2.2B and Table 2.1). Furthermore, replacing h0 residues of BimL with that of Bid removes the selective binding ^{V}BimL has for ^{C}BaxΔCTS over ^{C}BakΔCTS and enhances the binding affinity between ^{V}BimL and ^{C}BakΔCTS. In other words, our data demonstrate that Bid h0 residues, when inserted into Bim BH3, are sufficient to increase the binding affinity of ^{V}BimL to ^{C}BakΔCTS.

Our FP data with stapled Bid BH3 peptides (Bid SAHB) aligns with the FLIM-FRET data using full-length tBid, which shows that both I82 and I83 are necessary for binding to Bak (Figure 2.2 – Figure Supplement 1). However, I83A mutation affects the binding of Bid SAHB to BaxΔCTS in the cell-free FP assay but not ^{V}tBid to ^{C}BaxΔCTS in FLIM-FRET. This suggests that full-length tBid might have other non-BH3 regions aiding the Bid BH3 in Bax binding, thereby overcoming the negative effect of the I83A mutation on tBid-Bax interaction.

Although the exact reason why cBid is significantly more potent than BimL at activating Bak remains unclear, it is unlikely to be solely due to the differences in their BH3 motifs, despite these sequences having different binding affinities to the BH3-binding pocket of Bak. This was apparent when examining the Bak activation by cBid h0 mutants in the *in vitro* liposome assay. Mutating one or both h0 residues of cBid into alanine lowers but does not abolish cBid-mediated Bak activation as measured by the cell-free terbium release liposome permeabilization assay with recombinant cBid and full-length Bak (Figure 2.2D and Figure 2.2 – Figure Supplement 2C). Similarly, replacing the Bim BH3 with Bid BH3 or replacing Bim h0 regions with that of Bid does not significantly enhance BimL-mediated Bak activation (Figure 2.2E). These results suggest that the additional binding affinity conferred by the h0 region of Bid BH3 to the BH3-binding pocket of Bak is not sufficient to enhance Bak activation and that there must be other regions outside the Bid BH3 that, together with the BH3, account for the potency of Bid at activating Bak.

The CTS of Bak has been shown to play a role in Bak inhibition within Bak-VDAC2 high molecular weight complex (Lazarou *et al.*, 2010) as well as in Bak activation through mediating formation of high-order Bak oligomeric complex (Iyer *et al.*, 2015; Nguyen *et al*, 2024). Here, we demonstrate an additional role of Bak-CTS in its interaction with the activator BH3-only proteins Bid and Bim (Figure 2.3E). Importantly, we show that the Bak-CTS is required for efficient Bak activation by cBid (Figure 2.3B) beyond its role in binding Bak to the MOM (Figure 2.3D) as the Bak mutant with CTS scrambled can still be bound to isolated mitochondria but cannot be activated by cBid to cause MOMP. Nevertheless, we cannot rule out whether scrambling Bak-CTS did not affect Bak oligomerization, thereby reducing the pore-forming activity of activated Bak. On the other hand, we found that the binding of Bid to Bak-CTS is abolished if Bak-CTS is scrambled (CTSscr) in a construct expressing only the Bak-CTS (^{mT2}CTSBAK and ^{mT2}CTSscr$_{BAK}$) (Figure 2.3 – Figure Supplement 1B) or is reduced if Bak-CTS is scrambled in a full-length recombinant Bak (Figure 2.3C).

Furthermore, we showed that Bak-CTSscr can be recruited to the MOM via binding to cBid (Figure 2.3 – Figure Supplement 1A). Likely, the BH3-binding pocket in full-length Bak-CTSscr can still bind the Bid BH3 when they are co-recruited to the MOM. Altogether, our data support a model of Bak activation by Bid where the Bak-CTS binds the active p15 fragment of Bid (tBid), enabling the Bid BH3 to bind with high affinity to the BH3-binding pocket of Bak, inducing subsequent conformational changes in Bak for its eventual dimerization and oligomerization. Future studies are needed to elucidate the exact mechanism of how tBid binds Bak-CTS and where the binding interface locates on Bid. Such binding interface appears to be located outside the Bid BH3 region. This is evidenced by the fact that replacing the four key hydrophobic residues (h1–h4) in Bid BH3 with glutamic acid (4E) does not disrupt the binding to Bak-CTS (Figure 2.4A) or to full-length Bak with an inactivating mutation in its BH3-binding pocket (G126S) (Figure 2.4C). We hypothesize that this secondary binding site on Bid, which interacts with Bak-CTS and Bid BH3 binding to the BH3-binding pocket, enables highly efficient activation of Bak by cBid.

Nevertheless, like ^{V}tBid, ^{V}BimL can bind to ^{mT2}CTS$_{BAK}$ (Figure 2.3E) with very similar apparent K_D (Supplementary Table 3). Furthermore, we discovered that the Bim-CTS (^{V}CTS$_{BIM}$) directly binds Bak-CTS (Figure 2.5B) and is essential for BimL-mediated Bak activation (Figure 2.5E and G). This unexpected function of the Bim-CTS in Bak activation is independent of its membrane binding function as BimΔCTS-MAO, which binds liposome (Chi *et al.*, 2020), did not activate Bak (Figure 2.5 – Figure Supplement 3D). However, the binding of the Bim-CTS to Bak-CTS is not sufficient to activate Bak as Bim still requires its BH3 for Bak activation (Figure 2.5E and 2.5G). We conclude that both the Bim-BH3 and the Bim-CTS are necessary to activate Bak. Bim-CTS by itself is sufficient for binding to Bak-CTS but is not for Bak activation. Altogether, our functional data in cells and with liposomes validate the FLIM-FRET binding data, supporting the role of Bim-CTS in Bak activation via direct binding to the Bak-CTS to form a secondary binding site in addition to the Bim BH3. Our data suggest an 'avidity' model for BimL-mediated Bak activation where the Bim BH3 and Bim-CTS act as dual binding sites that engage Bak simultaneously at the BH3-binding pocket and the Bak-CTS, respectively. This dual-binding mechanism enables Bim to activate Bak despite the poor affinity of the Bim BH3 for Bak. Importantly, this Bak-activating mechanism by Bim is still not as efficient as the mechanism by which Bid activates Bak, as the EC_{50} for cBid is an order of magnitude lower than that of BimL.

Previous studies revealed that Bim-CTS binds to Bax and is essential for BimL-induced Bax activation (Chi *et al.*, 2020). Evidence from bismaleimidohexane (BMH) cross-linking with single-cysteine BimL (M123C or W137C) and Bax (W107C in helix α5) supports that Bim-CTS binds to the canonical groove of Bax (Chi *et al.*, 2020). However, since BMH is 13 Å long, the precise binding site of Bim-CTS on Bax remains unclear. Our FLIM-FRET data indicate that Bim-CTS does not bind to the Bax-CTS (Figure 2.3F, Supplement 3E) but instead binds to the Bak-CTS (Figure 2.3E, Figure 2.5A). This suggests that the pro-apoptotic function of Bim-CTS varies depending on the executioner protein target of BimL. The mechanism of the Bim-CTS binding to both the Bak-CTS and the BH3-binding pocket of Bax remains elusive, necessitating further studies to elucidate this interaction and its role in activating Bak and Bax.

We demonstrate that the cancer-associated R134L mutation in Bim-CTS (^{V}BIML-R134L) abolished its binding to Bak-CTS (Figure 2.5D) but did not affect the localization of BimL to mitochondria (Figure 2.5 – Figure Supplement 2C). This mutation significantly reduced ^{V}BimL-induced cell death in a Bak-dependent manner (Figure 2.5G). This finding has important implications for cancer therapy as chemotherapeutic agents like paclitaxel (Sunters *et al*, 2003; Tan *et al*, 2005) and doxorubicin (Yang *et al*, 2016) rely on Bim to induce apoptosis in cancer cells. BimL can also promote apoptosis by inhibiting anti-apoptotic proteins such as Bcl-XL and Bcl-2. Although Bim-CTS is not required for BimL to inhibit these proteins, it does bind a secondary site on Bcl-XL, forming a ‘double-bolt’ lock with Bim-BH3 at the primary binding site in the BH3-binding pocket. This confers resistance to BH3-mimetics displacement of ^{V}BimL from ^{C}Bcl-XL (Liu *et al.*, 2019). It remains unknown if the R134L mutation disrupts the binding interface between Bim-CTS and Bcl-XL. It would be important for future studies to investigate the effect of the R134L mutation on the direct activation of Bax. If the cancer mutations in the Bim-CTS reduce but do not completely abolish Bax or Bak activation, transcriptional induction of mutant Bim by chemotherapy could potentially cause non-lethal “minority MOMP” (Ichim *et al*, 2015) where a small number of mitochondria undergo MOMP without killing the cells as Bax and Bak are sub-optimally activated. This limited form of MOMP, which can be caused by sub-lethal doses of tBid, can trigger low-level caspase activation that leads to DNA fragmentation by caspase-activated DNase causing DNA damage and genomic instability. Such deleterious effects on the genomes of cancer cells can further drive oncogenesis and develop drug-resistant tumors.

In conclusion, our study reveals a novel mechanism for Bak activation involving Bid and Bim through their interactions with the Bak-CTS. We identified the Bim-CTS to directly bind Bak-CTS, creating a secondary binding site that is necessary but insufficient for BimL-mediated Bak activation (Figure 2.7). We also demonstrate that tBid can bind Bak-CTS through an unknown site outside the BH3 region of Bid and that the Bak-CTS is required for cBid-mediated Bak activation. This pro-apoptotic role of Bak-CTS, which is distinct from its membrane-binding function, represents a previously unknown mechanism by which Bak-CTS regulates Bak activation.

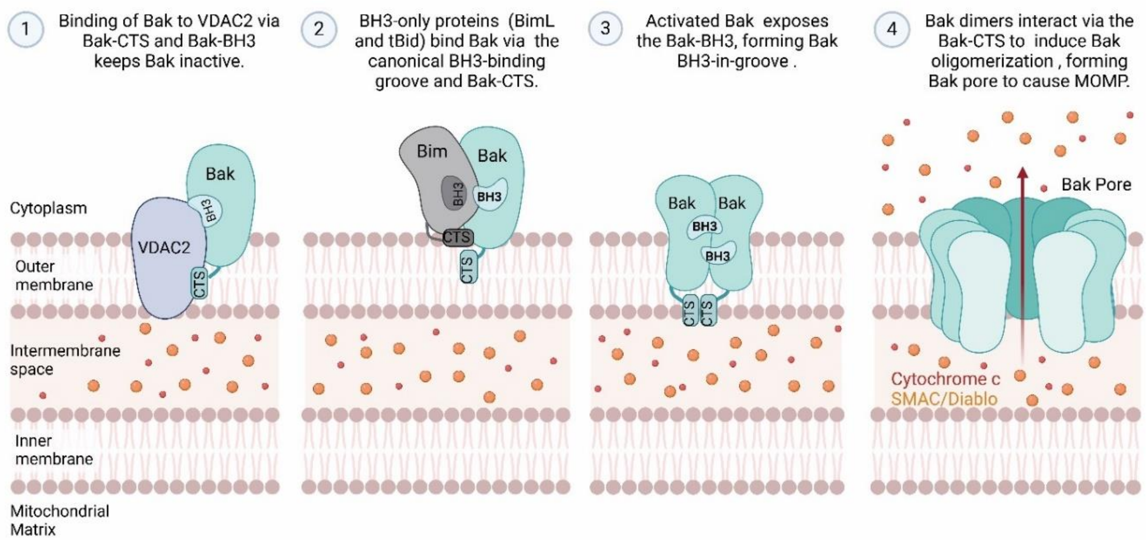

Figure 2.7. Model of Bak activation by BH3-only protein BimL. Inactive Bak at the MOM binds to VDAC2 via the Bak-CTS and Bak-BH3, keeping Bak inactivated (1). The direct activator BH3-only protein BimL (or tBid) binding to Bak via the Bak-CTS and the canonical BH3-binding groove displaces Bak from VDAC2. Specifically, the Bim-CTS of BimL interacts with Bak-CTS, while the Bim-BH3 binds the canonical BH3-binding groove, enhancing the binding avidity of BimL to Bak (2). This induces conformational changes that separate the core from the latch domain of Bak, leading to its homodimerization where the BH3-motif of one Bak is inserted into the BH3-binding groove of the second Bak, forming the Bak BH3-in-groove dimer (3). These Bak homodimers nucleate the formation of higher-order Bak oligomers where homotypic interactions between Bak-CTS potentially provide additional binding interfaces to expand the Bak pores and induce MOMP (4).

2.6 Methods

Key Resources Table

Reagent type (species) or resource	Designation	Source/Reference	Catalogue Identifier	Additional Information
Antibody	Antibody to GFP	Cell Signaling Technology	4B10	Dilution 1:1000
Antibody	Antibody to BAK	Cell Signaling Technology	D4E4	Dilution 1:1000
Antibody	Antibody to GAPDH	Cell Signaling Technology	14C10	Dilution 1:1000
Antibody	Donkey anti-rabbit (polyclonal)	Jackson Immuno Research Laboratories	Cat. #: 711-035-150	(1:40000) Dilution

Antibody	Donkey anti-mouse (polyclonal)	Jackson Immuno Research Laboratories	Cat. #: 711-035-152	(1:40000) Dilution
Cell line (M. musculus)	Baby mouse kidney - wild type (BMK-WT)	PMID: 11836241	N/A	Gift from E. White (Rutgers University, NJ)
Cell line (M. musculus)	Baby mouse kidney - BAK and BAX double knockout (BMK-DKO)	PMID: 11836241	N/A	Gift from E. White (Rutgers University, NJ)
Cell line (H. sapiens)	Human colorectal carcinoma – wild type (HCT-116 WT)	PMID: 9121588	CVCL_0291	Gift from B. Vogelstein (Johns Hopkins Sidney Kimmel Cancer Center, MD)
Cell line (H. sapiens)	Human colorectal carcinoma - BAK and BAX double knockout (HCT-116 DKO)	PMID: 11062132	CVCL_0291	Gift from B. Vogelstein (Johns Hopkins Sidney Kimmel Cancer Center, MD)
Cell line (H. sapiens)	Human embryonic kidney 293 cells (HEK293)	PMID: 886304	CVCL_0063	Gift from Frank Graham (McMaster University)
Recombinant protein	Alexa-647-conjugated AnnexinV	In house (PMID: 18314054)	N/A	Cellular death imaging
Peptides	TMR-labeled BID SAHB	Genscript (PMID: 17052454)	N/A	Custom stapled peptide for fluorescence assay
Chemical compound, drug	NucView® Caspase-3 Enzyme Substrates	Biotum	10406	Cellular death imaging
Chemical compound, drug	Hoescht 33258	ThermoFisher Scientific	Cat. # 4082S	Nuclear stain for live cell imaging
Chemical compound, drug	Draq5	ThermoFisher Scientific	Cat. #62251	Nuclear stain for live cell imaging
Chemical compound, drug	MitoTracker™ Green FM	ThermoFisher Scientific	M7514	Mitochondrial stain for live cell imaging
Chemical compound, drug	MitoTracker™ Red FM	ThermoFisher Scientific	M22425	Mitochondrial stain for live cell imaging
Chemical compound, drug	Q-VD-OPh	MedChemExpress	Cat. # HY-12305	Pan-caspase inhibitor
Chemical compound, drug	Alexa Fluor™ 647 C2 Maleimide	ThermoFisher Scientific	A20347	Protein labeling
Chemical compound, drug	Alexa Fluor™ 568 C_5 Maleimide	ThermoFisher Scientific	A20341	Protein labeling

Chemical compound, drug	*Trans*IT-X2® Dynamic Delivery System	Mirus bio	MIR 6000	Transfection reagent
Chemical compound, drug	PC (L-α-phosphatidylcholine)	Avanti Polar Lipids	Cat. #: 840051C	Phospholipids to synthesize liposomes
Chemical compound, drug	DOPS (1,2-dioleoyl-sn-glycero-3-phospho-L-serine)	Avanti Polar Lipids	Cat. #: 840035C	Phospholipids to synthesize liposomes
Chemical compound, drug	PI (L-α-phosphatidylinositol)	Avanti Polar Lipids	Cat. #: 840042C	Phospholipids to synthesize liposomes
Chemical compound, drug	PE (L-α-phosphatidylethanolamine	Avanti Polar Lipids	Cat. #: 841118C	Phospholipids to synthesize liposomes
Chemical compound, drug	TOCL, (18:1 Cardiolipin)	Avanti Polar Lipids	Cat. #: 710335C	Phospholipids to synthesize liposomes
Chemical compound, drug	Penicilin-streptomycin	Fisher Scientific	15140122	Cell culture media
Chemical compound, drug	Fetal bovine serum (FBS), Canada origin	Sigma	F1051	Cell culture media
Chemical compound, drug	Phosphate-buffered saline (PBS)	In-house (autoclaved)	N/A	Cell culture
Chemical compound, drug	Trypsin/EDTA (0.05%)	Wisent Bio Products	325-542 EL	Cell culture dissociation agent
Other	PhenoPlate™ 384-well microplate	Perkin Elmer	6057300	Live cell imaging
Other	Nonbinding surface 384-well black/clear flat bottom microplate	Corning	3544	Liposome assays with recombinant proteins
Other	Opera Phenix Plus High-Content Screening System	Perkin Elmer	HH14001000	Automated spinning disc confocal microscope used for live cell death assays
Other	INO-FHS	PMID: 35442739		Custom built by INO for DWA lab
Other	Infinite M1000	Tecan		Plate Reader
Software, algorithm	GraphPad Prism 9.5.0	GraphPad	https://www.graphpad.com/scientific-software/prism/	
Software, algorithm	MATLAB with toolboxes: Signal Processing, Image Processing, Curve Fitting, Version R2020a	MathWorks https://www.mathworks.com/products.html	RRID:SCR_00162	
Software, algorithm	Microsoft Excel 2010	Microsoft Corporation	www.microsoft.com/	
Software, algorithm	Harmony	PerkinElmer	https://www.perkinelmer.com/category/cellular-imaging-software	

Software, algorithm	Tecan i-control™	Tecan	https://lifesciences.tecan.com/plate_readers/infinite_200_pro?p=tab-3

Purification of Proteins

All recombinant proteins used in this study were expressed in Arabinose Induced (AI) *E. Coli* strain BL21-AI^{TM} (Life Technologies - Invitrogen, Carlsbad, CA). Bacterial cells were grown in Terrific Broth (TB) at 37ºC to an OD of 1.5 before inducing with Arabinose at 2g per Liter of culture. Induction was done overnight at 16ºC. For expressing all Bak constructs, 10 mM IPTG was added for induction, together with Arabinose. After the overnight induction, bacterial cultures were spun down at 500g for 30 minutes. Bacterial pellets were extracted and stored at -20ºC until purification. *E. Coli* cells expressing the constructs for BimL, Bid, Bax, and Bak were lysed in their respective lysis buffer by mechanical disruption with either a French press or a high-pressure homogenizer. All purified recombinant proteins were checked for purity on Coomassie Blue-stained SDS-PAGE gels.

Purification of murine His-tagged-BimL and BimL mutants was done as previously published (Liu *et al.*, 2019). Briefly, the Poly-Histidine sequence fused to the TEV protease recognition site (MHHHHHHGGSGGTGGSENLYFQGT) is present at the N-terminal of all recombinant BimL as they are left un-cleaved. The scrambled sequences of the carboxyl terminal of BimL was introduced in the BimL-CTSscr construct via PCR-directed fast cloning method [https://doi.org/10.1186/1472-6750-11-92 and https://doi.org/10.1371/journal.pone.0119221]. All recombinant BimL were purified using Nickle-NTA Affinity Chromatography followed by a High-Performance Phenyl Sepharose (HPPS) column. Final BimL elution was in a no-salt buffer and subsequently dialyzed against 10 mM HEPES pH 7, 20% Glycerol for 24-36 hours before flash-frozen.

Purification of murine PolyHis-tagged Bid and Bid mutants was carried out with Ni-NTA affinity chromatography as previously described (Kale *et al*, 2014). Cleavage of full-length

Bid to make cBid was done in 40 mM HEPES, 1mM EDTA, and 10 mM DTT using recombinant human caspase 8 (Enzo Life Sciences, Cat. #: BML-SE172-5000). After 48-56 hours of incubation with caspase 8, cBid is dialyzed against 10 mM HEPES, pH 7, 100mM NaCl, 0mM EDTA, and 10% Glycerol for 48 hours at 4ºC before flash frozen. Dialysis buffers for recombinant Bax and Bak were prepared using the same recipe as that for Bid. All recombinant cBid mutants and cBid WT were checked for cleavage efficiency by Coomassie Blue stained SDS-PAGE gel.

Purification of human Bax and the single-cysteine mutant of Bax (C126) was performed using chitin-affinity columns as previously published (Kale *et al.*, 2014). On-column cleavage to remove the chitin-binding domain (CBD) fused to Intein at the carboxyl terminal of Bax was done with 200mM Hydroxylamine at 4ºC for 48 hours. Bax cleaved off from the chitin column was collected and applied through a DEAE ion exchange column (DEAE Sepharose Fast Flow, Sigma-Aldrich, Cat. #: DFF100) to remove contaminant DNA before dialysis for 48 hours at 4ºC. Similarly, full-length human Bak with the triple mutations in Bak-CTS (V194K, L195S, V198D) with Intein-CBD fused to its carboxyl terminal was purified with a Chitin-Affinity column, followed by a DEAE ion exchange column and dialysis.

Protein-Labeling with Alexa Fluor™ Dyes

Single cysteine mutants of Bax (C62A) and Bak (C14A) were labeled with maleimide-conjugated Alexa Fluor™ 647 C_2 dye (ThermoFisher, Cat. #: A20347) using the same protocol that was previously described (Pogmore *et al.*, 2016). Labeling of single cysteine BimL (Q41C) and cBid with Alexa Fluor™ 568 C_5 (ThermoFisher, Cat. #: A20341) was done with the same protocol (Kale *et al.*, 2014) with the modification of adding 4M urea to the BimL-labeling buffer. Nickle-NTA columns were used to concentrate and remove the free dyes for both BimL and Bid, as these recombinant proteins have an N-terminal Poly-Histidine sequence. Further dialysis was carried out to remove the Urea from labeled BimL.

Terbium-Release Liposome Permeabilization Assay

A dry 2 mg lipid film with a molar composition resembling that of the MOM - 48% PC, 28% PE, 10% PI, 8% PS, and 6% Cardiolipin- was rehydrated with 1mL of the Assay Buffer containing 200mM KCl, 10mM HEPES pH 7, 1mM $MgCl_2$ supplemented with 1 mM $TbCl_3$, 3 mM dipicolinic acid (DPA). The lipid mixture underwent 10 freeze-thaw cycles and was extruded through a 0.1 µm pore-size membrane to ensure uniform liposome size. The resulting terbium liposomes were then applied to a 10 mL CL2B size-exclusion gel-filtration column to remove any unencapsulated Terbium:DPA complexes. Liposomes are collected in fractions 3 and 4, each measuring 1 mL mL. The 2 mL of collected terbium liposomes, now at a concentration of 1 mg/mL, were then diluted to 0.04 mg/mL for the liposome permeabilization assay using the assay buffer supplemented with 5 mM EDTA. Permeabilization of these liposomes by purified recombinant Bax or Bak releases DPA:Terbium into the EDTA-containing buffer outside the liposome, where EDTA chelates the terbium and quenches the fluorescence.

The terbium-release liposome permeabilization assay was carried out in a 384-well Corning plate (Cat. # 3544) without a cover. After adding proteins and liposomes to the wells, the 384-well plate was spun down using a microplate swinging bucket rotor for 30 seconds at 300g to ensure all the droplets were at the bottom of the wells. The setting of the plate reader (Tecan M1000), the assay set-up, and the data analysis were done as described previously, with the exception that the temperature was set to 30ºC instead of 37ºC to minimize evaporation (Bogner *et al*, 2020). In this assay, a fixed concentration of 100 nM Bak or Bax and an increasing amount of direct activator (cBid or BimL) were added to 0.04mg/mL of terbium-encapsulated liposomes.

Liposome binding Assay

Liposomes were prepared as described above. A568- or A647-labeled recombinant proteins at the specified concentrations were incubated with 0.2mg/mL liposomes for 1 hour at 37°C, then passed through a 2.5mL CL2B size-exclusion column. Twelve 250µL fractions were collected, and the fluorescence intensity of each fraction was measured using a Tecan M1000 plate reader. The fluorescence intensities of fractions 3 and 4 (containing the liposomes) were combined and divided by the total fluorescence intensity of all 12 fractions to calculate the percentage of liposome-bound protein.

Stapled BID-BH3 peptides

Stapled human Bid BH3 and mutated Bid BH3 peptides (Bid SAHB), conjugated N-terminally with a TMR fluorophore, were commercially purchased from Genscript, Piscataway, NJ. The design of the Bid SAHB was previously published (Walensky *et al.*, 2004). These peptides include two alpha-4-n-pentenylalaine residues, h3-1 and h4-1, originally Q92 and S96 in the human Bid (L) isoform, that form the stapling cross-linker.

Fluorescence Polarization Assay

TMR-conjugated Bid SAHBs were dissolved in DMSO to a concentration of 5 mM. 10 µL of 20nM of the indicated Bid SAHBs in Assay Buffer (10mM HEPES pH7, 200 mM KCL, 5mM $MgCl_2$) were added to the assay plate - a 384 well-plate Corning plate (Cat. # 3544). A 3x stock of recombinant BaxΔCTS and BakΔCTS proteins was prepared in a 96 well-plate with a 1-in-2 serial dilution including a blank (buffer alone). 5µL of the prepared proteins were transferred to each well in the assay plate, which contained 10µL of the 20nM Bid SAHB for a final indicated concentration of the proteins (1x) in a total volume of 15µL. The assay plates were then spun down at 300g for 30 seconds before being sealed. Following a 30-minute incubation at 37°C, fluorescence intensity and polarization were read on the Tecan M1000 using an excitation of 530 nm (5 nm slit-width) and an emission of 587nm (20 nm slit-width).

Mitochondria Assay

Heavy membrane fractions, including mitochondria, were isolated from BMK DKO cells with or without stable expression of SMAC-mCherry using nitrogen cavitation, as described in a previously published protocol (Niu *et al*, 2017). BMK DKO cells were washed with 1x PBS and harvested by a plastic cell scraper. After spun down to obtain a pellet, cells were resuspended in Mitolysis buffer containing 20mM HEPES pH 7.2, 250 mM sucrose, 150mM KCL, 1mM EDTA supplemented with protease inhibitor cocktail (Pierce^{TM} Protease Inhibitor Tablet, one tablet per 50mL of buffer). Cells were lysed by nitrogen cavitation at 150psi for 10 minutes on ice. Cell debris was removed by pelleting the cell lysate at 2000g for 4 minutes. Heavy membrane fractions, including mitochondria in the supernatant, were isolated by an additional step of centrifugation at 13000g for 10 minutes. The final pellet containing the mitochondria was resuspended in 50 to 100µL of the Mitolysis buffer. All centrifugation steps were carried out at 4ºC. The heavy membrane fraction was then diluted to 0.2mg/mL (determined by Bradford reagent) for the SMAC-mCherry release assay, the mitochondria-binding assay, and the *in vitro* FRET assay in the presence of mitochondria.

For the Smac-mCherry release assay, the isolated mitochondria were incubated with Bak and cBid for 1 hour at 37ºC. The release of SMAC-mCherry from the mitochondria was measured by the fluorescence intensity of mCherry in the supernatant (after a 10-minute 13000g spin) as a percentage of the total fluorescence intensity of mCherry in the supernatant and the pellet. mCherry fluorescence was read by the Tecan M1000 plate reader at the excitation of 587nm (6 nm slit-width) and emission of 610nm (12 nm slit-width).

For the mitochondria-binding assay, isolated mitochondria were incubated with the indicated concentration of either A647 labeled or unlabeled recombinant Bak for 1 hour at 37°C. The reaction was centrifuged at 13,000g for 10 minutes to separate the mitochondrial fraction (pellet) from the soluble fraction (supernatant). When A647 labeled Bak was used, the fluorescence intensity of A647 was measured in both fractions to determine the percentage of the fluorescence signal in the mitochondrial fraction relative to the total fluorescence signal. For assays with unlabeled Bak, western blot analysis was performed to calculate the percentage of Bak in the mitochondrial fraction.

In Vitro FRET Assay

In vitro FRET assay with Alexa-labeled single-cysteine acceptor A647-Bak C166 and donor A568-BimL Q41C /cBid C126 were carried out in the presence of membranes (liposome or isolated heavy membrane at 0.2 mg/mL as indicated). FRET results in a decrease in the fluorescence intensity of the donor (A568) proportional to the concentration of acceptor-donor complexes were recorded and expressed as %FRET efficiency. A detailed protocol was previously published (Pogmore *et al.*, 2016). Briefly, 5nM of the Donor A568 labeled cBid or BimL was added to liposomes in the assay plate - 384 well-plate (Corning, Cat. #3544). After sealing the plate, an initial fluorescence reading (F_0) for the Donor alone was recorded on the Tecan M1000 plate reader using the excitation of 567 nm and emission of 600 nm for the 'bottom read' mode. Temperatures were set to 37ºC. After 30-45 minutes, the A568 signals became stable, and the indicated concentration of A647 labeled or unlabeled Bak was added to the assay plate for two reactions: 1) A568 Donor + A647 labeled acceptor Bak and 2) A568 Donor + unlabeled acceptor Bak (to subtract out any environment-induced fluctuations introduced to the donor intensity by addition of another protein). The A568 signals were recorded after 1.5 to 2 hours of incubation at 37ºC. %FRET efficiency is calculated using the following formula:

$$\%\text{FRET efficiency} = (1 - \frac{F_{DA}}{F_A}) \times 100$$

where F_{DA} is the ratio F/F_0 of reaction 1 (the donor intensity in the presence of a labeled acceptor) and F_A is the ratio F/F_0 of reaction 2 (the donor intensity in the presence of an unlabeled acceptor). We then plotted the %FRET efficiency against the acceptor concentrations used in the experiment to generate a binding curve. A K_D value was calculated from a fitted model of the binding curve using a quadratic equation that accounts for the concentration of the donor protein (Pogmore *et al.*, 2016). This approach differs from Hill-equation fitting, which only considers the concentration of the acceptor (the ligand) and the percentage bound donor (the receptor) for K_D estimation.

One disadvantage of the *in vitro* FRET assay is that the apparent K_D from a curve with a low maximum FRET efficiency due to the stringent distance and orientation requirement of the two fluorophores is less accurate because of the increased contribution of collisions.

Cell Lines and Culture

Baby mouse kidney (BMK) and HCT116 (ATCC® CCL-247) colorectal carcinoma cells were cultured in Gibco high-glucose DMEM supplemented with 1% Pen Strep, 5% non-essential amino acids (NEAA, ThermoFisher), and 10% Fetal Bovine Serum (Sigma). HEK293 cells for lentivirus production were cultured in Gibco high-glucose DMEM supplemented with 10% Fetal Bovine Serum (Sigma). All cell lines were maintained in the CO_2 incubator (ThermoFisher) at 5% CO_2 and 37ºC. The BMK-DKO cell line was a kind gift from the originator - Dr. Eileen White, Rutgers Cancer Institute of New Jersey (Degenhardt *et al*, 2002). HCT116 and HCT116-DKO cells were a gift from Dr. Bert Vogelstein, The Johns Hopkins Kimmel Cancer Center (Lengauer *et al*, 1997; Zhang *et al*, 2000). HEK293 cells (293T) were a gift from the originator - Dr Frank Graham (McMaster University). HEK293 and HCT116 cell lines were authenticated at SickKids – the Hospital for Sick Children in Toronto by short tandem repeat genotyping. BMK cells were sent to the American Type Culture Collection (ATCC) for mouse tandem repeat profiling (18 loci) to validate and confirm murine origin. Western Blot analysis confirms no detectable level of Bax and Bak in the BMK and HCT116 DKO cell lines. All cells were tested and confirmed negative for Mycoplasma using MycoAlert® Mycoplasma Detection Kit (Lonza Group AG, Basel, Switzerland).

Generation of Cell Lines for FLIM-FRET

The BMK DKO ^{C}ActA cell line was generated by transient transfection of the mC3-ActA-pEGFP-C3 plasmid, followed by Fluorescence-activated cell sorting (FACS) to enrich for mCerulean3 positive clones with stable gene expression. All the other cell lines used in this study, including BMK DKO and HCT116 DKO expressing the donor mCerulean3 or mTurquoise2 N-terminally fused to the protein-of-interest, were generated by lentiviral infection, followed by FACS sorting. Lentiviral plasmids encode the indicated fusion protein derived from the FUGW-backbone (Addgene# 14883). For the generation of HCT116 DKO expressing ^{C}Bak G126S, antibiotic selection with Zeocin at 100 µg/mL for 1-2 weeks was required after FACS sorting to obtain stably expressing clones. Production of lentivirus by HEK293T was done following the protocol for 10-cm plates from MD Anderson Cancer Center at The University of Texas using VSVG, Pax2, and the relevant lentiviral plasmids. (https://www.mdanderson.org/patients-family/search-results.v2.html?q=Lentivirus%20production%20protocols.pdf#).

Generation of Dox-Inducible mC3-Bak Cell Line for Cell Death Assay

BMK DKO cells were first infected with lentivirus using the pLenti-CMV rtTA3 Blast (Addgene# 26429) to establish a Tet-On induction system. Stable clones were subsequently selected by Blasticidin selection in a 6-well plate (100k transfected cells/well). After one week of selection, surviving colonies are pooled and cultured in a 10cm plate with 5µg/mL Blasticidin for an additional four days until cells become confluent. Before the second lentiviral infection to introduce the Dox-inducible plvx-tight-mCerulean3-Bak Puro construct into the BMK DKO cell line stably expressing rtTA3, all cells (including the HEK293T for lentivirus production) were cultured in Tet-free DMEM containing Tet-System Approved FBS from ThermoFisher. Subsequent antibiotic selection with Blasticidin (5µg/mL) and Puromycin (6µg/mL) for 1 week produced clones positive for both rtTA3 and Dox-inducible ^{C}Bak. Clones were pooled and cultured in Tet-free media until confluence. All experiments with the Dox-inducible ^{C}Bak BMK DKO rtTA3 cell lines were done in Tet-Free DMEM.

FLIM-FRET

Two conditions are required to accurately determine apparent affinities by FRET measurements in live cells. First, an appropriate control for collisions is required due to the restricted localization of most fluorescence protein fusions in cells. Second, for separate proteins, FRET measurements must be accompanied by per-pixel measurements of protein concentration. This second requirement is most accurately determined by FLIM (Ma et al, 2016; Osterlund *et al.*, 2022).

Quantitative FLIM-FRET microscopy and analysis on the INO-FHS platform to detect the binding of proteins in live cells was conducted as previously described (Osterlund *et al.*, 2022; Pemberton *et al.*, 2023). In short, BMK DKO or HCT116 DKO cells stably expressing the mCerulean3 or mTurquoise2 fused to the POI were seeded into a CellCarrier-384 Ultra Microplate (Perkin Elmer) at 8000 cells/well. Cells were transfected, 4-5 hours post-seeding, with 150ng of plasmid DNA encoding Venus (or mCitrine)-Acceptor protein per well using the TransIT-x2 transfecting reagent (Mirus Bio) following the manufacturer's guidelines. After another 4-5 hours after transfection, media in each well were exchanged for fresh DMEM media containing 10µM pan-caspase inhibitor- Q-VD-OPH (MedChemExpress). The subsequent day image acquisition of the 384-well plate on the INO-FHS platform was carried out as previously described (Osterlund *et al.*, 2022). Importantly, the protein standards of purified mVenus, mCerulean3, fluorescein (10nM in 0.1M NaOH), and quenched fluorescein (30 µM Fluorescein in 8.3M NaI, 100 mM Na_2HPO_4 pH 10), were added to the assay plate for calibration and downstream analysis. Image analysis was done using specialized software developed to estimate fluorescence lifetime data using the phasor approach. Briefly, regions of interest (ROI) in each image were identified with a watershed algorithm based on the mCerulean3 or mTurquoise2 signals, which are the time-correlated Single Photon Counting (TCSPC) channel. Pixels within each ROI were combined. Within an ROI, the fluorescence intensity of the TCSPC and the hyperspectral (Venus or mCitrine) channels are recorded, and a fluorescence lifetime (τ) of the TCSPC was calculated for that ROI. If FRET occurs in an ROI, this causes a decrease in the fluorescence lifetime of the TCSPC channel. This decrease is measured as changes in the angular frequency ($\Delta\omega$**,** the y-values of the binding curves) of $\tau1$ on the universal circle of the phasor plot where $\tau1$ is the fluorescence lifetime of the non-transfected cells expressing the donor alone. Only ROIs with a physiological range of donor fluorophore equivalent to 1 – 3μM of mCerulean3 were selected for fluorescence lifetime analysis. This was done by utilizing the protein standards of mCerulean3. To calculate the free Venus (x-axis values) for the binding curves, we first converted the intensity from the Hyperspectral channel into the equivalent concentration of Venus in micromolar using a protein standard of recombinant Venus. Then, we subtracted the bound Venus concentration, assuming 1-to-1 binding to the Donor.

For each binding curve, binding data from 3 or more technical replicates (except for the experiment for Figure 2.5 – Figure Supplement 2B, where there are two technical replicates) were used to generate a single binding curve. If two threshold-based criteria are satisfied, this average binding curve is fitted to the Hill equation with a Hill constant (h) of 1. The first criterion is that the shape-ratio (s-ratio) of the binding data must be ≥2 to differentiate a binding curve from a linear increase in $\Delta\omega$ due to collisions between the donor and acceptor fluorophores. Briefly, the s-ratio is calculated as the area under the 'binding curve' divided by the area above the 'binding curve.' The lower the s-ratio correlates with more linear or 'less curvy' binding data. If the S-ratio is below 2, the binding data is fitted to a linear equation with no constraints. The second criterion is that the maximum $\Delta\omega$ (BMAX) determined from the Hill-fitted binding data must be above 0.05 to ensure only sufficient binding data are fitted with the Hill equation and to weed out noisy binding data due to inefficient binding. If the BMAX of the Hill-fitted binding data is below the threshold of 0.05, the binding data will then be re-fitted to a linear equation. For binding data fitted to the Hill equation, an apparent relative dissociation constant (K_D) value is calculated using GraphPad Prism 9.5.0. For Table 1, an additional step of subtracting the binding data of the respective negative collisional control (^{V}BimL-4E or ^{V}BimEL-4E or ^{V}tBid-4E) from the original binding data of the tested ^{V}BimL/^{V}Bim-EL/^{V}tBid construct was done before fitted to the Hill-equation for K_D value calculation. In this case, the second criterion of maximum $\Delta\omega$ (BMAX) must be above 0.04 for the binding data to be deemed sufficient.

Image Colocalization

The colocalization-imaging assay was conducted in a CellCarrier-384 Ultra Microplate (Perkin Elmer) with BMK DKO cells stably expressing ^{mT2}CTS$_{BAK}$, ^{mT2}CTSscr$_{BAK}$, or^{mT2}CTS-KSD$_{BAK}$. These cells were transiently transfected with the indicated Venus-fused constructs and stained with MitoTracker Red and Draq5 right before imaging. Draq5 was used to stain the cell nucleus and enable segmentation in the analysis. Cell seeding and transfection procedures were done in the same way as for the FLIM-FRET experiment. Image acquisition on the Opera Phenix microscope (Perkin Elmer) using a 63x water immersion objective (confocal mode) and the subsequent colocalization analysis for Pearson Correlation Coefficients (Pearson's r) using the Harmony software (V 4.9) were conducted as described previously (Pemberton *et al.*, 2023). Briefly, individual cells were segmented using the Draq5 signal. This created a mask for both the nucleus and cytoplasm. Areas of the mitochondrial network were identified by MitoTracker Red staining. A minimum threshold for the Venus channel was set based on non-fluorescent parental cells in a different well to enable the selection of only Venus-positive cells for colocalization analysis. A Pearson's r between the Venus or mTurquoise 2-fused query proteins and the fluorescently labeled mitochondria was calculated for all cells positive for Venus or mTurquoise 2. An additional colocalization analysis between the Venus and mTurquoise 2 channels was similarly done in the same analysis pipeline for each experiment. The median Pearson's r with interquartile range for each replicate was plotted in GraphPad Prism 9.5.0, which shows the indicated number of cells used for the plot.

Cell Death Assay

For the cell death assay using HCT116 DKO cells stably expressing mC3-Bak G126S, cells were seeded at a density of 8000 cells per well in a CellCarrier-384 Ultra Microplate (Perkin Elmer). The seeded cells were transfected with plasmids encoding either v-tBid or v-tBid-4E using the same method as for FLIM-FRET, but without adding the 10µM pan-caspase inhibitor Q-VD-OPH during the media exchange post-transfection. Twenty hours after transfection, the cells were stained with TMRE and A647 labeled Annexin V to measure mitochondrial membrane potential and detect externalized phosphatidylserine, respectively. Annexin V binds externalized phosphatidylserine on the outer plasma membrane of late apoptotic cells. Images were acquired with the Opera Phenix microscope (Perkin Elmer) using a 20x water immersion objective in confocal mode. Non-transfected cells served as a negative control. Cells positive for mCerulean3 and Venus were automatically selected using an analysis pipeline in Harmony software (V4.9) to quantify TMRE and A647-Annexin V intensities. Without a nuclear stain, the combined Venus and mCerulean3 channels created a mask for cell areas. Object-level data containing all cell areas were exported to GraphPad Prism 9.5.0 to compare median and range TMRE and Annexin V intensities between transfected and non-transfected groups. The threshold for Venus positivity was set at ≥2 standard deviations above the background Venus intensity in non-transfected cells. TMRE and Annexin V intensity of only Venus-positive cells were plotted in the transfected groups.

For the cell death assay with BMK DKO and BMK WT cells, cells were seeded and transfected with ^{V}BH3-only proteins as described in the previous paragraph. On the following day, before imaging, cells were stained with Hoechst 33258 for nuclear segmentation, and A647-Annexin V for detection of externalized phosphatidylserine on the outer leaflet of the plasma membrane indicating late-staged apoptotic cells. Image acquisition on the Opera Phenix microscope (Perkin Elmer) using a 20x water objective in confocal mode and analysis on the Harmony were done to evaluate the percentage of dead Venus-positive transfected cells. The Hoechst channel was used to identify cell nuclei and cytoplasmic area. Transfected Venus-positive cells were automatically selected using a threshold of ≥2 standard deviations above the background Venus intensity of non-transfected cells. Similarly, Annexin V positivity of the Venus-positive cell population was evaluated based on a threshold of ≥2 standard deviations above the background Annexin-V A647 intensity of non-transfected cells.

For the cell death assay with BMK DKO cells stably expressing rtTa3 and the Dox-inducible ^{C}Bak, cells were seeded at a density of 8000 cells per well in a CellCarrier-384

Ultra Microplate (Perkin Elmer). Four hours later, plasmids encoding the indicated ^{V}BH3-only proteins or Venus alone were transfected into the cells using the TransIT LT-1 Transfection Reagent (Mirus Bio) at the recommended transfection reagent to DNA ratio of 3 to 1, with 150ng of plasmid DNA per well. Three hours post-transfection, the media in each well were aspirated and replaced with new media containing either 500 ng/mL Doxycycline or no Doxycycline. Nine hours after the media change, the cells were stained with Draq5 and Nucview530 Caspase-3 Enzyme Substrate (Biotium, Fremont, CA) for nuclear segmentation and detection of active caspase 3, indicating apoptotic cells. Images were acquired using the Opera Phenix microscope (Perkin Elmer) with a 40x water immersion objective in confocal mode. Non-transfected cells and cells without Doxycycline treatment served as negative controls. Cells positive for mCerulean3 and Venus were selected based on the background intensity threshold in the no-Dox and non-transfected wells, respectively. These cells were then assessed for Caspase-3 activity by measuring the Nucview530 fluorescence intensity in the nucleus, as the Nucview530 Caspase-3 substrates re-localize to the nucleus (identified by Draq5) once cleaved by active Caspase-3. mCerulean3+ Venus+ cells with 2 standard deviations in nuclear Nucview530 intensity above the mean of non-transfected No-Dox-treated cells were scored as dead. The average percentage of dead cells expressing both Venus and mCerulean3 was calculated per well and plotted using GraphPad Prism 9.5.0 to compare Bak-induced cell death by different v-BH3-only proteins.

Immunoblotting

Immunoblotting for cell lysates was performed as previously described. Briefly, cell pellets in Eppendorf tubes were resuspended in lysis buffer (10mM Tris pH8, 150mM NaCl, 1% Triton) and left on ice for 30 minutes. Next, cellular debris was spun down at 14000 g for 15 minutes at 4ºC, and supernatants were collected for protein concentration determination by BCA assay. The volume needed in µL for 10µg (per lane) was added to 15µL 2x SDS Loading Buffer supplemented with 10 mM DTT. Samples were boiled at 95ºC for 15 minutes and then run through SDS-PAGE gels before transferring them to a PVDF membrane using a semi-dry Trans-Blot Turbo transfer system (Bio-Rad). PVDF membranes were then blocked by 5% Skim-milk powder in TBST 1x buffer before an overnight incubation at 4ºC with the primary antibodies at 1:1000 dilution. The next day, the blots were washed thrice with TBST 1x buffer before a 2-hour incubation at room temperature with the HRP-coupled secondary antibodies at 1:40000 dilution. A repeat wash with TBST 1x buffer was done thrice before the Ez-ECL solution (Biological Industries) was applied. Bands were detected using the MicroChemi 4.2 Gel Imager.

For immunoblotting of recombinant Bak in the heavy membrane (P) and soluble fraction (S), the above-described protocol for Western Blot was followed with the exception that all the P and S fractions were added, separately, to 10 µL of 2x SDS Loading Buffer supplemented with 10 mM DTT before loading to each lane of the SDS-PAGE gel (10% polyacrylamide gel). Band intensity for Bak was quantified using the 'Analyze gel' function in ImageJ.

Site-Directed Mutagenesis

The following primers were used for PCR-mediated fast cloning to generate the Venus-BimL CTS mutant constructs from the BimL template in Venus-BimL-pEGFP-C1 (Addgene# 166734). PCR conditions were optimized for Phusion Polymerase (NEB) with an Annealing Temperature between 60ºC and 65ºC.

1. BimL-CTS-scr

F:
CATTCCAACTCATCTTCCGAGTGTTAATGTGGAGAAGGCATTAACTCGAGCTC
AAGC

R:
GAGTTGGAATGGTACCAACTGGAGTCTTATGTGGTCTTCAGCCTCGCGGTAAT
C

2. BimL-M123I

F:
CTCTTGCGATTCATCTTCCGATTAGTGTGGAGAAGGCATTAACTCGAGCTCAAG
C

R:
TCGCAAGAGTTGCAATATTACTATCTGTGGGTGGTCTTCAGCCTCGCGGTAATC

3. BimL-I125V

F:
CTCTTGCGATTCATCTTCCGATTAGTGTGGAGAAGGCATTAACTCGAGCTCAAG
C

R:
TCGCAAGAGTTGCAAGACTACCATCTGTGGGTGGTCTTCAGCCTCGCGGTAAT
C

4. BimL-R130L

F:
CTCTTGCTGTTCATCTTCCGATTAGTGTGGAGAAGGCATTAACTCGAGCTCAAG
C

R:
CAGCAAGAGTTGCAATATTACCATCTGTGGGTGGTCTTCAGCCTCGCGGTAATC

5. BimL-I132N

F:
CTCTTGCGATTCAACTTCCGATTAGTGTGGAGAAGGCATTAACTCGAGCTCAA
GC

R:
TCGCAAGAGTTGCAATATTACCATCTGTGGGTGGTCTTCAGCCTCGCGGTAATC

6. BimL-R134L

F:
CTCTTGCGATTCATCTTCCTATTAGTGTGGAGAAGGCATTAACTCGAGCTCAAG
C

R:
TCGCAAGAGTTGCAATATTACCATCTGTGGGTGGTCTTCAGCCTCGCGGTAATC

To introduce the scrambled Bak-CTS sequence (GDKIVSQVNGRVFLNLVKLRGPFFLVGS) into the plasmid encoding recombinant human full-length BAK- pTYB1-Bak-Intein-Chitin Binding Domain for protein purification, we used the following pair of primers with PCR-mediated site-directed mutagenesis (fast-cloning method).

F:
CCTGAACTTAGTCAAACTTCGCGGTCCATTCTTTCTGGTGGGCTCATGCTTTGC
CAAGGG

R:
TAAGTTCAGGAATACTCTGCCGTTTACCTGCGAGACAATCTTGTCGCCCAAGTT
CAGGGC

Statistical analysis

Unpaired parametric t-tests or non-parametric Mann-Whitney test (GraphPad Prism 9.5.0.) were done to determine if the differences in Pearson's r values between the different transfectant groups for colocalization assay are statistically significant. Significance is denoted as $p<0.0001$. The apparent KD values are obtained from the fitted Hill-equation (h=1) of the binding data after subtracting the fitted binding data of the negative collisional control from each fitted construct's original binding data for each tBid construct. If the final binding curves' BMAX y values (ΔGↃ) are below the threshold of 0.04, the binding data are deemed insufficient (NSF). Unpaired student t-test with Welch's correction assuming Gaussian distribution with unequal standard deviation was used to determine K_D statistical significance between trasnfectant groups.

Data Availability

This work does not include data deposited in a public database.

Acknowledgments

We thank Justin Kale for providing us with the technical support to create the Dox-inducible mCerulean3-Bak cell line, and Elizabeth Osterlund and Nehad Hirmiz for providing the FLIM-FRET analysis tools. This work was supported by grant FDN143312 from the Canadian Institutes of Health Research (CIHR) to D.W.A and the Deutsche Forschungsgemeinschaft.

Disclosure Statement and Competing Interests

The authors declare no competing interests.

2.7 Supplementary Materials

FIGURE 2.1 – FIGURE SUPPLEMENTARY 1

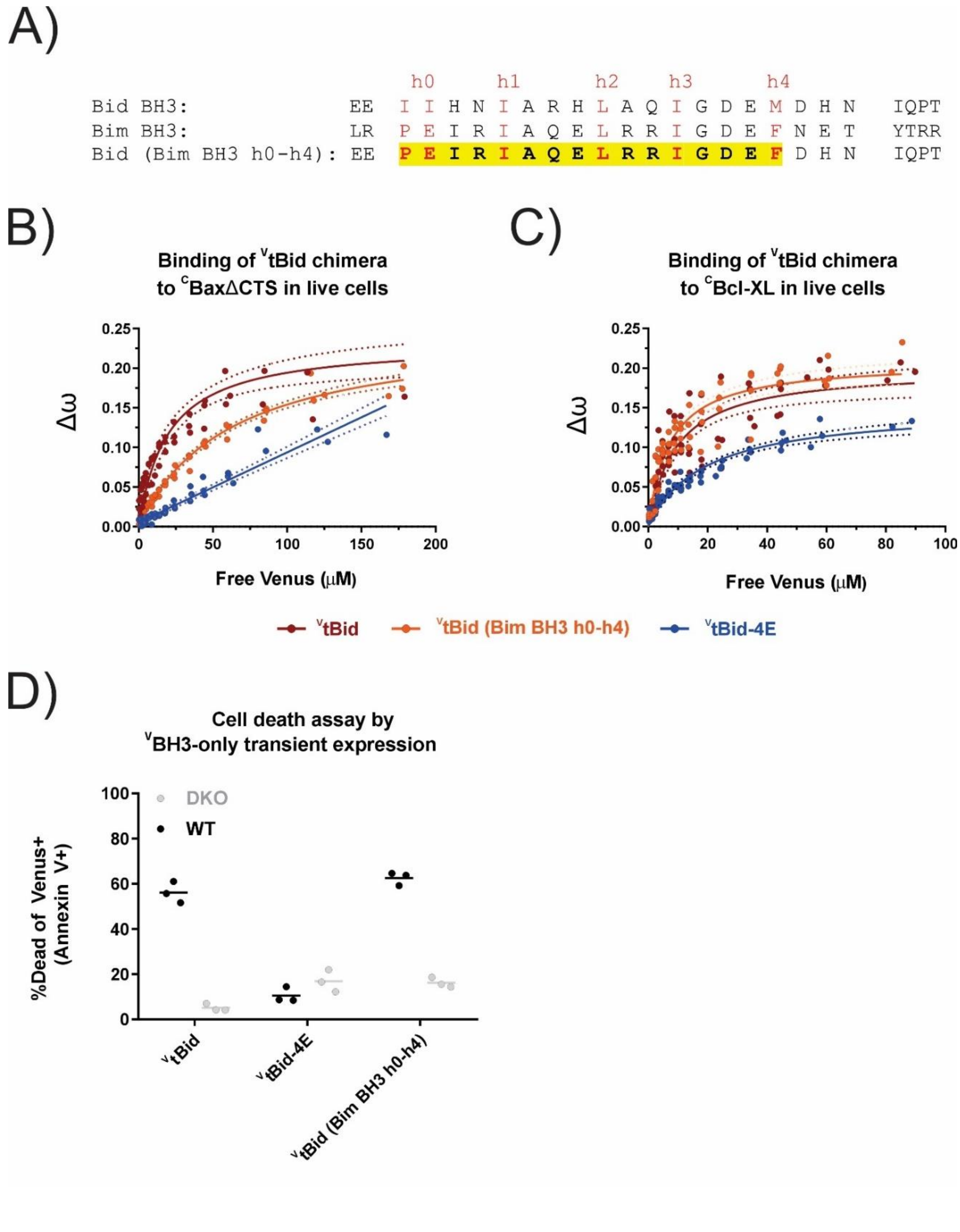

FIGURE 2.2 – FIGURE SUPPLEMENTARY 1

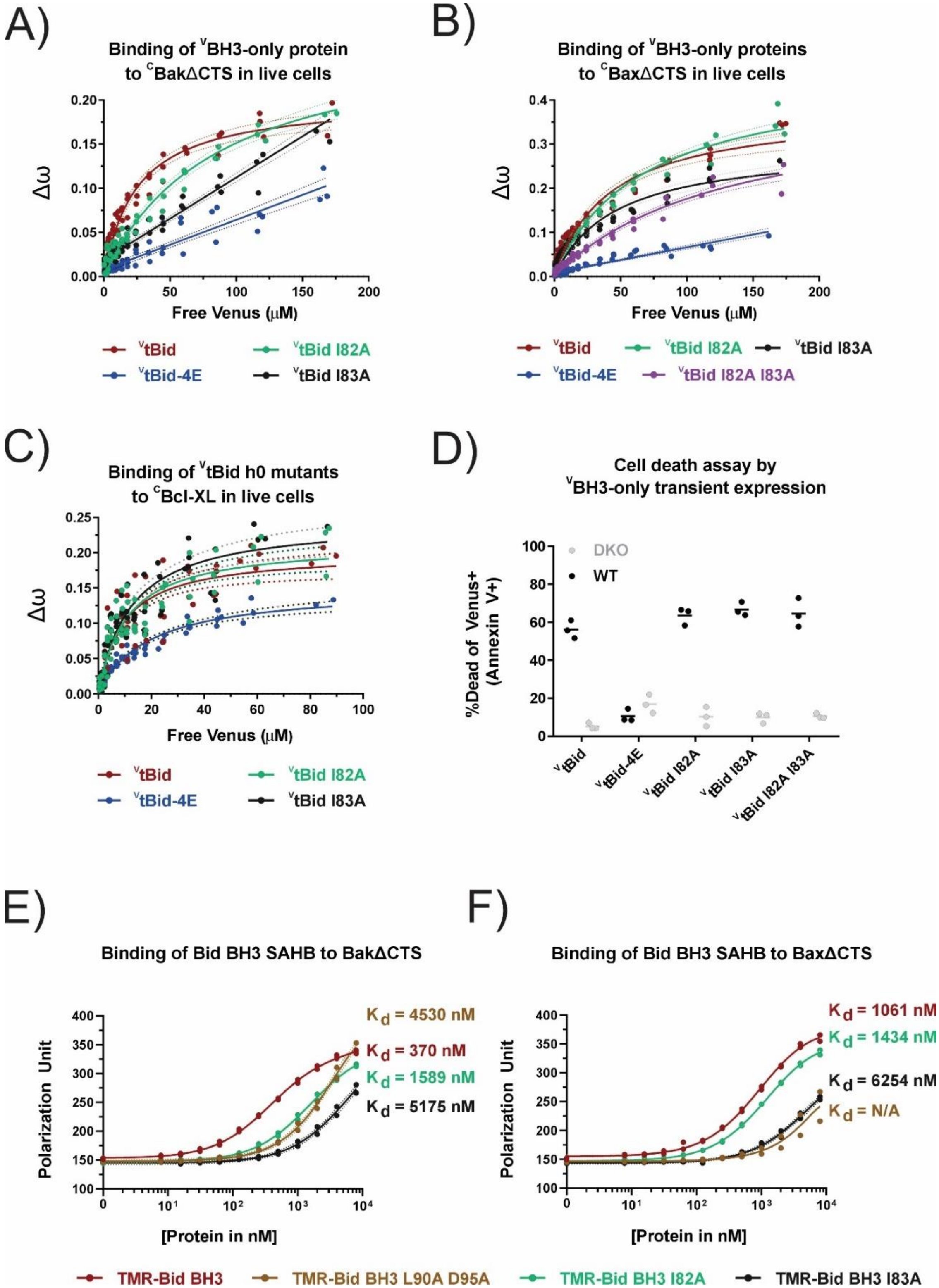

FIGURE 2.2 – FIGURE SUPPLEMENTARY 2

A)

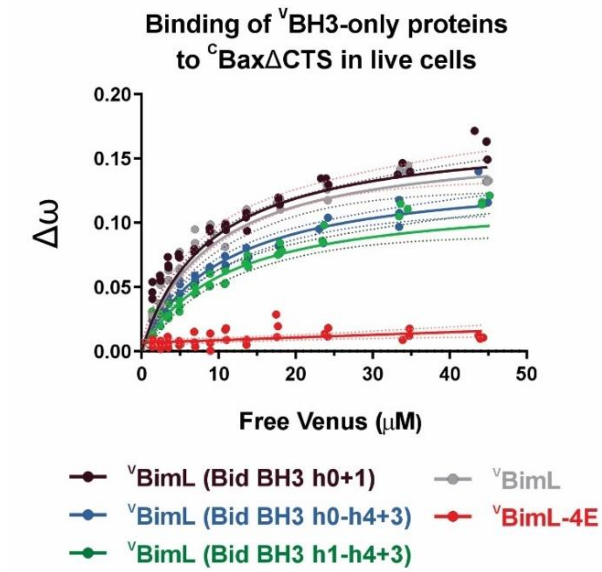

B)

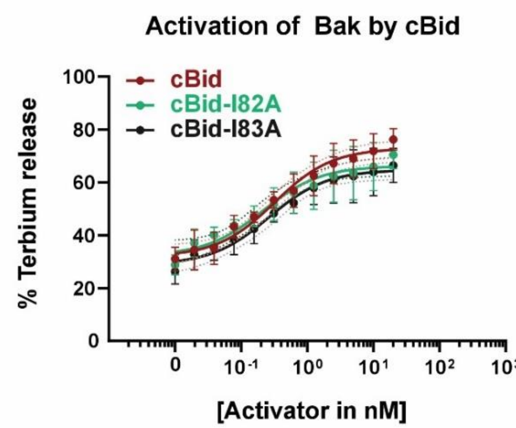

C)

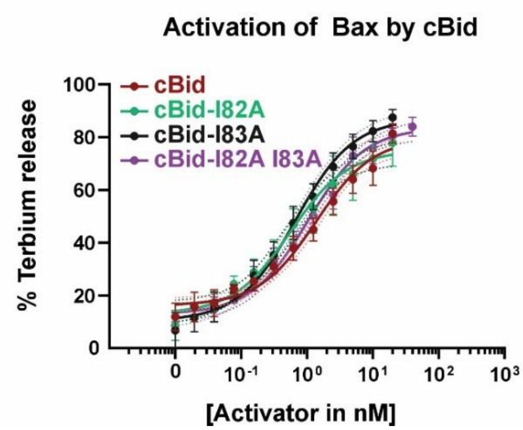

D)

EC_{50} (in nM)	BAK	BAX
cBid	0.3	1.4
cBid I82A	0.2	0.6
cBid I83A	0.3	0.7
cBid I82A I83A	0.4	1

FIGURE 2.3 – FIGURE SUPPLEMENTARY 1

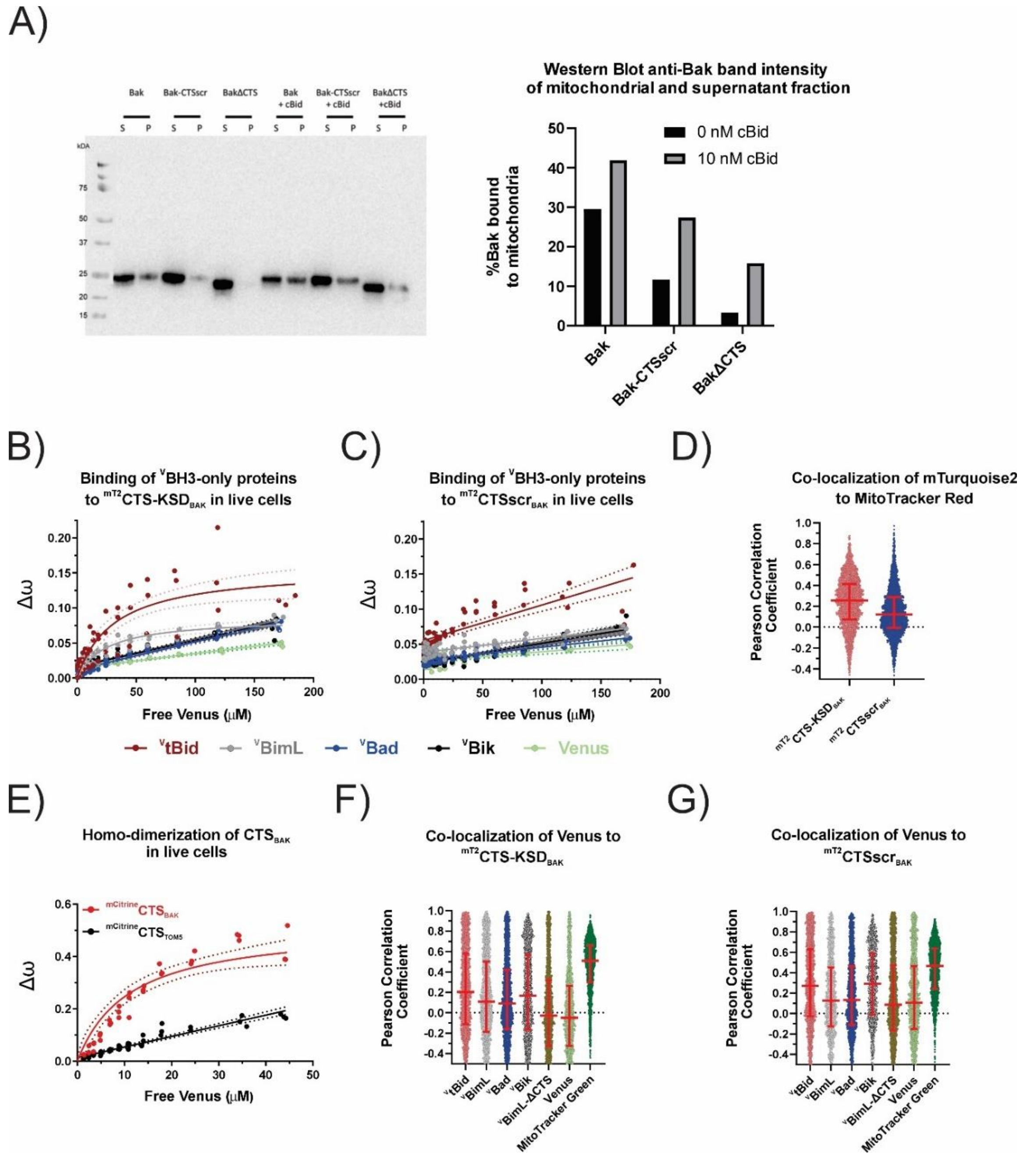

FIGURE 2.3 – FIGURE SUPPLEMENTARY 2

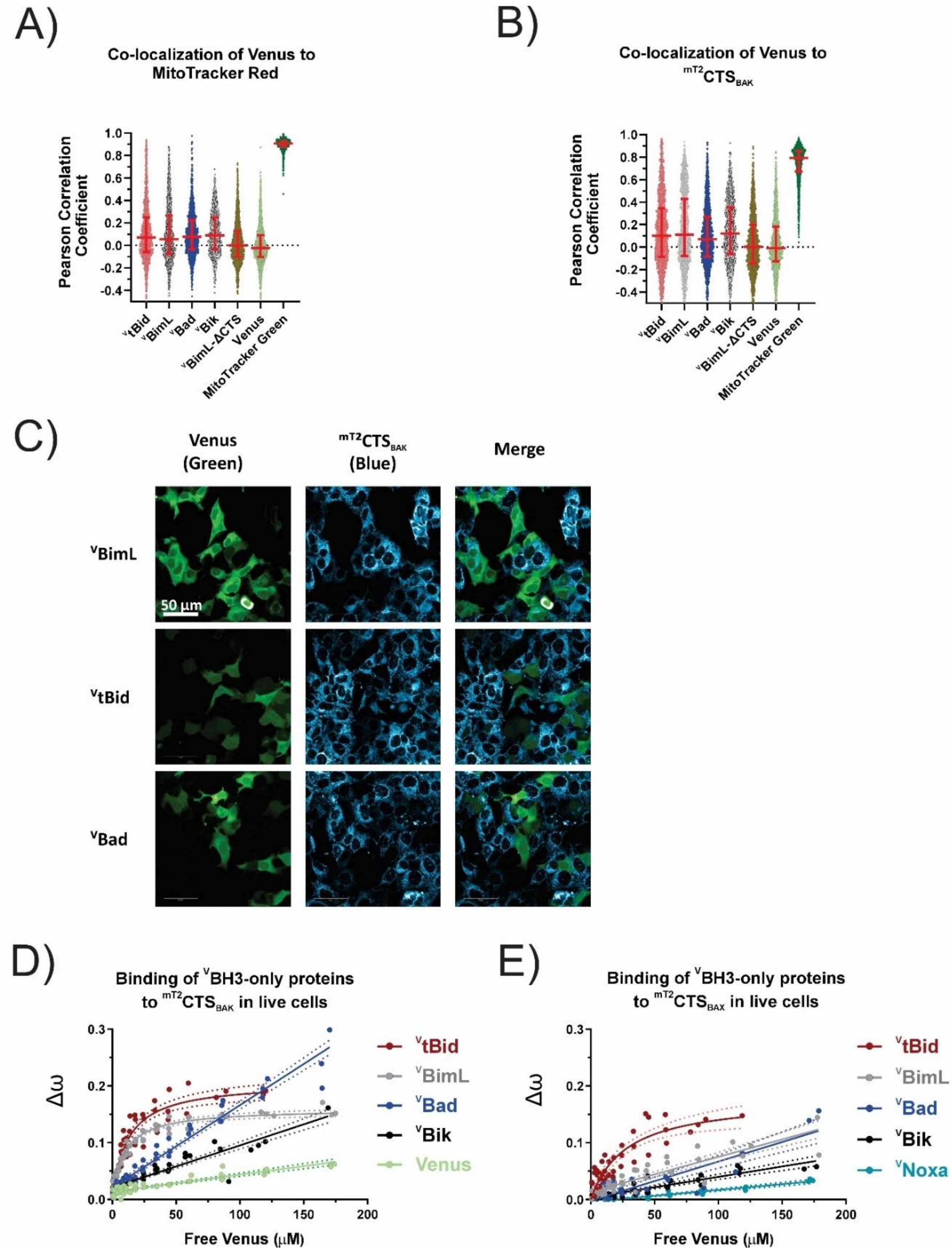

FIGURE 2.4 – FIGURE SUPPLEMENTARY 1

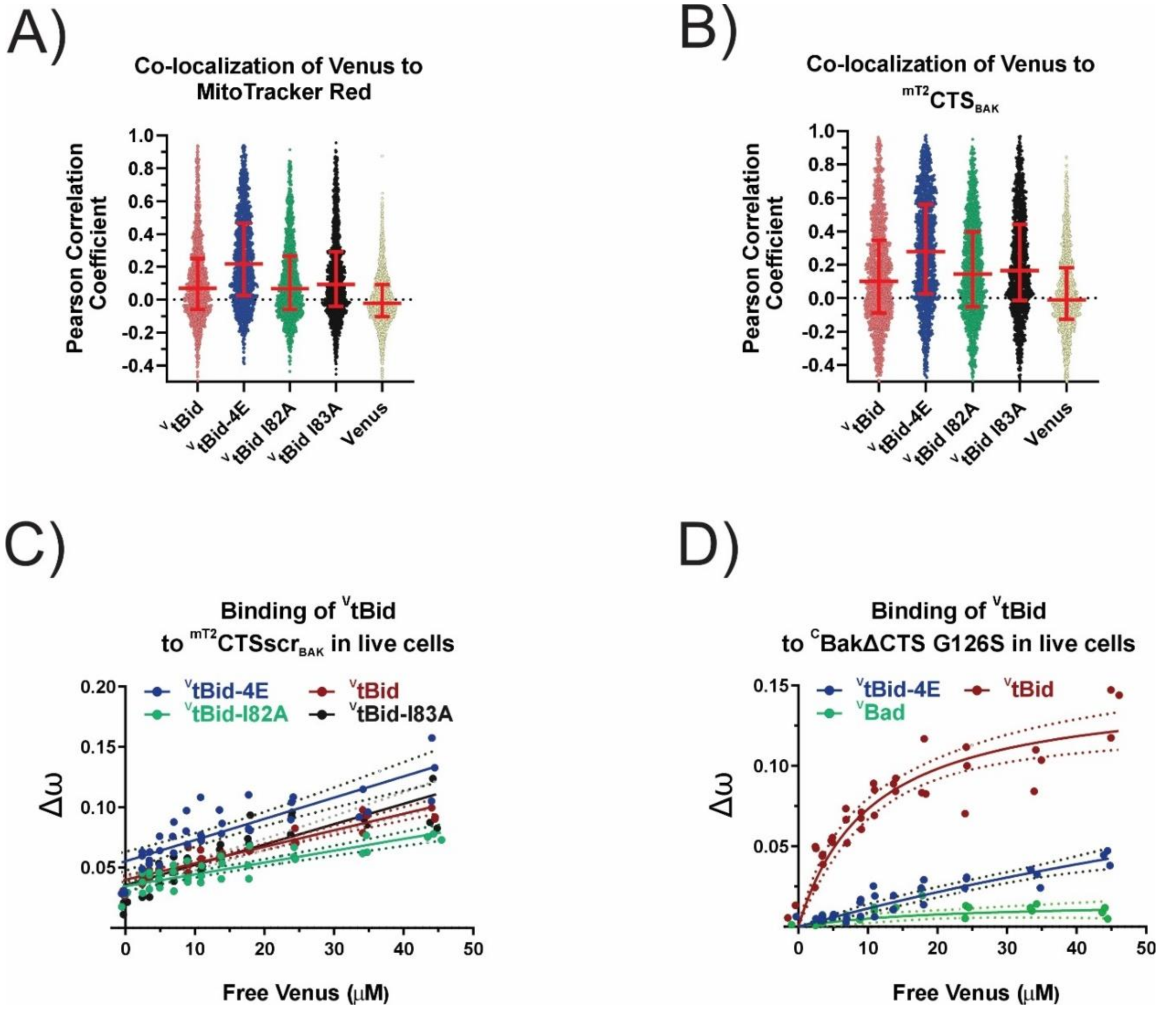

FIGURE 2.4 – FIGURE SUPPLEMENTARY 2

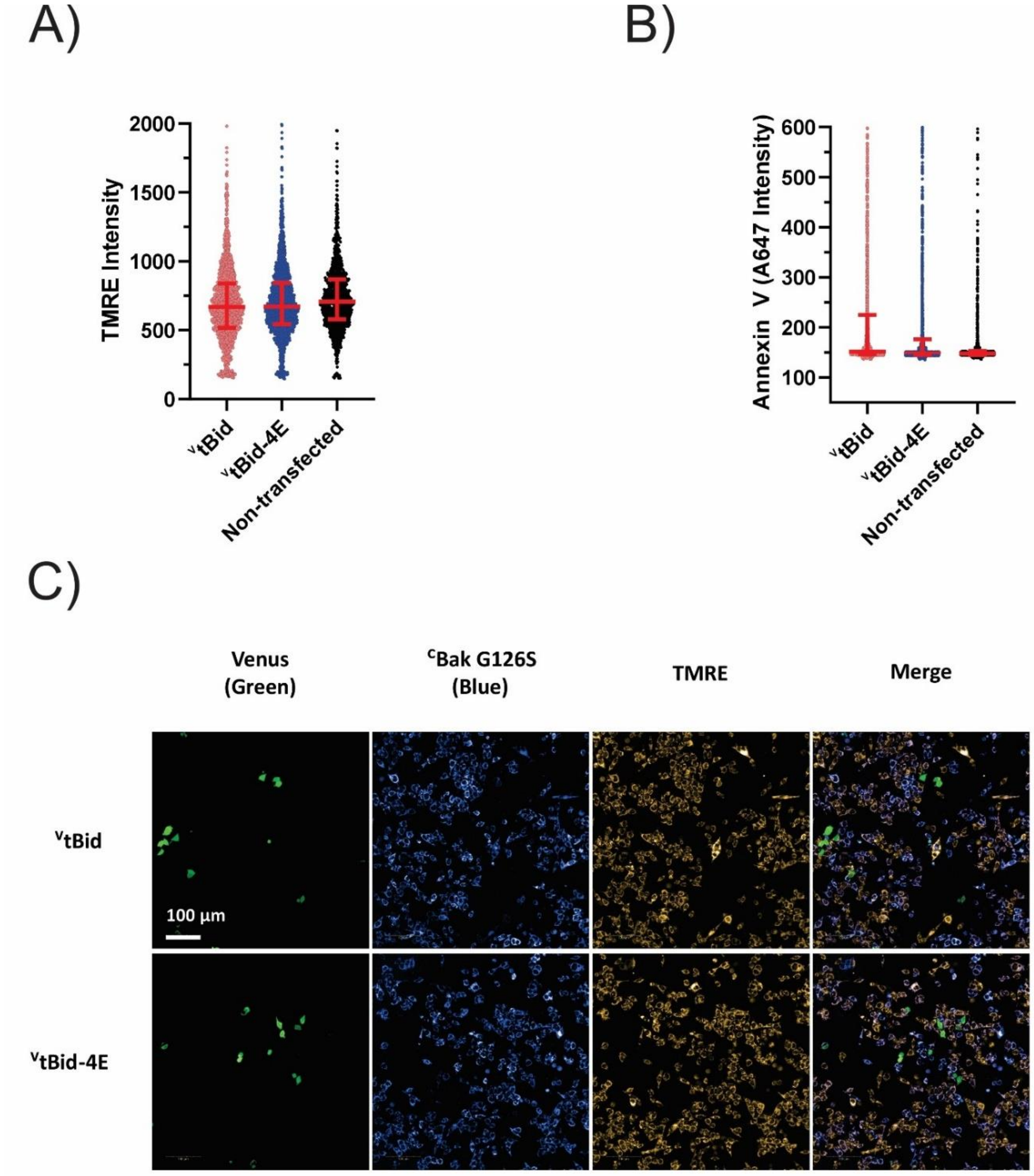

FIGURE 2.4 – FIGURE SUPPLEMENTARY 3

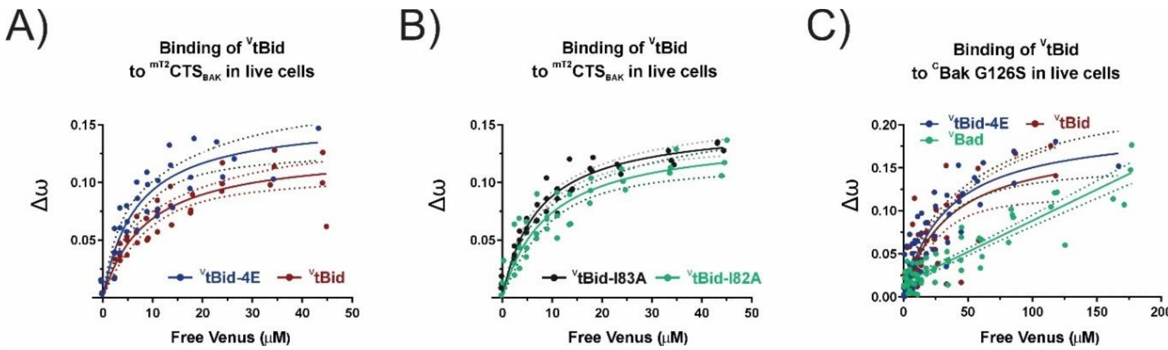

FIGURE 2.5 – FIGURE SUPPLEMENTARY 1

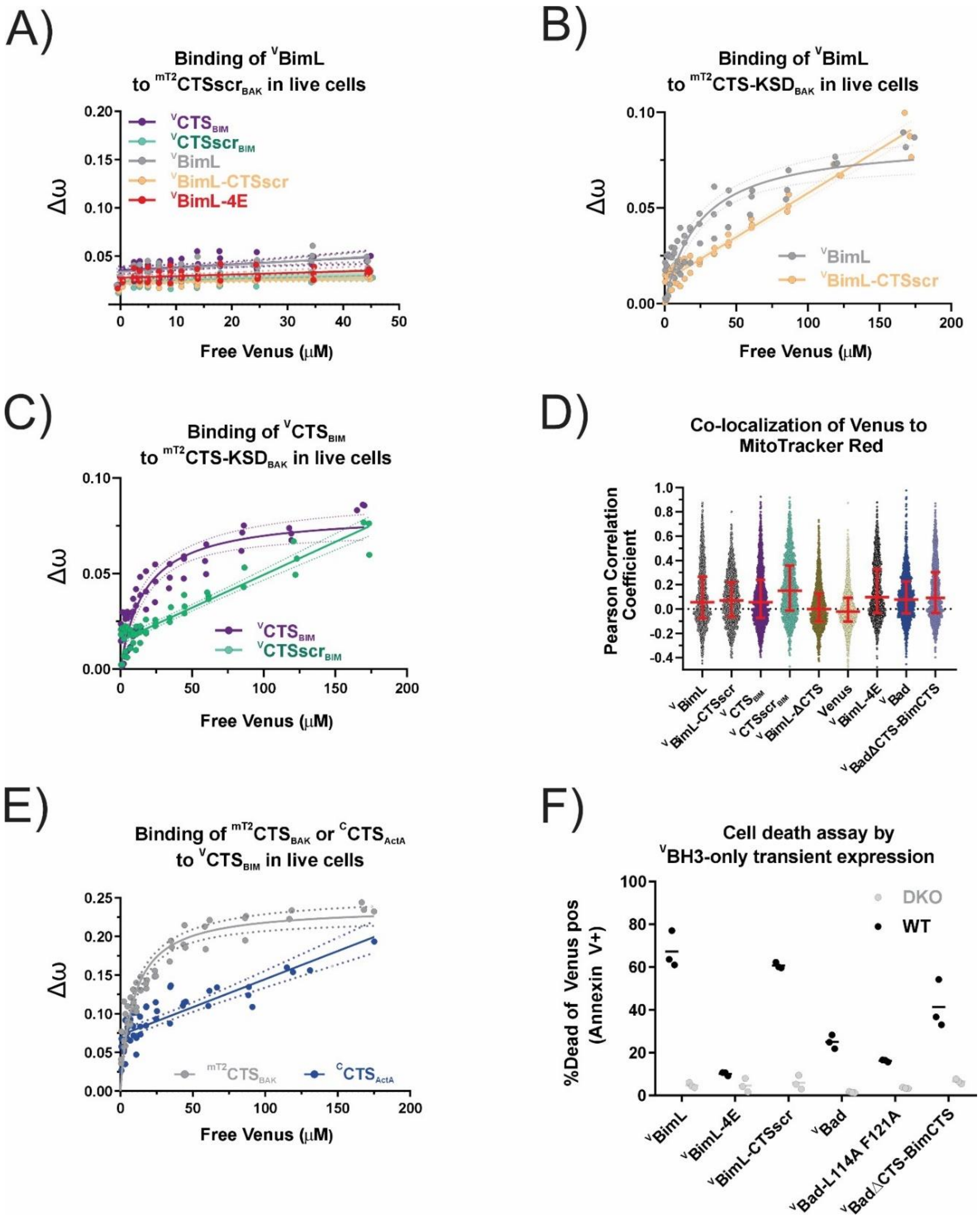

FIGURE 2.5 – FIGURE SUPPLEMENTARY 2

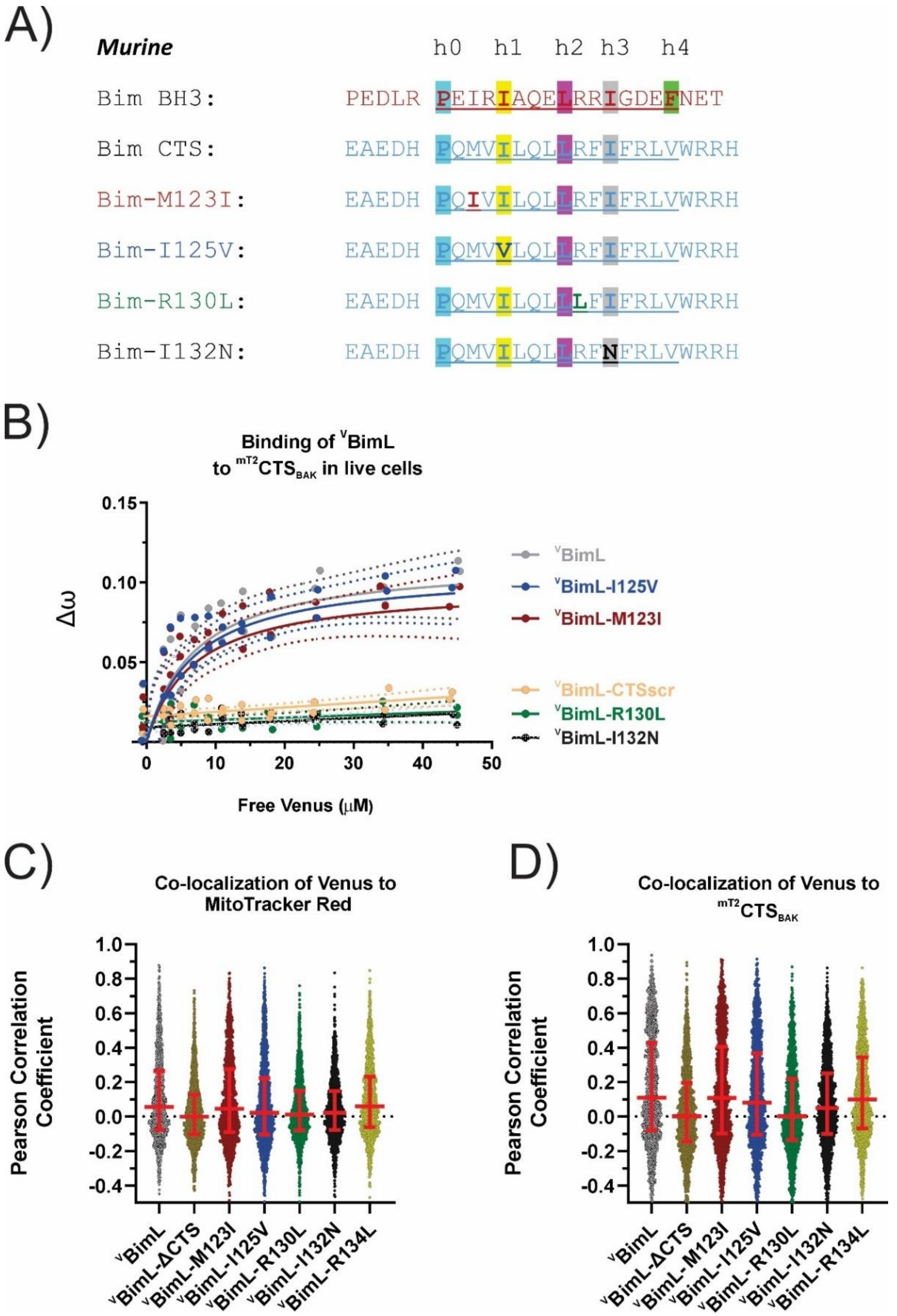

FIGURE 2.5 – FIGURE SUPPLEMENTARY 3

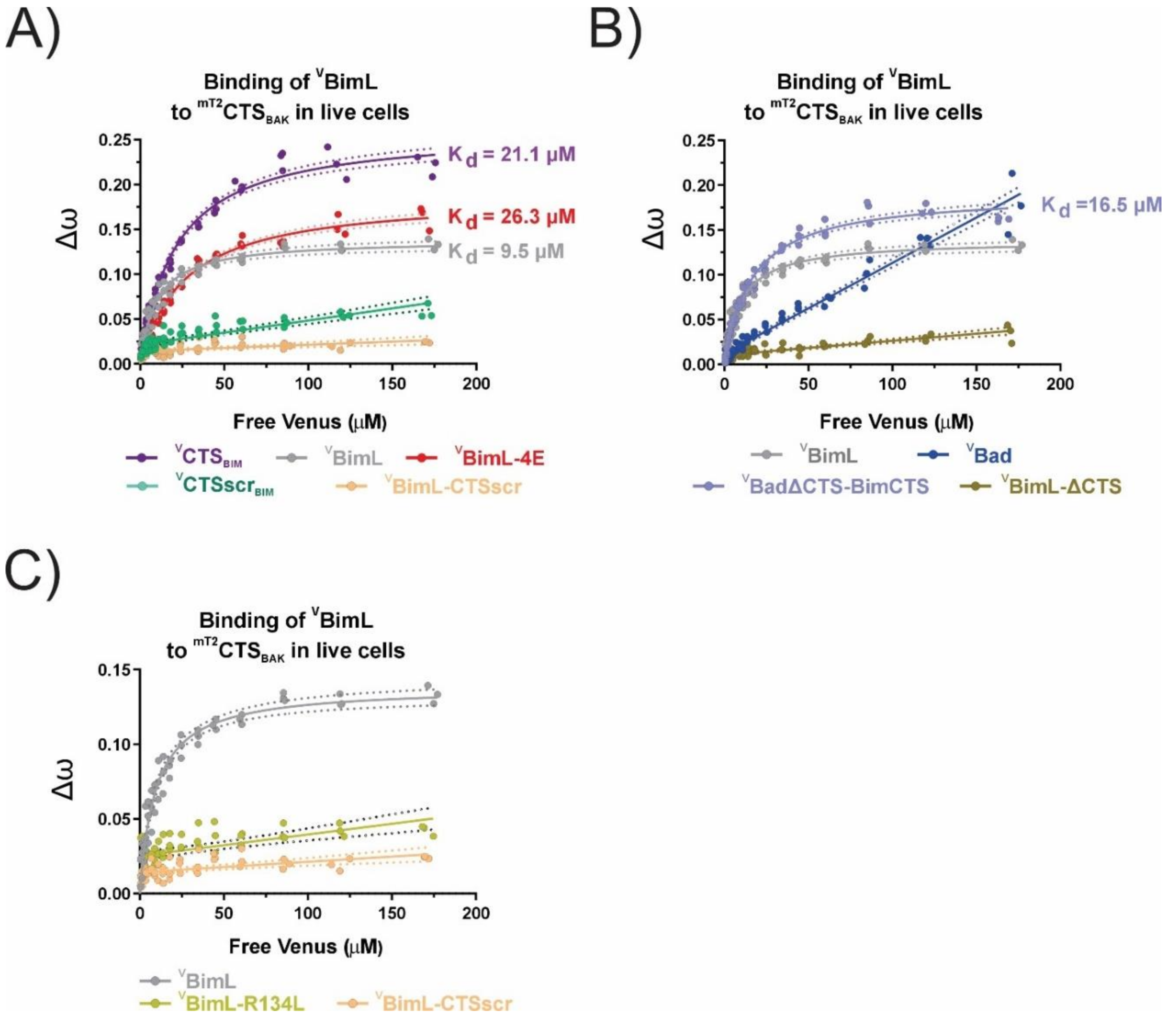

FIGURE 2.6 – FIGURE SUPPLEMENTARY 1

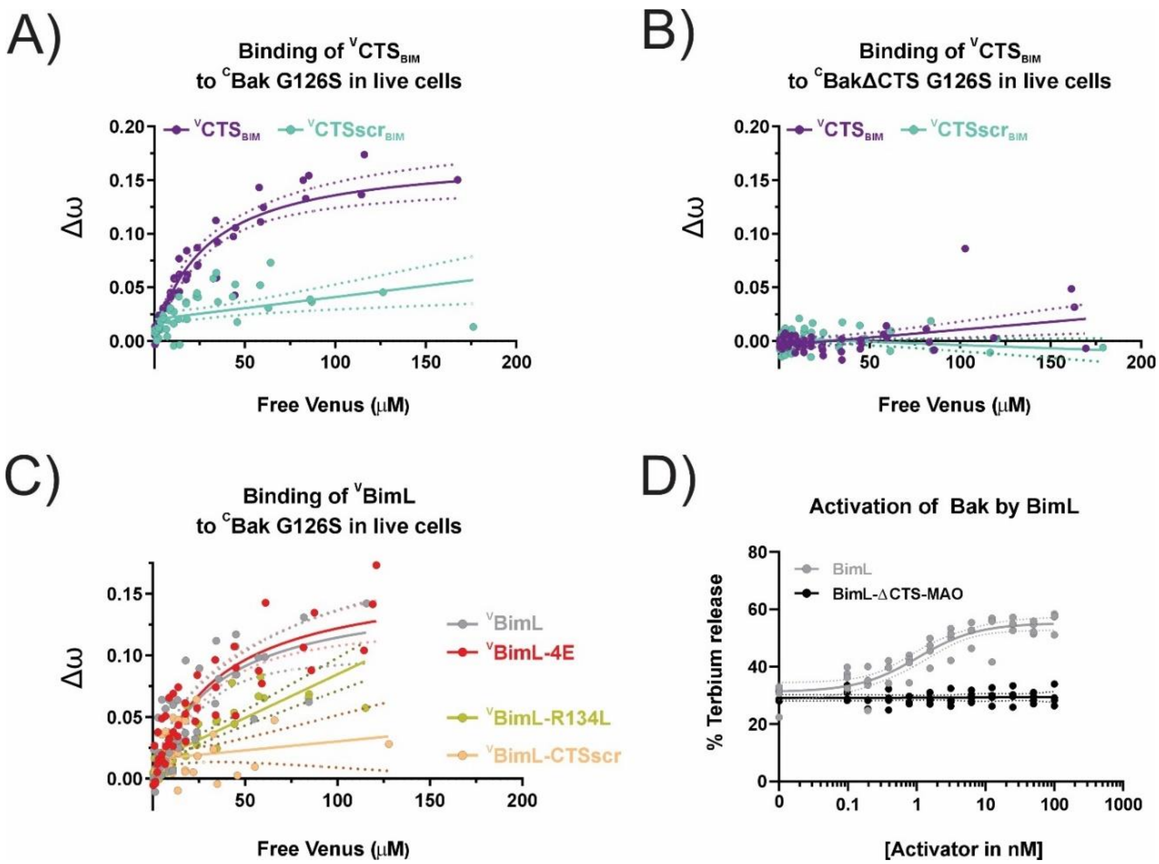

Appendix Table 2.S1. The apparent dissociation constant (KD) of ^{V}tBid and ^{V}tBid mutants in all independent replicates of FLIM-FRET experiments with ^{C}BaxΔCTS and ^{C}BakΔCTS. The apparent K_D values are obtained from the fitted Hill-equation (h=1) of the binding data after subtracting the fitted binding data of ^{V}tBid-4E (negative collisional control) from each fitted construct's original binding data for each tBid construct. If the final binding curves' BMAX y values (ΔGƆ) are below the threshold of 0.04, the binding data are deemed insufficient (NSF). Unpaired student t-test with Welch's correction assuming Gaussian distribution with unequal standard deviation was used to determine statistical signiificance. Average K_D values are shown in the right columns with standard deviation. N/A (not applicable) indicates that the construct was not tested in the replicate (column#). ‡ indicates one replicate. * indicates a statistically significant difference between compared tranfectant vs. ^{V}tBid for ^{C}BakΔCTS cells ($p \leq 0.05$). ** indicates a statistically significant difference between compared tranfectant vs. ^{V}tBid for ^{C}BaxΔCTS cells ($p \leq 0.05$).

K_d in µM	^{C}BakΔCTS					^{C}BaxΔCTS					
Replicate#	1	2	3	4	5	1	2	3	4	^{C}BakΔCTS (avg)	^{C}BaxΔCTS (avg)
^{V}tBid	6.44	6.33	7.39	12.44	5.31	8.79	11.7	11.9	18.43	7.6±2.5	12.7±3.5
^{V}tBid(Bim BH3 h0-h4)	NSF	NSF	NSF	NSF	N/A	14.23	21.44	20.3	N/A	NSF	18.7±3.2
^{V}tBid(Bim BH3 h0-h3)	NSF	NSF	NSF	NSF	N/A	15.22	14.71	15.41	N/A	NSF	15.1±0.3
^{V}tBid(Bim BH3 h1-h4)	6.51	7.52	5.56	15.30	N/A	7.30	7.39	7.467	N/A	8.1±3.9	7.4±0.1
^{V}tBid(Bim BH3 h0-PE)	NSF	NSF	NSF	NSF	N/A	NSF	NSF	NSF	N/A	NSF	NSF
^{V}tBid(Bim BH3 h0±2)	NSF	NSF	NSF	NSF	N/A	33.3	24.39	25.87	N/A	NSF	27.9±3.9**
^{V}tBid(Bim BH3 h0+2)	NSF	NSF	NSF	NSF	N/A	21.0	17.75	NSF	N/A	NSF	19.4±1.6
^{V}tBid(Bim BH3 h1-2)	6.54	5.93	5.47	6.60	N/A	8.77	12.25	9.18	N/A	7.8+0.5	10.1±1.6
^{V}tBid I82A I83A	N/A	NSF	NSF	NSF	N/A	N/A	23.68	9.9	N/A	NSF	16.8±6.9
^{V}tBid I82A	N/A	21.42	NSF	>1000	21.14	N/A	16.65	15.3	13.77	21.3±0.1*	15.2±1.2
^{V}tBid I83A	N/A	NSF	NSF	>1000	NSF	N/A	11.28	6.4	8.87	NSF	8.8±2.0
^{V}tBid(Bim BH3 h0-1,+2)	N/A	N/A	N/A	N/A	NSF	N/A	N/A	N/A	27.68	NSF	27.7‡
^{V}tBid(Bim BH3 h0±1)	N/A	N/A	N/A	N/A	NSF	N/A	N/A	N/A	NSF	NSF	NSF
^{V}tBid I83E	N/A	N/A	N/A	N/A	NSF	N/A	N/A	N/A	8.432	NSF	8.4‡
^{V}tBid I82P	N/A	N/A	N/A	N/A	NSF	N/A	N/A	N/A	20.18	NSF	20.2‡

Appendix Table 2.S2. The apparent dissociation constant (K_D) of ^{V}BimL, ^{V}BimEL, and their mutants in all independent replicates of FLIM-FRET experiments with ^{C}BaxΔCTS and ^{C}BakΔCTS. The apparent K_D values are obtained from the fitted Hill-equation (h=1) of the binding data after subtracting the fitted binding data of ^{V}BimL-4E or ^{V}BimEL-4E (negative collisional control) from each fitted construct's original binding data for each tBid construct. NSF (insufficient) is indicated for binding data that are deemed insufficient if the final binding curves' BMAX y values (ΔGЭ) are below the threshold of 0.04. Average K_D values are shown in the right columns with standard deviation. Unpaired student t-test with Welch's correction assuming Gaussian distribution with unequal standard deviation was used to determine statistical significance. N/A (not applicable) indicates that the construct was not tested in the replicate (column#). ‡ indicates one replicate. * indicates a statistically significant difference between compared transfectants and vtBid for CBakΔCTS cells ($p \leqslant 0.05$). There were no statistically significant differences between ^{V}BimL backbone transfectants vs. ^{V}BimL, or ^{V}BimEL backbone tranfectants with vs ^{V}BimEL for ^{C}BaxΔCTS cells ($p \leqslant 0.05$).

K_d in μM	**^{C}BakΔCTS**		**^{C}BaxΔCTS**			
Replicate#	**1**	**2**	**1**	**2**	**^{C}BakΔCTS (avg)**	**^{C}BaxΔCTS (avg)**
^{V}BimL	**NSF**	**NSF**	**7.22**	**9.091**	**NSF**	**8.2±0.9**
^{V}BimEL	**NSF**	**NSF**	**12.58**	**11.24**	**NSF**	**11.9±0.7**
^{V}BimL (Bid BH3 h0-h4+3)	**11.22**	**8.91**	**8.969**	**11.04**	**10.1±1.2**	**10.0±1.0**
^{V}BimEL (Bid BH3 h0-h4+3)	**17.95**	**14.65**	**8.531**	**11.26**	**16.3±1.7***	**9.9±1.4**
^{V}BimL (Bid BH3 h1-h4+3)	**NSF**	**NSF**	**14.82**	**11.63**	**NSF**	**13.2±1.6**
^{V}BimEL (Bid BH3 h1-h4+3)	**23.83**	**20.88**	**14.19**	**14.36**	**22.4±1.5***	**14.3±0.1**
^{V}BimL P86I E87I	**16.32**	**18.02**	**25.27**	**18.61**	**17.2±0.9***	**21.9±3.3**
^{V}BimEL P142I E143I	**12.66**	**NSF**	**10.83**	**9.82**	**12.7‡**	**10.3±0.5**
^{V}BimL (Bid BH3 h0+1)	**11.18**	**8.81**	**8.894**	**8.841**	**10.0±1.2**	**8.9±0.0**
^{V}BimEL (Bid BH3 h0+1)	**7.94**	**4.76**	**8.561**	**5.065**	**6.4±1.6**	**6.8±1.7**
^{V}BimL (Bid BH3 h0+2)	**6.83**	**15.65**	**8.947**	**9.0**	**11.2±4.4**	**9.0±0.0**
^{V}BimEL (Bid BH3 h0+2)	**9.88**	**6.97**	**8.788**	**8.83**	**8.4±1.5**	**8.8±0.0**
^{V}BimL (Bid BH3 h0±2)	**NSF**	**6.40**	**3.15**	**8.90**	**6.4‡**	**6.0±2.9**
^{V}BimEL (Bid BH3 h0±2)	**NSF**	**NSF**	**16.29**	**19.51**	**NSF**	**17.9±1.6**
^{V}BimL (Bid BH3 h1-2)	**NSF**	**NSF**	**8.952**	**8.97**	**NSF**	**9.0±0.0**
^{V}BimEL (Bid BH3 h1-2)	**NSF**	**NSF**	**15.66**	**22.82**	**NSF**	**19.2±3.6**

Appendix Table 2.S3. Calculated S-ratio, BMAX, and apparent K_D values for all FLIM-FRET experiments in this study are displayed. K_D values are obtained from the Hill-fitted original binding data for each binding curve in both main and supplementary figures. For each binding curve, the most complete independent replicate is chosen for s-ratio analysis. If the s-ratio is smaller than 2, the binding data is fitted to the linear regression model, and the energy transfer or FRET is interpreted as collisions between the acceptor and donor fluorophores. Suppose the binding data has an s-ratio larger than 2; in that case, the binding data for 3 technical replicates are fitted to the Hill equation to obtain a K_D value in µM of Free Acceptor (x-axis) and a BMAX value of the ΔGƆ (y-axis). If the BMAX value is below 0.05, the binding data is deemed insufficient, and the binding data is re-fitted to a linear regression model. Interpretation of the binding data is on the right. N/A = not applicable; binding data fails to qualify for the next step in the analysis.

Figure	Donor (mCerulean3- or mTurquoise2-)	Acceptor (Venus-)	Replicate#	Date of experiment	S-ratio (threshold ≥2)	BMAX of Hill equation (h=1, threshold>0.05)	Apparent K_D in µM (without subtracting collisional control)	Interpretation
1F-Main	BakΔCTS	tBid	2	24/11/2023	2.1	0.14	21.7	Binding curve
1F-Main	BakΔCTS	BimL	1	24/11/2023	1	N/A	N/A	Linear/FRET due to collision
1F-Main	BakΔCTS	Puma	1	24/11/2023	1.5	N/A	N/A	Linear/FRET due to collision
1F-Main	BakΔCTS	Bad	1	24/11/2023	1.5	N/A	N/A	Linear/FRET due to collision
1F-Main	BakΔCTS	Noxa	1	24/11/2023	1.8	N/A	N/A	Linear/FRET due to collision
1F-Main	BakΔCTS	Bik	2	24/11/2023	0.9	N/A	N/A	Linear/FRET due to collision
1F-Main	BakΔCTS	Venus	1	24/11/2023	0.8	N/A	N/A	Linear/FRET due to collision
1G-Main	BaxΔCTS	tBid	1	24/11/2023	2.6	0.19	13.1	Binding curve
1G-Main	BaxΔCTS	BimL	3	24/11/2023	2.3	0.16	36	Binding curve
1G-Main	BaxΔCTS	Puma	1	24/11/2023	2	0.16	15	Binding curve
1G-Main	BaxΔCTS	Bad	1	24/11/2023	1.2	N/A	N/A	Linear/FRET due to collision
1G-Main	BaxΔCTS	Noxa	1	24/11/2023	0.9	N/A	N/A	Linear/FRET due to collision
1G-Main	BaxΔCTS	Bik	2	24/11/2023	1.6	N/A	N/A	Linear/FRET due to collision
1G-Main	BaxΔCTS	Venus	1	24/11/2023	1.3	N/A	N/A	Linear/FRET due to collision
1H-Main	BakΔCTS	tBid	1	18/05/2023	2.3	0.15	14.4	Binding curve
1H-Main	BakΔCTS	tBid (BimBH3 h0-h4)	1	18/05/2023	1	N/A	N/A	Linear/FRET due to collision
1H-Main	BakΔCTS	tBid-4E	2	18/05/2023	0.6	N/A	N/A	Linear/FRET due to collision
2B-Main	BakΔCTS	tBid	2	13/05/2023	2	0.14	11	Binding curve
2B-Main	BakΔCTS	tBid-4E	2	13/05/2023	0.7	N/A	N/A	Linear/FRET due to collision
2B-Main	BakΔCTS	tBid-I82A I83A	1	13/05/2023	0.6	N/A	N/A	Linear/FRET due to collision
2C-Main	BakΔCTS	BimL	2	13/02/2023	1.2	N/A	N/A	Linear/FRET due to collision

2C-Main	BakΔCTS	BimL-4E	2	13/02/2023	1.5	N/A	N/A	Linear/FRET due to collision
2C-Main	BakΔCTS	BimL (BidBH3 h0+1)	1	13/02/2023	3.4	0.16	17.1	Binding curve
2C-Main	BakΔCTS	BimL (BidBH3 h0-h4+3)	3	13/02/2023	4.2	0.12	15.4	Binding curve
2C-Main	BakΔCTS	BimL (BidBH3 h1-h4+3)	1	13/02/2023	0.9	N/A	N/A	Linear/FRET due to collision
3E-Main	CTS$_{BAK}$	BimL	1	15/06/2024	4.3	0.12	6.2	Binding curve
3E-Main	CTS$_{BAK}$	tBid	1	15/06/2024	2.1	0.14	7.9	Binding curve
3E-Main	CTS$_{BAK}$	Bad	1	15/06/2024	1.4	N/A	N/A	Linear/FRET due to collision
3E-Main	CTS$_{BAK}$	Bik	1	15/06/2024	1.6	N/A	N/A	Linear/FRET due to collision
3E-Main	CTS$_{BAK}$	Venus	1	15/06/2024	1.4	N/A	N/A	Linear/FRET due to collision
3F-Main	CTS$_{BAX}$	BimL	2	23/07/2024	1.2	N/A	N/A	Linear/FRET due to collision
3F-Main	CTS$_{BAX}$	tBid	2	23/07/2024	2.6	0.17	6.6	Binding curve
3F-Main	CTS$_{BAX}$	Bad	2	23/07/2024	1.2	N/A	N/A	Linear/FRET due to collision
3F-Main	CTS$_{BAX}$	Bik	3	23/07/2024	1.3	N/A	N/A	Linear/FRET due to collision
3F-Main	CTS$_{BAX}$	Noxa	2	23/07/2024	1	N/A	N/A	Linear/FRET due to collision
4A-Main	CTS$_{BAK}$	tBid	3	02/03/2024	2.5	0.21	12.7	Binding curve
4A-Main	CTS$_{BAK}$	tBid-4E	1	02/03/2024	2.1	0.18	4.7	Binding curve
4B-Main	CTS$_{BAK}$	tBid-I82A	2	02/03/2024	2.3	0.21	12.3	Binding curve
4B-Main	CTS$_{BAK}$	tBid-I83A	1	02/03/2024	2.2	0.2	7.9	Binding curve
4C-Main	Bak G126S	tBid	2	03/04/2024	2	0.12	24	Binding curve
4C-Main	Bak G126S	tBid-4E	1	03/04/2024	3	0.17	36.6	Binding curve
4C-Main	Bak G126S	Bad	2	03/04/2024	1.7	N/A	N/A	Linear/FRET due to collision
5B-Main	CTS$_{BAK}$	BimL	3	02/03/2024	2.7	0.16	9	Binding curve
5B-Main	CTS$_{BAK}$	CTS$_{BIM}$	1	02/03/2024	2.5	0.3	13.1	Binding curve
5B-Main	CTS$_{BAK}$	CTSscr$_{BIM}$	2	02/03/2024	1.5	N/A	N/A	Linear/FRET due to collision
5B-Main	CTS$_{BAK}$	BimL-4E	1	02/03/2024	2.4	0.2	15.8	Binding curve
5B-Main	CTS$_{BAK}$	BimL-CTSscr	2	02/03/2024	2.6	0.04	N/A	Insufficient FRET
5C-Main	CTS$_{BAK}$	Bad	2	02/03/2024	1.1	N/A	N/A	Linear/FRET due to collision
5C-Main	CTS$_{BAK}$	BadΔCTS-BimCTS	1	02/03/2024	2.2	0.23	13.9	Binding curve
5C-Main	CTS$_{BAK}$	BimΔCTS	2	02/03/2024	1.3	N/A	N/A	Linear/FRET due to collision
5D-Main	CTS$_{BAK}$	BimL-R134L	1	02/03/2024	2.84	0.04	N/A	Insufficient FRET
1B-Sup1	BaxΔCTS	tBid	2	24/11/2023	2.6	0.23	19.6	Binding curve
1B-Sup1	BaxΔCTS	tBid-4E	3	24/11/2023	1.6	N/A	N/A	Linear/FRET due to collision

1B-Sup1	BaxΔCTS	tBid (Bim BH3 h0-h4)	2	24/11/2023	2.4	0.25	62	Binding curve
1C-Sup1	Bcl-XL	tBid	1	20/02/2024	3	0.2	9.4	Binding curve
1C-Sup1	Bcl-XL	tBid-4E	1	20/02/2024	2	0.15	18.9	Binding curve
1C-Sup1	Bcl-XL	tBid (Bim BH3 h0-h4)	1	20/02/2024	4	0.2	7.2	Binding curve
2A-Sup1	BakΔCTS	tBid	1	13/05/2023	3.3	0.2	25	Binding curve
2A-Sup1	BakΔCTS	tBid-4E	1	13/05/2023	0.8	N/A	N/A	Linear/FRET due to collision
2A-Sup1	BakΔCTS	tBid I82A	1	13/05/2023	2	0.28	86	Binding curve
2A-Sup1	BakΔCTS	tBid I83A	1	13/05/2023	1	N/A	N/A	Linear/FRET due to collision
2B-Sup1	BaxΔCTS	tBid	1	13/05/2023	2	0.38	42	Binding curve
2B-Sup1	BaxΔCTS	tBid-4E	3	13/05/2023	1.1	N/A	N/A	Linear/FRET due to collision
2B-Sup1	BaxΔCTS	tBid I82A	3	13/05/2023	2	0.46	67	Binding curve
2B-Sup1	BaxΔCTS	tBid I83A	3	13/05/2023	2	0.29	46	Binding curve
2B-Sup1	BaxΔCTS	tBid I82A I83A	2	13/05/2023	2.1	0.4	131	Binding curve
2C-Sup1	Bcl-XL	tBid	2	20/02/2024	2	0.2	9.4	Binding curve
2C-Sup1	Bcl-XL	tBid-4E	2	20/02/2024	2	0.15	18.9	Binding curve
2C-Sup1	Bcl-XL	tBid-I82A	1	20/02/2024	3.6	0.21	10.6	Binding curve
2C-Sup1	Bcl-XL	tBid-I83A	1	20/02/2024	2.6	0.24	12.3	Binding curve
2A-Sup2	BaxΔCTS	BimL	2	13/02/2023	2.3	0.16	9	Binding curve
2A-Sup2	BaxΔCTS	BimL-4E	1	13/02/2023	0.9	N/A	N/A	Linear/FRET due to collision
2A-Sup2	BaxΔCTS	BimL (BidBH3 h0+1)	1	13/02/2023	2	0.17	8.8	Binding curve
2A-Sup2	BaxΔCTS	BimL (BidBH3 h0-h4+3)	3	13/02/2023	2.4	0.14	10.5	Binding curve
2A-Sup2	BaxΔCTS	BimL (BidBH3 h1-h4+3)	1	13/02/2023	2.2	0.12	10.9	Binding curve
3A-Sup1	CTS-KSD$_{BAK}$	BimL	3	24/03/2024	2.2	0.08	22.8	Binding curve
3A-Sup1	CTS-KSD$_{BAK}$	tBid	3	24/03/2024	3.1	0.16	31.7	Binding curve
3A-Sup1	CTS-KSD$_{BAK}$	Bad	3	24/03/2024	1.4	N/A	N/A	Linear/FRET due to collision
3A-Sup1	CTS-KSD$_{BAK}$	Bik	1	24/03/2024	1.4	N/A	N/A	Linear/FRET due to collision
3A-Sup1	CTS-KSD$_{BAK}$	Venus	1	24/03/2024	1.5	N/A	N/A	Linear/FRET due to collision
3B-Sup1	CTSscr$_{BAK}$	BimL	3	24/03/2024	1.2	N/A	N/A	Linear/FRET due to collision
3B-Sup1	CTSscr$_{BAK}$	tBid	3	24/03/2024	1.9	N/A	N/A	Linear/FRET due to collision
3B-Sup1	CTSscr$_{BAK}$	Bad	2	24/03/2024	1.8	N/A	N/A	Linear/FRET due to collision
3B-Sup1	CTSscr$_{BAK}$	Bik	1	24/03/2024	0.9	N/A	N/A	Linear/FRET due to collision
3B-Sup1	CTSscr$_{BAK}$	Venus	1	24/03/2024	1.6	N/A	N/A	Linear/FRET due to collision
3C-Sup1	CTS$_{BAK}$	CTS$_{BAK}$	2	23/08/2022	2.1	0.52	11.1	Binding curve

3C-Sup1	CTS_{BAK}	CTS_{TOM5}	2	23/08/2022	1.4	N/A	N/A	Linear/FRET due to collision
3D-Sup2	CTS_{BAK}	tBid	2	02/03/2024	2.8	0.21	11.84	Binding curve
3D-Sup2	CTS_{BAK}	BimL	1	02/03/2024	5.6	0.16	9.2	Binding curve
3D-Sup2	CTS_{BAK}	Bad	1	02/03/2024	1.4	N/A	N/A	Linear/FRET due to collision
3D-Sup2	CTS_{BAK}	Bik	2	02/03/2024	0.7	N/A	N/A	Linear/FRET due to collision
3D-Sup2	CTS_{BAK}	Venus	1	02/03/2024	1.5	N/A	N/A	Linear/FRET due to collision
3E-Sup2	CTS_{BAX}	tBid	3	24/08/2024	2.3	0.18	27.9	Binding curve
3E-Sup2	CTS_{BAX}	BimL	1	24/08/2024	1.9	N/A	N/A	Linear/FRET due to collision
3E-Sup2	CTS_{BAX}	Bad	2	24/08/2024	0.8	N/A	N/A	Linear/FRET due to collision
3E-Sup2	CTS_{BAX}	Bik	1	24/08/2024	1.5	N/A	N/A	Linear/FRET due to collision
3E-Sup2	CTS_{BAX}	Noxa	1	24/08/2024	1.3	N/A	N/A	Linear/FRET due to collision
4C-Sup1	$CTSscr_{BAK}$	tBid	1	24/03/2024	1.5	N/A	N/A	Linear/FRET due to collision
4C-Sup1	$CTSscr_{BAK}$	tBid-4E	1	24/03/2024	1.5	N/A	N/A	Linear/FRET due to collision
4C-Sup1	$CTSscr_{BAK}$	tBid-I82A	1	24/03/2024	1.4	N/A	N/A	Linear/FRET due to collision
4C-Sup1	$CTSscr_{BAK}$	tBid-I83A	2	24/03/2024	1.3	N/A	N/A	Linear/FRET due to collision
4D-Sup1	BakΔCTS G126S	tBid	1	03/04/2024	2.1	0.15	10.4	Binding curve
4D-Sup1	BakΔCTS G126S	tBid-4E	1	03/04/2024	0.9	N/A	N/A	Linear/FRET due to collision
4D-Sup1	BakΔCTS G126S	Bad	3	03/04/2024	1.5	N/A	N/A	Linear/FRET due to collision
4A-Sup3	CTS_{BAK}	tBid	1	17/02/2024	2.1	0.13	8.7	Binding curve
4A-Sup3	CTS_{BAK}	tBid-4E	1	17/02/2024	3.5	0.16	6.7	Binding curve
4B-Sup3	CTS_{BAK}	tBid-I82A	1	17/02/2024	2.2	0.14	9.1	Binding curve
4B-Sup3	CTS_{BAK}	tBid-I83A	1	17/02/2024	3.2	0.15	7.2	Binding curve
4C-Sup3	Bak G126S	tBid	2	28/03/2024	2.8	0.18	34	Binding curve
4C-Sup3	Bak G126S	tBid-4E	1	05/07/2024	2.3	0.2	32.9	Binding curve
4C-Sup3	Bak G126S	Bad	2	05/07/2024	1.5	N/A	N/A	Linear/FRET due to collision
5A-Sup1	$CTSscr_{BAK}$	BimL	2	24/03/2024	2.9	0.05	N/A	Insufficient FRET
5A-Sup1	$CTSscr_{BAK}$	BimL-4E	1	24/03/2024	1.2	N/A	N/A	Linear/FRET due to collision
5A-Sup1	$CTSscr_{BAK}$	BimL-CTSscr	2	24/03/2024	0.6	N/A	N/A	Linear/FRET due to collision
5A-Sup1	$CTSscr_{BAK}$	CTS_{BIM}	2	24/03/2024	3.2	0.05	N/A	Insufficient FRET
5A-Sup1	$CTSscr_{BAK}$	$CTSscr_{BIM}$	1	24/03/2024	1	N/A	N/A	Linear/FRET due to collision
5B-Sup1	$CTS\text{-}KSD_{BAK}$	BimL	2	24/03/2024	2.6	0.08	22.8	Binding curve
5B-Sup1	$CTS\text{-}KSD_{BAK}$	BimL-CTSscr	1	24/03/2024	1.2	N/A	N/A	Linear/FRET due to collision

5C-Sup1	CTS-KSD$_{BAK}$	CTS$_{BIM}$	2	24/03/2024	2.2	0.08	17.1	Binding curve
5C-Sup1	CTS-KSD$_{BAK}$	CTSscr$_{BIM}$	1	24/03/2024	1	N/A	N/A	Linear/FRET due to collision
5E-Sup1	CTS$_{BAK}$	CTS$_{BIM}$	3	03/06/2024	4.9	0.24	9.3	Binding curve
5E-Sup1	CTS$_{ActA}$	CTS$_{BIM}$	3	03/06/2024	1.5	N/A	N/A	Linear/FRET due to collision
5B-Sup2	CTS$_{BAK}$	BimL	1	05/05/2024	2.2	0.1	6.9	Binding curve
5B-Sup2	CTS$_{BAK}$	BimL-CTSscr	1	05/05/2024	1.3	N/A	N/A	Linear/FRET due to collision
5B-Sup2	CTS$_{BAK}$	BimL-M123I	1	05/05/2024	2.4	0.1	6.8	Binding curve
5B-Sup2	CTS$_{BAK}$	BimL-I125V	1	05/05/2024	2.1	0.1	6.9	Binding curve
5B-Sup2	CTS$_{BAK}$	BimL-R130L	1	05/05/2024	1.8	N/A	N/A	Linear/FRET due to collision
5B-Sup2	CTS$_{BAK}$	BimL-I132N	1	05/05/2024	2.5	0.02	N/A	Insufficient FRET
5A-Sup3	CTS$_{BAK}$	BimL	1	17/02/2023	6	0.14	9.5	Binding curve
5A-Sup3	CTS$_{BAK}$	CTS$_{BIM}$	1	17/02/2024	10.8	0.26	21.1	Binding curve
5A-Sup3	CTS$_{BAK}$	CTSscr$_{BIM}$	1	17/02/2024	2.3	0.05	N/A	Insufficient FRET
5A-Sup3	CTS$_{BAK}$	BimL-4E	1	17/02/2024	3.4	0.19	26.4	Binding curve
5A-Sup3	CTS$_{BAK}$	BimL-CTSscr	2	17/02/2024	2.3	0.02	N/A	Insufficient FRET
5B-Sup3	CTS$_{BAK}$	Bad	1	17/02/2024	1.3	N/A	N/A	Linear/FRET due to collision
5B-Sup3	CTS$_{BAK}$	BadΔCTS-BimCTS	1	17/02/2024	10.7	0.19	16.5	Binding curve
5B-Sup3	CTS$_{BAK}$	BimΔCTS	1	17/02/2024	1.2	N/A	N/A	Linear/FRET due to collision
5C-Sup3	CTS$_{BAK}$	BimL-R134L	1	17/02/2024	4.1	0.04	N/A	Insufficient FRET
6A-Sup1	Bak G126S	CTS$_{BIM}$	1	03/04/2024	3.1	0.17	27.9	Binding curve
6A-Sup1	Bak G126S	CTSscr$_{BIM}$	2	03/04/2024	0.7	N/A	N/A	Linear/FRET due to collision
6B-Sup1	BakΔCTS G126S	CTS$_{BIM}$	2	03/04/2024	0.5	N/A	N/A	Linear/FRET due to collision
6B-Sup1	BakΔCTS G126S	CTSscr$_{BIM}$	2	03/04/2024	0.7	N/A	N/A	Linear/FRET due to collision
6C-Sup1	Bak G126S	BimL-4E	1	03/04/2024	3	0.17	36.2	Binding curve
6C-Sup1	Bak G126S	BimL	3	05/07/2024	2.3	0.15	34.2	Binding curve
6C-Sup1	Bak G126S	BimL-R134L	1	03/04/2024	1.4	N/A	N/A	Linear/FRET due to collision
6C-Sup1	Bak G126S	BimL-CTSscr	3	05/07/2024	0.9	N/A	N/A	Linear/FRET due to collision

Appendix Table 2.S4: All cell lines were tested for Mycoplasma using MycoAlert® Mycoplasma Detection Kit from Lonza. Ratio A/B is an indicator of ATP level which is measured by the luminescence intensity before (read A) and after (read B) adding the substrate. Samples with ratio A/B <1 are negative for Mycoplasma. N/A: not applicable.

Sample ID	Cell line	Ratio A/B
1	BMK DKO rtTA3	0.57
2	BMK DKO rtTA3 - ^{C}Bak	0.48
3	HCT116 DKO - ^{C}BaxΔCTS	0.47
4	HCT116 DKO - ^{C}BakΔCTS	0.55
5	HCT116 DKO - ^{C}Bak G126S	0.51
6	HCT116 DKO - ^{C}BakΔCTS G126S	0.44
7	BMK DKO - $^{mT2}CTS_{BAX}$	0.46
8	BMK DKO - $^{mT2}CTS\text{-}KSD_{BAK}$	0.47
9	BMK DKO - $^{mT2}CTS_{BAK}$	0.50
10	BMK DKO - $^{C}CTS_{ActA}$	0.45
11	BMK DKO - $^{mT2}CTSscr_{BAK}$	0.42
Negative control	N/A	0.15
Positive control	N/A	68.02

Appendix Figure 2.S5. Western blot of cell lysates from cell lines used for FLIM-FRET. Expression of the donor-fusion proteins was verified by immunoblotting on the left panel. GAPDH loading control is shown on the right panel.

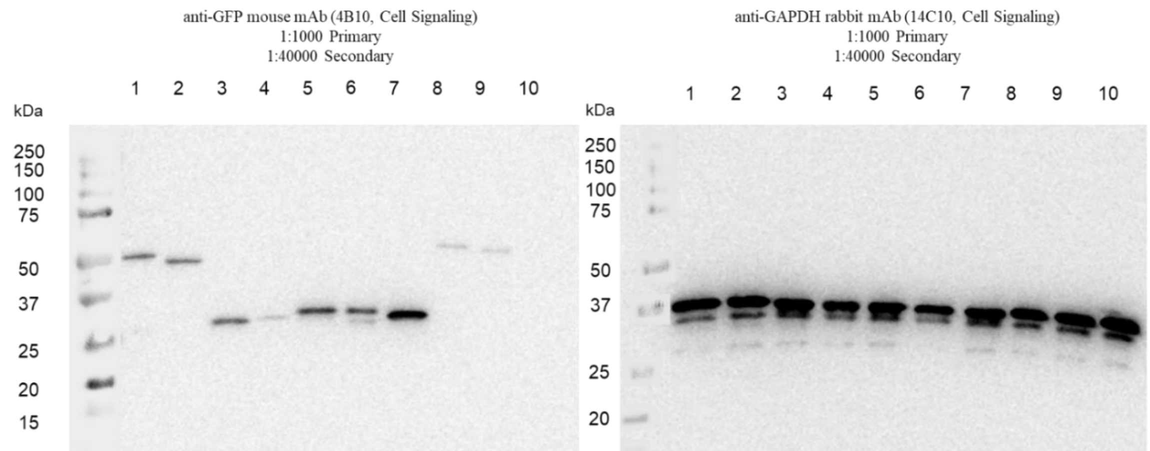

Lane# 10μg of cell lysate/lane

1) HCT116 DKO – ^{C}BakΔCTS
2) HCT116 DKO – ^{C}BaxΔCTS
3) BMK DKO – ^{mT2}CTS$_{BAK}$
4) BMK DKO – ^{mT2}CTS$_{BAX}$
5) BMK DKO – ^{mT2}CTSscr$_{BAK}$
6) BMK DKO – ^{mT2}CTS-KSD$_{BAK}$
7) BMK DKO – ^{C}CTS$_{ActA}$
8) HCT116 DKO – ^{C}Bak G126S
9) HCT116 DKO – ^{C}BakΔCTS G126S
10) Parental HCT116 DKO

Molecular Weight
^{C}BakΔCTS ≈ 48 kDa
^{C}BaxΔCTS ≈ 46 kDa
^{mT2}CTS$_{BAK}$ ≈ 31 kDa
^{mT2}CTS$_{BAX}$ ≈ 31 kDa
^{C}CTS$_{ActA}$ ≈ 30 kDa
^{C}Bak G126S ≈ 51 kDa
GAPDH ≈ 36 kDa

2.8 References

Alberts B (2022) *Molecular biology of the cell*. W. W. Norton & Company, New York

Beigl TB, Paul A, Fellmeth TP, Nguyen D, Barber L, Weller S, Schäfer B, Gillissen BF, Aulitzky WE, Kopp HG *et al* (2024) BCL-2 and BOK regulate apoptosis by interaction of their C-terminal transmembrane domains. *EMBO Rep* 25: 3896-3924

Bogner C, Kale J, Pogmore J, Chi X, Shamas-Din A, Fradin C, Leber B, Andrews DW (2020) Allosteric Regulation of BH3 Proteins in Bcl-x(L) Complexes Enables Switch-like Activation of Bax. *Mol Cell* 77: 901-912.e909

Brahmbhatt H, Uehling D, Al-Awar R, Leber B, Andrews D (2016) Small molecules reveal an alternative mechanism of Bax activation. *Biochem J* 473: 1073-1083

Brouwer JM, Lan P, Cowan AD, Bernardini JP, Birkinshaw RW, van Delft MF, Sleebs BE, Robin AY, Wardak A, Tan IK *et al* (2017) Conversion of Bim-BH3 from Activator to Inhibitor of Bak through Structure-Based Design. *Mol Cell* 68: 659-672.e659

Brouwer JM, Westphal D, Dewson G, Robin AY, Uren RT, Bartolo R, Thompson GV, Colman PM, Kluck RM, Czabotar PE (2014) Bak core and latch domains separate during activation, and freed core domains form symmetric homodimers. *Mol Cell* 55: 938-946

Cartron PF, Juin P, Oliver L, Martin S, Meflah K, Vallette FM (2003) Nonredundant role of Bax and Bak in Bid-mediated apoptosis. *Mol Cell Biol* 23: 4701-4712

Cerami E, Gao J, Dogrusoz U, Gross BE, Sumer SO, Aksoy BA, Jacobsen A, Byrne CJ, Heuer ML, Larsson E *et al* (2012) The cBio cancer genomics portal: an open platform for exploring multidimensional cancer genomics data. *Cancer Discov* 2: 401-404

Certo M, Del Gaizo Moore V, Nishino M, Wei G, Korsmeyer S, Armstrong SA, Letai A (2006) Mitochondria primed by death signals determine cellular addiction to antiapoptotic BCL-2 family members. *Cancer Cell* 9: 351-365

Cheng EH, Sheiko TV, Fisher JK, Craigen WJ, Korsmeyer SJ (2003) VDAC2 inhibits BAK activation and mitochondrial apoptosis. *Science* 301: 513-517

Chi X, Nguyen D, Pemberton JM, Osterlund EJ, Liu Q, Brahmbhatt H, Zhang Z, Lin J, Leber B, Andrews DW (2020) The carboxyl-terminal sequence of bim enables bax activation and killing of unprimed cells. *Elife* 9

Dai H, Smith A, Meng XW, Schneider PA, Pang YP, Kaufmann SH (2011) Transient binding of an activator BH3 domain to the Bak BH3-binding groove initiates Bak oligomerization. *J Cell Biol* 194: 39-48

Das AT, Tenenbaum L, Berkhout B (2016) Tet-On Systems For Doxycycline-inducible Gene Expression. *Curr Gene Ther* 16: 156-167

Day CL, Smits C, Fan FC, Lee EF, Fairlie WD, Hinds MG (2008) Structure of the BH3 domains from the p53-inducible BH3-only proteins Noxa and Puma in complex with Mcl-1. *J Mol Biol* 380: 958-971

de Bruijn I, Kundra R, Mastrogiacomo B, Tran TN, Sikina L, Mazor T, Li X, Ochoa A, Zhao G, Lai B *et al* (2023) Analysis and Visualization of Longitudinal Genomic and Clinical Data from the AACR Project GENIE Biopharma Collaborative in cBioPortal. *Cancer Res* 83: 3861-3867

Deckwerth TL, Elliott JL, Knudson CM, Johnson EM, Jr., Snider WD, Korsmeyer SJ (1996) BAX is required for neuronal death after trophic factor deprivation and during development. *Neuron* 17: 401-411

Degenhardt K, Sundararajan R, Lindsten T, Thompson C, White E (2002) Bax and Bak independently promote cytochrome C release from mitochondria. *J Biol Chem* 277: 14127-14134

Del Gaizo Moore V, Letai A (2013) BH3 profiling--measuring integrated function of the mitochondrial apoptotic pathway to predict cell fate decisions. *Cancer Lett* 332: 202-205

Deng J, Carlson N, Takeyama K, Dal Cin P, Shipp M, Letai A (2007) BH3 profiling identifies three distinct classes of apoptotic blocks to predict response to ABT-737 and conventional chemotherapeutic agents. *Cancer Cell* 12: 171-185

Dewson G, Kratina T, Czabotar P, Day CL, Adams JM, Kluck RM (2009) Bak activation for apoptosis involves oligomerization of dimers via their alpha6 helices. *Mol Cell* 36: 696-703

Gallenne T, Gautier F, Oliver L, Hervouet E, Noël B, Hickman JA, Geneste O, Cartron PF, Vallette FM, Manon S *et al* (2009) Bax activation by the BH3-only protein Puma promotes cell dependence on antiapoptotic Bcl-2 family members. *J Cell Biol* 185: 279-290

Gao J, Aksoy BA, Dogrusoz U, Dresdner G, Gross B, Sumer SO, Sun Y, Jacobsen A, Sinha R, Larsson E *et al* (2013) Integrative analysis of complex cancer genomics and clinical profiles using the cBioPortal. *Sci Signal* 6: pl1

Gossen M, Freundlieb S, Bender G, Müller G, Hillen W, Bujard H (1995) Transcriptional activation by tetracyclines in mammalian cells. *Science* 268: 1766-1769

Hockings C, Alsop AE, Fennell SC, Lee EF, Fairlie WD, Dewson G, Kluck RM (2018) Mcl-1 and Bcl-x(L) sequestration of Bak confers differential resistance to BH3-only proteins. *Cell Death Differ* 25: 721-734

Hockings C, Anwari K, Ninnis RL, Brouwer J, O'Hely M, Evangelista M, Hinds MG, Czabotar PE, Lee EF, Fairlie WD *et al* (2015) Bid chimeras indicate that most BH3-only proteins can directly activate Bak and Bax, and show no preference for Bak versus Bax. *Cell Death Dis* 6: e1735

Huang K, O'Neill KL, Li J, Zhou W, Han N, Pang X, Wu W, Struble L, Borgstahl G, Liu Z *et al* (2019) BH3-only proteins target BCL-xL/MCL-1, not BAX/BAK, to initiate apoptosis. *Cell Res* 29: 942-952

Ichim G, Lopez J, Ahmed SU, Muthalagu N, Giampazolias E, Delgado ME, Haller M, Riley JS, Mason SM, Athineos D *et al* (2015) Limited mitochondrial permeabilization causes DNA damage and genomic instability in the absence of cell death. *Mol Cell* 57: 860-872

Iyer S, Bell F, Westphal D, Anwari K, Gulbis J, Smith BJ, Dewson G, Kluck RM (2015) Bak apoptotic pores involve a flexible C-terminal region and juxtaposition of the C-terminal transmembrane domains. *Cell Death Differ* 22: 1665-1675

Jakubowska MA, Kerkhofs M, Martines C, Efremov DG, Gerasimenko JV, Gerasimenko OV, Petersen OH, Bultynck G, Vervliet T, Ferdek PE (2019) ABT-199 (Venetoclax), a BH3-mimetic Bcl-2 inhibitor, does not cause Ca(2+) -signalling dysregulation or toxicity in pancreatic acinar cells. *Br J Pharmacol* 176: 4402-4415

Kale J, Chi X, Leber B, Andrews D (2014) Examining the molecular mechanism of bcl-2 family proteins at membranes by fluorescence spectroscopy. *Methods Enzymol* 544: 1-23

Kale J, Osterlund EJ, Andrews DW (2018) BCL-2 family proteins: changing partners in the dance towards death. *Cell Death Differ* 25: 65-80

Kamada S, Shimono A, Shinto Y, Tsujimura T, Takahashi T, Noda T, Kitamura Y, Kondoh H, Tsujimoto Y (1995) bcl-2 deficiency in mice leads to pleiotropic abnormalities: accelerated lymphoid cell death in thymus and spleen, polycystic kidney, hair hypopigmentation, and distorted small intestine. *Cancer Res* 55: 354-359

Kerr JF, Wyllie AH, Currie AR (1972) Apoptosis: a basic biological phenomenon with wide-ranging implications in tissue kinetics. *Br J Cancer* 26: 239-257

Kiefer MC, Brauer MJ, Powers VC, Wu JJ, Umansky SR, Tomei LD, Barr PJ (1995) Modulation of apoptosis by the widely distributed Bcl-2 homologue Bak. *Nature* 374: 736-739

Kim H, Tu HC, Ren D, Takeuchi O, Jeffers JR, Zambetti GP, Hsieh JJ, Cheng EH (2009) Stepwise activation of BAX and BAK by tBID, BIM, and PUMA initiates mitochondrial apoptosis. *Mol Cell* 36: 487-499

Knudson CM, Tung KS, Tourtellotte WG, Brown GA, Korsmeyer SJ (1995) Bax-deficient mice with lymphoid hyperplasia and male germ cell death. *Science* 270: 96-99

Korsmeyer SJ, Wei MC, Saito M, Weiler S, Oh KJ, Schlesinger PH (2000) Pro-apoptotic cascade activates BID, which oligomerizes BAK or BAX into pores that result in the release of cytochrome c. *Cell Death Differ* 7: 1166-1173

Krajewski S, Krajewska M, Reed JC (1996) Immunohistochemical analysis of in vivo patterns of Bak expression, a proapoptotic member of the Bcl-2 protein family. *Cancer Res* 56: 2849-2855

Ku B, Liang C, Jung JU, Oh BH (2011) Evidence that inhibition of BAX activation by BCL-2 involves its tight and preferential interaction with the BH3 domain of BAX. *Cell Res* 21: 627-641

Kurosaka K, Takahashi M, Watanabe N, Kobayashi Y (2003) Silent cleanup of very early apoptotic cells by macrophages. *J Immunol* 171: 4672-4679

Lazarou M, Stojanovski D, Frazier AE, Kotevski A, Dewson G, Craigen WJ, Kluck RM, Vaux DL, Ryan MT (2010) Inhibition of Bak activation by VDAC2 is dependent on the Bak transmembrane anchor. *J Biol Chem* 285: 36876-36883

Lee EF, Grabow S, Chappaz S, Dewson G, Hockings C, Kluck RM, Debrincat MA, Gray DH, Witkowski MT, Evangelista M *et al* (2016) Physiological restraint of Bak by Bcl-xL is essential for cell survival. *Genes Dev* 30: 1240-1250

Lengauer C, Kinzler KW, Vogelstein B (1997) Genetic instability in colorectal cancers. *Nature* 386: 623-627

Leshchiner ES, Braun CR, Bird GH, Walensky LD (2013) Direct activation of full-length proapoptotic BAK. *Proc Natl Acad Sci U S A* 110: E986-995

Letai A, Bassik MC, Walensky LD, Sorcinelli MD, Weiler S, Korsmeyer SJ (2002) Distinct BH3 domains either sensitize or activate mitochondrial apoptosis, serving as prototype cancer therapeutics. *Cancer Cell* 2: 183-192

Li H, Zhu H, Xu CJ, Yuan J (1998) Cleavage of BID by caspase 8 mediates the mitochondrial damage in the Fas pathway of apoptosis. *Cell* 94: 491-501

Lindsten T, Ross AJ, King A, Zong WX, Rathmell JC, Shiels HA, Ulrich E, Waymire KG, Mahar P, Frauwirth K *et al* (2000) The combined functions of proapoptotic Bcl-2 family members bak and bax are essential for normal development of multiple tissues. *Mol Cell* 6: 1389-1399

Liu Q, Leber B, Andrews DW (2012) Interactions of pro-apoptotic BH3 proteins with anti-apoptotic Bcl-2 family proteins measured in live MCF-7 cells using FLIM FRET. *Cell Cycle* 11: 3536-3542

Liu Q, Osterlund EJ, Chi X, Pogmore J, Leber B, Andrews DW (2019) Bim escapes displacement by BH3-mimetic anti-cancer drugs by double-bolt locking both Bcl-XL and Bcl-2. *Elife* 8

Martínez-Senac Mdel M, Corbalán-García S, Gómez-Fernández JC (2002) The structure of the C-terminal domain of the pro-apoptotic protein Bak and its interaction with model membranes. *Biophys J* 82: 233-243

McIlwain DR, Berger T, Mak TW (2013) Caspase functions in cell death and disease. *Cold Spring Harb Perspect Biol* 5: a008656

Morris RG, Hargreaves AD, Duvall E, Wyllie AH (1984) Hormone-induced cell death. 2. Surface changes in thymocytes undergoing apoptosis. *Am J Pathol* 115: 426-436

Motoyama N, Wang F, Roth KA, Sawa H, Nakayama K, Nakayama K, Negishi I, Senju S, Zhang Q, Fujii S *et al* (1995) Massive cell death of immature hematopoietic cells and neurons in Bcl-x-deficient mice. *Science* 267: 1506-1510

Naghdi S, Várnai P, Hajnóczky G (2015) Motifs of VDAC2 required for mitochondrial Bak import and tBid-induced apoptosis. *Proc Natl Acad Sci U S A* 112: E5590-5599

Nakayama K, Nakayama K, Negishi I, Kuida K, Shinkai Y, Louie MC, Fields LE, Lucas PJ, Stewart V, Alt FW *et al* (1993) Disappearance of the lymphoid system in Bcl-2 homozygous mutant chimeric mice. *Science* 261: 1584-1588

Nguyen D, Osterlund E, Kale J, Andrews DW (2024) The C-terminal sequences of Bcl-2 family proteins mediate interactions that regulate cell death. *Biochem J* 481: 903-922

Niu X, Brahmbhatt H, Mergenthaler P, Zhang Z, Sang J, Daude M, Ehlert FGR, Diederich WE, Wong E, Zhu W *et al* (2017) A Small-Molecule Inhibitor of Bax and Bak Oligomerization Prevents Genotoxic Cell Death and Promotes Neuroprotection. *Cell Chem Biol* 24: 493-506.e495

Oh KJ, Singh P, Lee K, Foss K, Lee S, Park M, Lee S, Aluvila S, Park M, Singh P *et al* (2010) Conformational changes in BAK, a pore-forming proapoptotic Bcl-2 family member, upon membrane insertion and direct evidence for the existence of BH3-BH3 contact interface in BAK homo-oligomers. *J Biol Chem* 285: 28924-28937

Osterlund EJ, Hirmiz N, Pemberton JM, Nougarède A, Liu Q, Leber B, Fang Q, Andrews DW (2022) Efficacy and specificity of inhibitors of BCL-2 family protein interactions assessed by affinity measurements in live cells. *Sci Adv* 8: eabm7375

Osterlund EJ, Hirmiz N, Tardif C, Andrews DW (2019) Rapid Imaging of BCL-2 Family Interactions in Live Cells Using FLIM-FRET. *Methods Mol Biol* 1877: 305-335

Osterlund EJ, Liu Q, Andrews DW (2015) The use of FLIM-FRET for the detection of mitochondria-associated protein interactions. *Methods Mol Biol* 1264: 395-419

Pemberton JM, Nguyen D, Osterlund EJ, Schormann W, Pogmore JP, Hirmiz N, Leber B, Andrews DW (2023) The carboxyl-terminal sequence of PUMA binds to both anti-apoptotic proteins and membranes. *Elife* 12

Pogmore JP, Pemberton JM, Chi X, Andrews DW (2016) Using Förster-Resonance Energy Transfer to Measure Protein Interactions Between Bcl-2 Family Proteins on Mitochondrial Membranes. *Methods Mol Biol* 1419: 197-212

Sandow BA, West NB, Norman RL, Brenner RM (1979) Hormonal control of apoptosis in hamster uterine luminal epithelium. *Am J Anat* 156: 15-35

Sandow JJ, Tan IK, Huang AS, Masaldan S, Bernardini JP, Wardak AZ, Birkinshaw RW, Ninnis RL, Liu Z, Dalseno D *et al* (2021) Dynamic reconfiguration of pro-apoptotic BAK on membranes. *Embo j* 40: e107237

Sarosiek KA, Chi X, Bachman JA, Sims JJ, Montero J, Patel L, Flanagan A, Andrews DW, Sorger P, Letai A (2013) BID preferentially activates BAK while BIM preferentially activates BAX, affecting chemotherapy response. *Mol Cell* 51: 751-765

Savill J, Fadok V (2000) Corpse clearance defines the meaning of cell death. *Nature* 407: 784-788

Shamas-Din A, Satsoura D, Khan O, Zhu W, Leber B, Fradin C, Andrews DW (2014) Multiple partners can kiss-and-run: Bax transfers between multiple membranes and permeabilizes those primed by tBid. *Cell Death Dis* 5: e1277

Shivakumar S, Kurylowicz M, Hirmiz N, Manan Y, Friaa O, Shamas-Din A, Masoudian P, Leber B, Andrews DW, Fradin C (2014) The proapoptotic protein tBid forms both superficially bound and membrane-inserted oligomers. *Biophys J* 106: 2085-2095

Singh G, Guibao CD, Seetharaman J, Aggarwal A, Grace CR, McNamara DE, Vaithiyalingam S, Waddell MB, Moldoveanu T (2022) Structural basis of BAK activation in mitochondrial apoptosis initiation. *Nat Commun* 13: 250

Singh R, Letai A, Sarosiek K (2019) Regulation of apoptosis in health and disease: the balancing act of BCL-2 family proteins. *Nat Rev Mol Cell Biol* 20: 175-193

Souers AJ, Leverson JD, Boghaert ER, Ackler SL, Catron ND, Chen J, Dayton BD, Ding H, Enschede SH, Fairbrother WJ *et al* (2013) ABT-199, a potent and selective BCL-2 inhibitor, achieves antitumor activity while sparing platelets. *Nat Med* 19: 202-208

Stehle D, Grimm M, Einsele-Scholz S, Ladwig F, Johänning J, Fischer G, Gillissen B, Schulze-Osthoff K, Essmann F (2018) Contribution of BH3-domain and Transmembrane-domain to the Activity and Interaction of the Pore-forming Bcl-2 Proteins Bok, Bak, and Bax. *Scientific reports* 8: 12434

Sunters A, Fernández de Mattos S, Stahl M, Brosens JJ, Zoumpoulidou G, Saunders CA, Coffer PJ, Medema RH, Coombes RC, Lam EW (2003) FoxO3a transcriptional regulation of Bim controls apoptosis in paclitaxel-treated breast cancer cell lines. *J Biol Chem* 278: 49795-49805

Tait SW, Parsons MJ, Llambi F, Bouchier-Hayes L, Connell S, Muñoz-Pinedo C, Green DR (2010) Resistance to caspase-independent cell death requires persistence of intact mitochondria. *Dev Cell* 18: 802-813

Tan TT, Degenhardt K, Nelson DA, Beaudoin B, Nieves-Neira W, Bouillet P, Villunger A, Adams JM, White E (2005) Key roles of BIM-driven apoptosis in epithelial tumors and rational chemotherapy. *Cancer Cell* 7: 227-238

Tartaglia LA, Ayres TM, Wong GH, Goeddel DV (1993) A novel domain within the 55 kd TNF receptor signals cell death. *Cell* 74: 845-853

Todt F, Cakir Z, Reichenbach F, Emschermann F, Lauterwasser J, Kaiser A, Ichim G, Tait SW, Frank S, Langer HF *et al* (2015) Differential retrotranslocation of mitochondrial Bax and Bak. *Embo j* 34: 67-80

Tsujimoto Y, Cossman J, Jaffe E, Croce CM (1985) Involvement of the bcl-2 gene in human follicular lymphoma. *Science* 228: 1440-1443

Veis DJ, Sorenson CM, Shutter JR, Korsmeyer SJ (1993) Bcl-2-deficient mice demonstrate fulminant lymphoid apoptosis, polycystic kidneys, and hypopigmented hair. *Cell* 75: 229-240

Walensky LD, Kung AL, Escher I, Malia TJ, Barbuto S, Wright RD, Wagner G, Verdine GL, Korsmeyer SJ (2004) Activation of apoptosis in vivo by a hydrocarbon-stapled BH3 helix. *Science* 305: 1466-1470

Wang K, Yin XM, Chao DT, Milliman CL, Korsmeyer SJ (1996) BID: a novel BH3 domain-only death agonist. *Genes Dev* 10: 2859-2869

Wyllie AH, Kerr JF, Currie AR (1980) Cell death: the significance of apoptosis. *Int Rev Cytol* 68: 251-306

Wyllie AH, Morris RG, Smith AL, Dunlop D (1984) Chromatin cleavage in apoptosis: association with condensed chromatin morphology and dependence on macromolecular synthesis. *J Pathol* 142: 67-77

Yang MC, Lin RW, Huang SB, Huang SY, Chen WJ, Wang S, Hong YR, Wang C (2016) Bim directly antagonizes Bcl-xl in doxorubicin-induced prostate cancer cell apoptosis independently of p53. *Cell Cycle* 15: 394-402

Ye K, Meng WX, Sun H, Wu B, Chen M, Pang YP, Gao J, Wang H, Wang J, Kaufmann SH *et al* (2020) Characterization of an alternative BAK-binding site for BH3 peptides. *Nat Commun* 11: 3301

Zhang L, Yu J, Park BH, Kinzler KW, Vogelstein B (2000) Role of BAX in the apoptotic response to anticancer agents. *Science* 290: 989-992

3 Concluding Remarks

Activation of Bak by BH3-only proteins requires binding BH3 sequences of activators to the BH3-binding pocket of Bak. This study demonstrates that BimL is less efficient than cBid in activating Bak (Figure 1A and B), consistent with previous data (Sarosiek *et al.*, 2013). While the exact reasons for the greater potency of cBid over BimL in Bak activation remain unclear, it is unlikely due to the differences in their BH3 motifs, despite these sequences having different binding affinities to the BH3-binding pocket of Bak. This suggests that the additional binding affinity provided by the h0 region of Bid BH3 to the BH3-binding pocket of Bak is not sufficient to enhance Bak activation and that there must be other regions outside the Bid BH3 that, together with the BH3, account for the potency of Bid at activating Bak. Future studies classifying the Bid carboxyl terminal region could provide a target to characterize cBid activation mechanisms outside of the h0 region.

A key challenge in studying Bak is the difficulty of analyzing the full-length proteins within membranes, coupled with Bak's specific role in inducing cell death upon activation in live cells. Previous research has utilized truncated forms of Bcl-2 family proteins, with Bak often studied as a carboxyl terminal-truncated cytosolic multi-BH domain protein. In this study, to address this challenge, binding and activation of Bak were systematically investigated by examining activation of Bak by BH3-only activator protein of Bak utilizing either:

1. The carboxyl terminally-truncated cytosolic version of Bak (BakΔCTS) used in previous studies.
2. The membrane-binding CTS region of Bak alone, addressed the function of the CTS directly.
3. Full-length protein Bak, where it was possible to set up those assays.

Further, one of the difficulties of interpreting FLIM-FRET data is its high rate of false negatives due to stringent requirements for donor/acceptor fluorophore to align appropriately and be in close proximity (<10nm). To overcome this, an orthogonal in-vitro binding assay using recombinant proteins was carried out to validate our FLIM-FRET findings.

Lastly, examining the activation of cell death using live cell death assays is particularly challenging due to cell priming by upregulation of anti-apoptotic proteins. This challenge was overcome by creating a BMK DKO cell line stably expressing rtTa3 and the doxycycline-inducible mC3-Bak. The addition of doxycycline enabled a controlled and rapid activation of the executioner protein Bak in cells transfected with BH3-only activator proteins 5 hours previously. The rapid expression of Bak within 12 hours produced a population of cells that did not yet adapt by priming. It allowed a time point at which the activation of Bak by Bim took place. Cells were scored for apoptosis, measuring the Nucview530 fluorescence intensity in the nucleus for caspase-3 activity. Apoptosis markers were visible and imaged before the cell progressed into protein degradation and later stages of apoptosis.

CTS of Bak retains a functional regulation of proteins that is markedly different from CTS of Bax, which may be partially responsible for most organ systems cells retaining copies of both genes. Bak knockout mice exhibit limited developmental dysfunction, while Bax knockout mice exhibit much higher physiological deficits (Deckwerth *et al.*, 1996; Lindsten *et al.*, 2000). Double knockout Bax−/−Bak−/− animals are largely not viable, with only 10% surving into adulthood (Lindsten *et al.*, 2000). In cells, this points to a biological interchangibility of Bax for Bak, however, Bak cannot be substituted for Bax to retain homeostasis. Bax provides cells with higher flexibility to regulate cell death. From a biological standpoint, flexible regulation of cell death in organ systems such as the brain, is a much more advantageous strategy.

In conclusion, this study reveals a novel mechanism for Bak activation by Bid and Bim through interactions with the Bak-CTS. Classifying the motifs involved in the activation of the executioner proteins opens avenues for potential pharmaceutical interventions selectively targeting Bak- or Bax-mediated apoptosis. Bim-CTS bind directly to the Bak-CTS, creating a secondary binding site that is necessary but insufficient for BimL-mediated Bak activation (Figure 7). Further, this study demonstrates that tBid can bind Bak-CTS through an unknown site outside the BH3 region of Bid and that the Bak-CTS is required for cBid-mediated Bak activation. The pro-apoptotic role of Bak-CTS, distinct from its membrane-binding function, represents a previously unknown mechanism by which Bak-CTS regulates Bak activation.